

The Influence of Matrix Bound Nanovesicles on Inflammation-Driven Prosthetic Heart Valve Failure

by

Madeline Claire Cramer

Bachelor of Science in Materials Science and Engineering with a secondary degree in Biomedical Engineering, Carnegie Mellon University, 2014

Master of Science in Biomedical Engineering, Carnegie Mellon University, 2015

Submitted to the Graduate Faculty of the
Swanson School of Engineering in partial fulfillment
of the requirements for the degree of
Doctor of Philosophy

University of Pittsburgh

2022

UNIVERSITY OF PITTSBURGH

SWANSON SCHOOL OF ENGINEERING

This dissertation was presented

by

Madeline Claire Cramer

It was defended on

January 26, 2022

and approved by

Frederick J. Schoen, MD, PhD, Professor
Department of Pathology, Brigham and Women's Hospital and Harvard Medical School

Sanjeev G. Shroff, PhD, Distinguished Professor and Chair
Department of Bioengineering

Heth R. Turnquist, PhD, Associate Professor
Departments of Surgery and Immunology

William Wagner, PhD, Distinguished Professor
Departments of Surgery, Chemical Engineering and Bioengineering

Justin S. Weinbaum, PhD, Assistant Professor
Departments of Bioengineering and Pathology

Dissertation Director: Stephen F. Badylak, DVM, PhD, MD, Professor
Departments of Surgery and Bioengineering

Copyright © by Madeline Claire Cramer

2022

The Influence of Matrix Bound Nanovesicles on Inflammation-Driven Prosthetic Heart Valve Failure

Madeline Claire Cramer, PhD

University of Pittsburgh, 2022

Bioprosthetic tissue valves consisting of glutaraldehyde-fixed bovine pericardium (gluBP) are the standard of care for aortic valve replacement. However, failure of bioprosthetic tissue valves typically occurs after 10-15 years due to structural valve degeneration (SVD), a gradual process of stenosis or regurgitation resulting from calcification, fibrotic tissue deposition, or cusp tearing. The mechanisms are not fully understood, but macrophage-driven inflammation is thought to contribute to the pathologic remodeling of SVD.

Extracellular matrix (ECM) bioscaffolds promote an anti-inflammatory macrophage phenotype and facilitate a constructive remodeling outcome in multiple clinical applications. Extracellular vesicles embedded within the ECM, termed matrix bound nanovesicles (MBV), and their associated lipid, miRNA and protein cargo have recently been shown to recapitulate anti-inflammatory effects in macrophages. Alteration of the MBV intraluminal cargo can have dramatic implications on their bioactivity. More specifically, elimination of the cytokine interleukin-33 (IL-33) within MBV negates their anti-inflammatory effects.

The present dissertation first expands our current understanding of MBV and then evaluates the therapeutic potential of MBV in altering cellular processes associated with SVD of bioprosthetic valves, including macrophage activation, fibrosis, and calcification, both *in vitro* and *in vivo*. The contribution of IL-33 cargo to MBV-mediated effects are also examined. Results show that MBV are a distinct subpopulation of extracellular vesicle with lipid, protein, and miRNA

composition that changes with cell source and disease progression. The anti-inflammatory effects induced by MBV in macrophages is dependent on the repertoire of genes regulated by IL-33 cargo independently of its canonical receptor. MBV direct phenotypical changes in fibroblast activation and mineralization primarily through indirect, macrophage-mediated effects. In a rodent subcutaneous implant model, systemic administration of MBV containing IL-33 cargo shifted the host inflammatory response to a gluBP implant toward an anti-inflammatory phenotype but did not significantly impact the calcification response. These results signify the importance of the MBV cargo protein IL-33 in eliciting an anti-inflammatory phenotype in macrophages and provides guidance for the designing of next generation biomaterials and tissue engineering strategies.

Table of Contents

| | |
|---|-----------|
| Preface..... | xiv |
| Table of Abbreviations | xvi |
| 1.0 Biomaterial Approaches to Aortic Valve Replacement..... | 1 |
| 1.1 Clinical Significance of Aortic Valve Failure..... | 1 |
| 1.2 Current Standard of Care for Aortic Valve Replacements..... | 2 |
| 1.3 Mechanisms of Failure of Bioprosthetic Heart Valves | 4 |
| 2.0 Extracellular Matrix Bioscaffolds and Their Influence on Cell Behavior..... | 7 |
| 2.1 Immune Response to Implantation of ECM Scaffolds..... | 9 |
| 2.2 Factors that Affect the Immune Response to ECM-Based Biomaterials | 13 |
| 2.3 Matrix Bound Nanovesicles Recapitulate Anti-Inflammatory Effects..... | 15 |
| 3.0 Significance..... | 16 |
| 4.0 Central Hypothesis and Specific Aims..... | 18 |
| 4.1 Central Hypothesis | 18 |
| 4.2 Specific Aims..... | 18 |
| 4.2.1 Specific Aim 1 | 18 |
| 4.2.2 Specific Aim 2 | 19 |
| 4.2.3 Specific Aim 3..... | 20 |
| 5.0 Matrix Bound Nanovesicles Represent a Distinct Subset of Extracellular Vesicle | 21 |
| 5.1 Introduction | 21 |
| 5.2 Materials and Methods | 23 |
| 5.2.1 Overview of Experimental Design | 23 |

| | |
|--|----|
| 5.2.1 Source of Vesicle Subtypes | 23 |
| 5.2.2 Isolation of Vesicles | 26 |
| 5.2.3 Transmission Electron Microscopy | 27 |
| 5.2.4 Nanoparticle Tracking Analysis | 27 |
| 5.2.5 RNA Isolation and miRNA-Sequencing..... | 27 |
| 5.2.6 Characterization of Vesicle Proteins | 28 |
| 5.2.7 Lipidomic Analysis of Phospholipids | 29 |
| 5.2.8 Statistical Analysis | 29 |
| 5.3 Results..... | 30 |
| 5.3.1 MBV are Distinct from Exosomes and Calcifying Matrix Vesicles..... | 30 |
| 5.3.1.1 Vesicles Have Similar Physical Characteristics | 30 |
| 5.3.1.2 Vesicles Have Unique Protein Signatures..... | 30 |
| 5.3.1.3 Vesicles Have Distinctive Lipid Composition..... | 33 |
| 5.3.1.4 Vesicle Subtypes Have Distinct miRNA Cargo..... | 35 |
| 5.3.2 MBV are Distinct from Exosomes of a Given Cell Type | 37 |
| 5.3.2.1 3T3-derived MBV and Liquid-Phase Exo Have Similar Sizes | 37 |
| 5.3.2.2 3T3-derived MBV and Exosomes Have Unique Protein Markers | 37 |
| 5.3.2.3 3T3-derived MBV and Exosomes Have Unique Lipid Composition | 38 |
| 5.3.2.4 3T3-derived MBV and Exosomes Have Unique Lipid Composition | 40 |
| 5.3.2.5 3T3-derived MBV and Exosomes Have Unique miRNA Cargo..... | 41 |
| 5.3.1 MBV Vary with Cell Source..... | 43 |
| 5.3.1.1 Cell Source Does Not Affect MBV Size..... | 43 |
| 5.3.1.2 MBV miRNA Cargo Varies with Cell Source..... | 44 |

| | |
|---|-----------|
| 5.3.2 MBV Change with Disease | 46 |
| 5.3.2.1 MBV Size and Abundance are Similar with Heart Disease..... | 46 |
| 5.3.2.2 MBV Protein Cargo Changes with Disease..... | 46 |
| 5.3.2.3 MBV miRNA Cargo Changes with Disease | 49 |
| 5.4 Discussion | 51 |
| 6.0 The Influence of Matrix Bound Nanovesicle Associated Interleukin-33 On | |
| Macrophage Phenotype, Fibrosis and Osteogenesis | 58 |
| 6.1 Introduction | 58 |
| 6.2 Methods | 60 |
| 6.2.1 Overview of Experimental Design | 60 |
| 6.2.2 Animals | 62 |
| 6.2.3 Isolation of MBV | 62 |
| 6.2.4 Isolation and Stimulation of Bone Marrow-derived Macrophages..... | 63 |
| 6.2.5 RNA Isolation | 64 |
| 6.2.6 RNA-Sequencing and Bioinformatic Analysis | 64 |
| 6.2.7 qPCR Validation | 65 |
| 6.2.8 Evaluation of MBV Effect on Inflammatory Macrophages..... | 65 |
| 6.2.9 Immunolabeling of Stimulated Macrophages | 66 |
| 6.2.10 Characterization of Fibroblast to Myofibroblast Transition..... | 67 |
| 6.2.11 Characterization of Osteogenic Differentiation of Fibroblasts..... | 68 |
| 6.2.12 Statistical Analysis | 69 |
| 6.3 Results..... | 69 |
| 6.3.1 MBV are Internalized by Macrophages and Deliver IL-33 to the Nucleus.. | 69 |

| | |
|--|-----|
| 6.3.2 MBV Alter Gene Expression in Macrophages Independently of ST2 Receptor | 71 |
| 6.3.3 IL-33 Cargo within MBV Differentially Regulates Gene Expression in Macrophages..... | 73 |
| 6.3.4 MBV-associated IL-33 Regulates Pathways of the Inflammatory Response | 77 |
| 6.3.5 IL-33 ⁺ MBV can Alleviate and Prevent Pro-inflammatory Activation of Macrophages..... | 79 |
| 6.3.6 MBV-Induced Macrophage Secretome Limits Myofibroblast Activation ... | 81 |
| 6.3.7 MBV Directly and Indirectly Modulate Osteogenic Differentiation | 84 |
| 6.4 Discussion | 90 |
| 7.0 MBV Modulate Host Response to Implanted Bioprosthetic Tissue Valve | 97 |
| 7.1 Introduction | 97 |
| 7.2 Materials and Methods | 98 |
| 7.2.1 Overview of Experimental Design | 98 |
| 7.2.2 Preparation of gluBP | 99 |
| 7.2.3 Dorsal Subcutaneous Implantation in Rats | 100 |
| 7.2.4 Intravenous Injection of MBV | 100 |
| 7.2.5 Histologic Evaluation | 101 |
| 7.2.6 Evaluation of Macrophage Phenotype | 101 |
| 7.2.7 Radiographic Analysis | 102 |
| 7.2.8 Quantification of Calcium Content within gluBP Implants..... | 103 |
| 7.2.9 Statistical Analysis | 103 |

| | |
|---|------------|
| 7.3 Results..... | 103 |
| 7.3.1 Cellular Infiltration..... | 103 |
| 7.3.2 Neovascularization | 106 |
| 7.3.3 Macrophage Phenotype | 107 |
| 7.3.4 Susceptibility to Calcification..... | 109 |
| 7.4 Discussion | 112 |
| 8.0 Dissertation Summary | 115 |
| 8.1 Major Findings | 116 |
| 8.2 Overall Conclusions..... | 118 |
| Bibliography | 120 |

List of Tables

| | |
|--|-----------|
| Table 1. Commercially available ECM bioscaffolds..... | 8 |
| Table 2. Summary of experimental design for Specific Aim 1. | 24 |
| Table 3. Patient characteristics of human left ventricle tissue samples..... | 26 |
| Table 4. miRNA name, fold change, and p-value for a subset of the top differentially expressed miRNA..... | 50 |
| Table 5. Number of differentially expressed genes (DEGs) with $p < 0.05$ between each treatment group. | 73 |
| Table 6. Top regulated genes are associated with anti-inflammatory activation of macrophages..... | 76 |

List of Figures

| | |
|--|-----------|
| Figure 1. cMV, Exo and MBV have similar physical characteristics. | 31 |
| Figure 2. cMV, Exo and MBV have distinct vesicle-associated proteins. | 32 |
| Figure 3. Lipid composition of cMV and Exo are distinct from MBV. | 34 |
| Figure 4. miRNA cargo of cMV, Exo, and MBV are distinct. | 36 |
| Figure 5. MBV and liquid-phase EV from 3T3 cells have similar physical characteristics. | 38 |
| Figure 6. MBV and liquid-phase EV from 3T3 cells have unique protein markers. | 39 |
| Figure 7. Lipidomic analysis reveals distinct lipid composition of 3T3 cells, MBV and liquid-phase EV. | 41 |
| Figure 8. miRNA cargo is selectively packaged into liquid-phase EV and MBV. | 42 |
| Figure 9. MBV from unique cellular origins are similar in size. | 43 |
| Figure 10. MBV miRNA content varies with cell source. | 45 |
| Figure 11. MBV size and abundance are similar with heart disease. | 47 |
| Figure 12. MBV protein cargo changes with disease state. | 48 |
| Figure 13. miRNA cargo of MBV changes with disease state. | 49 |
| Figure 14. Top pathways regulated by healthy vs. failing MBV miRNA cargo. | 51 |
| Figure 15. Schematic overview of experiments to evaluate direct and indirect effects of MBV on pathologic processes. | 61 |
| Figure 16. Schematic overview of experiments to characterize MBV effect on inflammatory macrophages. | 66 |
| Figure 17. Schematic overview of experiments to evaluate myofibroblast activation. | 67 |
| Figure 18. Schematic overview of experiments to evaluate MBV effects on osteogenesis. .. | 68 |

| | |
|---|------------|
| Figure 19. IL-33 translocates to the nucleus after uptake into macrophages. | 70 |
| Figure 20. MBV IL-33-induced gene expression in macrophages is independent of ST2 receptor. | 72 |
| Figure 21. IL-33 content differentially regulates gene expression in macrophages. | 74 |
| Figure 22. Top pathways regulated by MBV-associated IL-33 are related to the inflammatory response. | 78 |
| Figure 23. MBV containing IL-33 alleviate a pro-inflammatory macrophage phenotype. . | 79 |
| Figure 24. MBV containing IL-33 can prevent pro-inflammatory macrophage activation. | 80 |
| Figure 25. Direct exposure to MBV does not affect myofibroblast activation. | 82 |
| Figure 26. Macrophage secretome induced by WT MBV prevents myofibroblast activation. | 83 |
| Figure 27. Direct effect of MBV on osteogenesis..... | 85 |
| Figure 28. Dose response of direct MBV effects on osteogenesis..... | 87 |
| Figure 29. Indirect effect of MBV-induced macrophage secretome on osteogenesis. | 89 |
| Figure 30. Overview of experimental design for Specific Aim 3. | 99 |
| Figure 31. Cellular response to gluBP implantation. | 105 |
| Figure 32. Endothelial cell and neovascularization response to gluBP..... | 106 |
| Figure 33. Macrophage response to gluBP..... | 108 |
| Figure 34. Histologic assessment of calcification. | 109 |
| Figure 35. Radiographic assessment of calcification. | 110 |
| Figure 36. Calcium content of gluBP samples..... | 111 |
| Figure 37. Schematic summary of MBV effects on cellular processes..... | 119 |

Preface

First and foremost, I would like to thank my thesis advisor and mentor Dr. Badylak. I am forever grateful for the opportunity to work in his laboratory. His patience and encouragement was persistent, even when it seemed like nothing was going my way. I am confident that the quality of training and breadth of experiences that I have received along this path could not have been achieved in any other lab. Dr. Badylak's own unique career path and strong focus on translational research have shaped my perspective as a scientist and guided my vision for the future.

I want to thank my entire advisory committee for their invaluable insights, feedback, and encouragement along the way. Thank you, Dr. Frederick Schoen, Dr. Sanjeev Shroff, Dr. Heth Turnquist, Dr. William Wagner and Dr. Justin Weinbaum for your time and support. I would like to express additional gratitude to Dr. Frederick Schoen and Dr. Heth Turnquist who have been important collaborators throughout much of my work.

Thank you to the numerous former and current Badylak lab members for their help during my academic journey. Each and every person made coming to the lab every day enjoyable. Dr. Neill Turner, Dr. Li Zhang, Scott Johnson, and Janet Reing have been a source immense knowledge and patience- the lab would not be able to function without them. Thank you to Dr. Brian Sicari, Dr. Luai Huleihel, Dr. George Hussey, Dr. Lisa White, Dr. Michelle Scarritt, Dr. Juan Diego Naranjo, Dr. Jonas Erikson, Dr. Anjani Ravindra, Dr. Nazia Mehrban, Dr. William D'Angelo, Dr. Arthi Shridhar, Dr. Hector Capella Monsonis, Dr. Marley Dewey, Dr. Remya Kommeri, Jordan Chang, David Nascari, Salma El-Mossier, and Kelsey Hall for their mentorship, guidance and friendship. My fellow graduate students over the years, Dr. Jenna Dziki, Dr. Lindsey Saldin, Dr. Catalina Pineda Molina, Dr. Lina Quijano Luque, Dr. Yoojin Lee, Dr. Joseph

Bartolacci, Dr. Mark Murdock, Raphael Crum, and Gabrielle Lorenz have made each day more enjoyable. I would not have survived the hardest parts of this journey without their friendship.

I also want to thank all the current and former administrators for keeping us organized. The work of Rachel Thomas, Emily Henderson, Nicole Wenturine, Tynneal Grant, Hadley Pratt, Emily Staysich, and Jocelyn Runyon has been imperative to the success of every single lab member.

During my time in the laboratory, I have had the opportunity to mentor many undergraduate and rotational students. Thank you, Dr. Neil Khurana, Brian Kolich, Eric Sobieski, Devin Vo, Alvin Liu, Paula Sarmiento Huertas, Lucille Marchal, Ethan Paules, Anisha Verma, and Anika Kulkarni for your help and for teaching me to be a better mentor.

I am grateful for the financial support and training opportunities that have been provided by the Cardiovascular Bioengineering Training Program and the National Institutes of Health F31 fellowship. This work would not have been possible without them.

This dissertation is dedicated to all of my family and friends, but especially my parents Blake and Nancy Cramer. Your unconditional love and encouragement have kept me going over the years. I thank you for always making sure I am happy, safe, and healthy, and most importantly ensuring that I am always doing something that I love. Your excitement and pride over some of the seemingly smallest accomplishments have kept me motivated and reminded me of how exciting science really can be. I am forever grateful for your patience with me during some of the most stressful years of my life.

Finally, thank you to my love, Nicholas Dulac. I could not have done this without you. You make even the most stressful days better and have been my source of comfort, encouragement, commiseration, and distraction at all the right times. Nick, thank you for loving me through all the ups and downs. I can't wait to see what the future holds for us.

Table of Abbreviations

| Abbreviation | Definition |
|--------------------------------|--|
| gluBP | Glutaraldehyde-fixed bovine pericardium |
| SVD | Structural valve degeneration |
| ECM | Extracellular matrix |
| MBV | Matrix bound nanovesicles |
| IL | Interleukin |
| AVD | Aortic valve disease |
| CAVD | Calcific aortic valve disease |
| BHV | Bioprosthetic tissue valve |
| TAVI | Transcatheter valve implantation |
| TEHV | Tissue engineered heart valve |
| ETR | Endogenous tissue restoration |
| TGF-β | Transforming growth factor-beta |
| αSMA | Alpha smooth muscle actin |
| TNFα | Tumor necrosis factor alpha |
| ALP | Alkaline phosphatase |
| Tregs | Regulatory T cells |
| IV | Intravenous |
| EV | Extracellular vesicles |
| TNAP | Tissue non-specific alkaline phosphatase |
| cMV | Calcifying matrix vesicles |
| Exo | Exosomes |
| DMEM | Dulbecco's modified Eagle's medium |
| PBS | Phosphate buffered saline |
| BMSC | Bone marrow-derived stem cell |
| ASC | Adipose stem cell |
| UCSC | Umbilical cord stem cell |
| α-MEM | α -minimum essential medium |
| FBS | Fetal bovine serum |
| TEM | Transmission electron microscopy |
| cDNA | Complementary DNA |
| ANOVA | Analysis of variance |
| SEM | Standard error of the mean |
| PCA | Principal component analysis |
| EGF | Epidermal growth factor |
| LPL | Lysophospholipid |
| PC | Phosphatidylcholine |
| PE | Phosphatidylethanolamine |
| PG | Phosphatidylglycerol |

| | |
|----------------|--|
| PI | Phosphatidylinositol |
| PS | Phosphatidylserine |
| SL | Sphingolipid |
| LPC | Lysophosphatidylcholine |
| LPE | Lysophosphatidylethanolamine |
| LPG | Lysophosphatidylglycerol |
| NTA | Nanoparticle tracking analysis |
| LC-MS | Liquid chromatography-mass spectrometry |
| BMP | Bis-monoacylglycerophosphate |
| CL | Cardiolipin |
| PA | Phosphatidic acid |
| SM | Sphingomyelin |
| LPS | Lysophosphatidylserine |
| LPI | Lysophosphoinositol |
| LPA | Lysophosphatidic acid |
| mCL | Monolysocardiolipin |
| IPA | Ingenuity Pathway Analysis |
| ST2 | Stimulation-2 |
| WT | Wildtype |
| BMDM | Bone marrow-derived macrophages |
| MCSF | Macrophage colony stimulating factor |
| rIL-33 | Recombinant interleukin-33 |
| DAPI | 4'6-diamidino-2-phenylindole |
| OS | Osteogenic supplements |
| DEG | Differentially expressed gene |
| H&E | Hematoxylin and eosin |
| CT | Computed tomography |
| ICP-MS | Inductively-coupled plasma mass spectrometry |
| sST2 | Soluble stimulation-2 |

1.0 Biomaterial Approaches to Aortic Valve Replacement¹

1.1 Clinical Significance of Aortic Valve Failure

Over 100 million people worldwide are affected by valvular heart disease [1] and an estimated 6.4% of people 65 years or older have undiagnosed moderate to severe valvular heart disease [2,3]. Aortic valve disease (AVD) accounts for almost 50% of all valvular conditions and is caused by aortic valve stenosis, regurgitation, or a combination of both [4]. Aortic stenosis is the most common AVD diagnosis and is primarily caused by congenital defects in children and young adults or calcific aortic valve disease (CAVD) in the aging population. In an Italian study, an estimated 0.5% of primary school students had a bicuspid aortic valve, a congenital defect that is the most common cause of aortic stenosis in young adults [5]. The prevalence of aortic stenosis is approximately 4.3% in patients over 70 years old and is expected to double by 2040 and triple by 2060 [3,6].

There are currently no therapeutic modalities available to slow or prevent progression valvular disease, therefore implantation of a prosthetic aortic valve remains the standard of care for severe AVD. In developed countries, CAVD resulting in aortic stenosis is the main indication for aortic valve replacement [1]. Surgical placement of a mechanical or bioprosthetic tissue valve (BHV) was the standard for more than six decades, however since 2002 transcatheter valve implantation (TAVI) has become more prominent [7]. In the United States, the number of TAVI

¹ Excerpts of this chapter have been adapted from the following publication:

M.C. Cramer, J. Chang, M. Cox, H. Li, A. Serrero, M. El-Kurdi, F.J. Schoen, S.F. Badylak, Tissue response, macrophage phenotype, and intrinsic calcification induced by cardiovascular biomaterials: Can clinical regenerative potential be predicted in a rat subcutaneous implant model?, *J Biomed Mater Res Part A*. (2021) 1–12.

procedures exceeded the number of open surgical replacements (72,991 vs. 57,626) as of 2019 and the predominance of TAVI is expected to increase as the FDA approved TAVI for low-risk patients in 2019 [7,8].

1.2 Current Standard of Care for Aortic Valve Replacements

Currently available prosthetic heart valves are broadly characterized into mechanical or bioprosthetic tissue valves (BHV) based on the composition of the leaflet. Mechanical valves are composed of materials such as titanium or carbon and generally fall under one of three basic designs: ball-in-cage, bileaflet, or single tilting disc [9]. Mechanical valves offer improved long-term durability over BHV, however they carry a high risk of thromboembolic complications for which patients require lifelong anticoagulation therapy. Improved hemocompatibility of BHV and the ability to deliver them minimally invasively with TAVI technology has led to their more frequent use, accounting for approximately 80% of all aortic valve replacements [7,10,11]. Most BHV are xenogeneic in origin, though autografts and homografts are occasionally used in clinical practice [12].

Clinically used xenogeneic BHV typically consist of porcine aortic valve or bovine pericardium that has been crosslinked with glutaraldehyde. Glutaraldehyde fixation serves to enhance the durability of the graft by mitigating collagen denaturation and to alleviate immunogenicity by masking xenogeneic antigens [11]. Commercially available BHV are further processed with anti-calcification treatments such as α -amino-oleic-acid (e.g. Medtronic's MosaicTM, AVALUSTM, and FreestyleTM), ethanol (e.g. Abbott TrifectaTM GT), or surfactants (e.g. Medtronic HancockTM II) to extend the lifetime of the device [13–17]. Despite improved

technologies throughout the years, commercial BHV are still susceptible to multiple modes of failure that limit their efficacy to 10 - 15 years [11,18]. These mechanisms of failure will be discussed in more detail below.

A wide range of strategies are being explored at the pre-clinical level in an effort to improve long-term outcomes associated with BHV. These methods include, but are certainly not limited to, using alternative non-glutaraldehyde crosslinkers (e.g. epoxy compounds, genipin, tannic acid, and carbodiimide) [19–23], decellularizing the source tissue [24,25], and genetically modifying donor animals to eliminate xenoantigens (e.g. α -Gal and NeuGc) [12,26–28].

The creation of tissue engineered heart valves (TEHV) has been proposed as an alternative to the use of mechanical and BHV [29,30]. The classical approach to creating TEHV involves *in vitro* seeding of cells onto a degradable scaffold in a bioreactor [31–33]. While some early studies have shown promise, poor long-term pre-clinical results, high manufacturing costs, and complex regulatory hurdles have hindered clinical translation [34–36]. An emerging strategy that addresses many of the limitations of both BHV and *in vitro* seeded TEHV is *in situ* bioengineering or Endogenous Tissue Restoration (ETR) in which an acellular restorative device is implanted into the body, becomes gradually infiltrated by host cells, and remodels over time [34]. Various materials have been investigated as a template for ETR including decellularized matrices from donor valves [37–41], small intestinal submucosa [42,43] or *in vitro* engineered ECM [32,44–46], and synthetic bioabsorbable polymers [36,44,47–50]. Though ETR-based scaffolds have not yet reached the clinic for aortic valve replacement, an electrospun supramolecular polymer graft produced by Xeltis (Eindhoven, The Netherlands) has shown promise in early pre-clinical application as an aortic valve [51], and in pediatric clinical studies as an extracardiac conduit [52] and as a pulmonary valved conduit for RVOT reconstruction [53].

1.3 Mechanisms of Failure of Bioprosthetic Heart Valves

Clinical failure of BHV can occur by various mechanisms that are commonly classified as thrombosis, endocarditis, nonstructural dysfunction and structural dysfunction [54]. Thrombosis and infective endocarditis generally occur in the acute phase and are affected by patient and procedural factors [4,55]. Nonstructural dysfunction is considered as alterations that are not intrinsic to the prosthetic valve itself such as pannus formation, suture entrapment and perivalvular leak. Pannus is a form of valve degeneration in which host tissue grows onto the BHV and can contribute to valve stenosis by limiting leaflet movement. Pannus formation is stimulated by the minor thrombus and inflammation that results from surgical implantation of the valve. The pannus tissue is composed of a heterogeneous cell population that includes endothelial cells, myofibroblasts, and various immune cells, including macrophages [56,57]. The mechanisms of pannus overgrowth are not well studied, but likely involve transforming growth factor-beta (TGF- β) signaling which induces myofibroblast activation and excessive extracellular matrix deposition [12]. Teshima *et al.* showed abundant infiltration of macrophages expressing high levels of TGF- β and TGF- β receptor 1, and alpha smooth muscle actin (α SMA) positive myofibroblasts expressing TGF- β receptor 1 within the pannus of explanted BHV, potentially indicating a role of intercellular cross-talk in the pathologic fibrosis [57].

Structural dysfunction, or structural valve degeneration (SVD), is classified as permanent intrinsic changes of the BHV, such as calcification or cusp tearing, that cause hemodynamic or clinical failure. Calcification is the primary contributor to SVD and is the most important pathology limiting the long-term success of heart valve replacement with BHV [18,58]. Calcification of BHV is a complex and incompletely understood process that is thought to involve

both passive and cell-mediated processes that are regulated by three primary factors: (1) biological factors (local environment of function and recipient's metabolic state); (2) biomaterial factors (structure and chemistry of the substrate biomaterial); and (3) biomechanical factors (degree and locations of stress and strain) [11,17,18,59]. Both intrinsic and extrinsic mineralization of a biomaterial are generally enhanced at the sites of intense mechanical stress [58,60], however the mechanism of stress-induced calcification is not fully understood. Pre-treatment with glutaraldehyde is considered an important biomaterial factor for passive calcification of bioprosthetic tissue [61,62]. Passive calcification results from calcium binding to negatively charged phospholipids within the scaffold which can be accelerated by release of cellular debris induced by cytotoxic free aldehyde groups [63,64].

The role of host cells in calcification of biomaterials is uncertain [65]. However, multiple studies have associated increased macrophage infiltration to calcification of BHV [66] and native aortic valves [67,68], clinically significant processes with likely distinctly different mechanisms. Li *et al.* observed significantly more pro-inflammatory (M1-like) macrophages and higher expression of tumor necrosis factor alpha (TNF α) in calcified native aortic valves compared to noncalcified valves [67]. Pro-inflammatory cytokines produced by M1-like macrophages, such as TNF α , promote calcification of valvular interstitial cells *in vitro* through increased nuclear factor kappa B activation, bone morphogenetic protein 2 expression, and alkaline phosphatase (ALP) activity [69,70]. Conversely, it is hypothesized that anti-inflammatory M2-like macrophages are protective against calcification by synthesizing increased inorganic pyrophosphate, a direct inhibitor of calcium phosphate deposition, and downregulating ALP expression [71].

Despite studies correlating macrophage phenotype to calcific responses, the contribution of macrophages to clinical SVD remains controversial in the field. Proponents for the relevance of inflammatory processes in SVD cite the presence of antibodies against xenogeneic valve components and brisk mononuclear cell inflammation within some failed BHV [72–74]. On the other hand, areas of valve calcification are frequently not associated with inflammation and calcification still occurs with similar severity in the absence of interaction with immune cells [75,76]. It is likely that inflammatory processes are a primary contributor to SVD in only a small proportion of patients. Nevertheless, understanding the potential impact of the pro-inflammatory response to BHV is increasingly becoming an area of interest [77–80].

2.0 Extracellular Matrix Bioscaffolds and Their Influence on Cell Behavior²

Biologic materials composed of mammalian extracellular matrix (ECM) have been effectively used for the repair and reconstruction of a variety of tissues, including skeletal muscle [81–84], esophagus [85–88], tendon [89–93], lower urinary tract [94–98], and heart [99–104], among others [105–108] in both preclinical animal studies and human clinical studies. These studies have largely shown constructive, functional tissue remodeling with the partial restoration of site appropriate tissue [109]. This deviation from the default tissue injury response of inflammation and scar tissue formation is consistently associated with modulation of the host innate and adaptive immune response [110–114] and the recruitment and differentiation of endogenous stem cells [114–116]. However, not all studies in which ECM-based materials have been used report this type of constructive healing response [117,118]. Alternative and less favorable outcomes include serous fluid accumulation at the implant site, rapid degradation of the material with associated mechanical failure in load bearing sites, or a lack of biomaterial degradation and an associated foreign body response [117–122]. These alternative outcomes have typically been associated with variations in manufacturing methods and/or source tissues. A partial list of commercially available ECM bioscaffolds is provided in Table 1 to show the variability of source materials and approved clinical indications. The present chapter provides an overview of the immune response to appropriately prepared ECM bioscaffolds and the effects of production methods upon the quality of the cellular response.

² Portions of this chapter have been adapted from the following publication:
M.C. Cramer, S.F. Badylak, Extracellular matrix-based biomaterials and their influence upon cell behavior, *Ann. Biomed. Eng.* 48 (2020) 2132–2153.

Table 1. Commercially available ECM bioscaffolds.

Source tissue, application focus and post-decellularization processing steps of common commercially available ECM bioscaffolds.

| Product | Manufacturer | Source Tissue | Application Focus | Form | Crosslinking Agent | Terminal Sterilization |
|-------------------------|--------------------|-------------------------|-------------------------|----------|--------------------|------------------------|
| AlloDerm RTM | BioHorizons | Human dermis | Soft tissue, dentistry | Dry | --- | --- |
| AlloMax | BD Bard | Human dermis | Soft tissue | Dry | --- | Gamma |
| AlloPatch HD | ConMed | Human dermis | Tendon | Dry | --- | --- |
| Avalus | Medtronic | Bovine pericardium | Valve replacement | Hydrated | Glu | Liquid Chemical |
| Biodesign Hernia Graft | Cook Biotech | Porcine small intestine | Soft tissue | Dry | --- | EtO |
| CardioCel | Admedus | Bovine pericardium | Cardiac tissue | Dry | Glu | Propylene Oxide |
| DermaSpan | Zimmer Biomet | Human dermis | Soft tissue, tendon | Dry | --- | Gamma |
| FlexHD Pliable | Mentor | Human dermis | Breast | Hydrated | --- | --- |
| Fortiva | RTI Surgical | Porcine dermis | Soft tissue | Hydrated | --- | Gamma |
| Freestyle | Medtronic | Porcine heart valve | Valve replacement | Hydrated | Glu | Liquid Chemical |
| Gentrix Surgical Matrix | Acell | Porcine urinary bladder | Soft tissue | 6 Layer | --- | E-beam |
| GraftJacket | Wright Medical | Human dermis | Soft tissue | Dry | --- | --- |
| Grafton DBM | Medtronic | Human bone | Bone | Powder | --- | --- |
| InteguPly | Aziyo Biologicals | Human dermis | Soft tissue, wound care | Dry | --- | Gamma |
| Meso BioMatrix | DSM | Porcine mesothelium | Soft tissue | Dry | --- | EtO |
| MicroMatrix | Acell | Porcine urinary bladder | Wound care | Powder | --- | E-beam |
| Miroderm | Reprise Biomedical | Porcine liver | Soft tissue | Hydrated | --- | E-beam |
| Oasis Ultra | Cook Biotech | Porcine small intestine | Wound care | 3 Layer | --- | EtO |
| Peri-Guard Repair Patch | Baxter | Bovine pericardium | Soft tissue | Hydrated | Glu | Liquid Chemical |
| Permacol | Medtronic | Porcine dermis | Soft tissue | Hydrated | HMDI | Gamma |
| ProLayer | Stryker | Human dermis | Soft tissue | Hydrated | --- | E-beam |
| Strattice | LifeCell Corp. | Porcine dermis | Soft tissue | Hydrated | --- | E-beam |
| Trifecta | Abbott | Bovine pericardium | Valve replacement | Hydrated | Glu | Liquid Chemical |
| TutoPatch | RTI Surgical | Bovine pericardium | Soft tissue | Dry | --- | Gamma |
| Tutoplast Pericardium | Coloplast | Human pericardium | Soft tissue | Dry | --- | Gamma |
| VentriGel* | Ventrix | Porcine ventricle | Cardiac tissue | Hydrogel | --- | --- |
| XenMatrix | BD Bard | Porcine dermis | Soft tissue | Hydrated | --- | E-beam |

2.1 Immune Response to Implantation of ECM Scaffolds

As described in detail below, there are many factors that contribute to the overall quality of an ECM bioscaffold and each of these can affect the host response to the material. The seemingly endless variables involved in producing an ECM scaffold and the wide range of clinical applications make the definition of an “ideal” ECM bioscaffold impossible. However, when close attention is given to the variables known to affect the host response the chance for a favorable outcome can be maximized.

The term “constructive remodeling” has been used to describe the *in vivo* events that occur following implantation of a thoroughly decellularized, sterile ECM bioscaffold [81,82,84,85,109,112]. Constructive remodeling is characterized by degradation and gradual replacement of the bioscaffold with site appropriate functional tissue. This type of *in vivo* response is in stark contrast to the default response to an implanted biomaterial that is associated with a pro-inflammatory environment and the deposition of dense scar tissue.

As stated above, the remodeling outcomes following ECM bioscaffold implantation have not always been constructive [117–122]. A mild or intense inflammatory response and/or a serous fluid accumulation have occurred with associated scar tissue formation as occurs with the default wound healing response. Such results are commonly associated with ECM-based products that have significant cell remnants, residual chemicals from disinfection and decellularization processes, or the use of chemical crosslinking methods that alter structural and functional protein constituents and that inhibit or delay degradation of the scaffold [111,112,123–125].

Though the specific mechanisms by which ECM bioscaffolds promote positive constructive tissue remodeling are not fully understood, the following processes are consistently associated with such outcomes: 1) degradation of the ECM bioscaffold to release bioactive

signaling molecules [126–128], 2) modulation of the host immune response toward a pro-remodeling and regulatory type 2 phenotype [110–114], and 3) recruitment and differentiation of endogenous stem/progenitor cells [115,116,129]. The potential favorable response of immune cells to ECM bioscaffolds is described in detail below.

Implantation of any material, including ECM scaffolds, is associated with the immediate adsorption of proteins to the surface. Competitive protein exchange results in a dynamic mixture of adsorbed proteins (Vroman effect) [130]. At early time points the composition is dominated by high concentration proteins that are eventually displaced by proteins with a higher affinity for the implanted material. Protein adsorption is followed by activation of the innate immune response, including dendritic cells, neutrophils and macrophages [131,132]. The adaptive immune system consisting of lymphocytes (B and T cells) may also be indirectly stimulated depending on the type of biomaterial [133,134]. Both macrophages and T helper cells can assume diverse phenotypes that are characterized by their gene and protein expression profiles, and associated functions. In simplified terms, a pro-inflammatory (Type I) phenotype of macrophages and T helper cells is associated with expression of cytotoxic signaling molecules, and a pro-healing and regulatory (Type 2) phenotype is associated with anti-inflammatory and regulatory signaling molecules [135–140]. ECM-based biomaterials that are devoid of cellular material, retain the ultrastructure and bioactive components of the native ECM, and that can be readily degraded by infiltrating host cells have been repeatedly shown to stimulate a strong pro-healing phenotype of both the adaptive and innate immune systems [110–114].

A seminal study by Allman et al. in 2001 showed that there is a robust host immune response to implanted ECM bioscaffolds with activation of T helper cells to a “Th2” phenotype. Implantation of porcine-derived ECM in a murine host elicited production of anti-inflammatory

cytokines, including interleukin (IL)-4 and IL-10, and noncomplement fixing IgG1 antibody isotype. Both of these responses were consistent with recognition of the presence of the biomaterial, acceptance of the decellularized xenogeneic scaffold, and lack of an adverse immune response. The constructive remodeling response to the scaffold was reported as T cell independent in this model although macrophage participation and macrophage phenotype were not examined [141]. Importantly, the strong Th2 response induced by ECM scaffolds was maintained following a secondary exposure to the scaffold [141] and therefore was not associated with an adverse sensitization phenomenon. The same group subsequently showed that ECM bioscaffold implantation did not cause generalized immune suppression, did not impair the antibody-mediated immune response to viral or bacterial infection, and did not impair the cell-mediated immune response to contact or xenogeneic skin graft rejection [110].

In 2009 Valentin et al. showed that ECM bioscaffolds induce a favorable host innate immune response, specifically the macrophage phenotype component of the innate response. This macrophage response was not only sufficient, but was required, for constructive remodeling of the scaffold [128]. Further, the early macrophage phenotypic profile induced by degradation of an ECM bioscaffold *in vivo* was predictive of downstream remodeling responses [111]. That is, increased infiltration of M2-like CD206⁺ macrophages and higher ratios of M2:M1 macrophages within the implantation site at 14 days were associated with more positive remodeling outcomes [111]. Macrophages exposed to the degradation products of ECM bioscaffolds can directly activate macrophages towards an anti-inflammatory “M2-like” (iNOS⁻/Fizz1⁺) phenotype [142,143]. The ECM-induced macrophage phenotype has been extensively characterized and is broadly associated with upregulation of anti-inflammatory genes and proteins [129,144,145], downregulation or suppression of pro-inflammatory genes and proteins [146,147], high antigen presenting

capabilities [148] and presence of damage associated molecular patterns (DAMPs) [149]. Increased presence of DAMPs is hypothesized to contribute to a constructive wound healing response by amplifying endogenous wound-associated signaling pathways [149].

The macrophage phenotype induced by ECM bioscaffolds is complex and varies depending on the source and/or processing of the ECM [143,147,148]. The phenotype in response to ECM scaffolds is distinct from that induced by IFN γ + LPS (classically activated), IL-4 (alternatively activated), cellular xenogeneic scaffolds and synthetic scaffolds [147,149]. Importantly, the phenotype elicited by ECM-based bioscaffolds is different from that of tumor associated macrophages, another subset of M2 macrophages [150]. The activation of M2-like macrophages by ECM bioscaffolds is dependent on the presence of Th2 cells [145,150]. Although the exact mechanisms by which the ECM promotes a type 2-like immune response is only partially understood, it is known that degradation of the ECM and subsequent release of cryptic peptides, growth factors, matrix bound nanovesicles (MBV), and other bioactive molecules is required. MBV alone can recapitulate the immunomodulatory properties of the parent ECM [151,152].

Recent studies have characterized the ECM-induced immune cells infiltrating the bioscaffold and in the adjacent native tissue with a multicolor flow cytometry panel and have shown robust populations of macrophages, dendritic cells, T cells and B cells [145,148,149]. The overall profile of infiltrating immune cells was significantly different between ECM bioscaffolds prepared from different source tissues (bone, cardiac, liver, spleen and lung), but the general pattern was similar [148]. ECM bioscaffolds in general elicited a higher proportion of T helper cells than cytotoxic T cells [145,148,153]. Regulatory T cells (Tregs) were also recruited to the site of and were associated with increased levels of anti-inflammatory IL-10 cytokine secretion compared to autograft or saline [144,145,148,154].

Wang et al. used a humanized mouse model to characterize the temporal human immune response to xenogeneic and allogeneic decellularized myocardial ECM hydrogels. Although both decellularized scaffolds elicited a Th2 and M2-like macrophage phenotype, the quantity of cells and Th2 phenotype were more robust in response to the xenogeneic scaffold compared to the allogeneic scaffold. However, it is unknown if the amplified type 2 response was due to the xenogeneity of the bioscaffold or to differences in the source tissue, including older source age, greater collagen crosslinking and a more vigorous decellularization protocol associated with the allogeneic ECM [153].

2.2 Factors that Affect the Immune Response to ECM-Based Biomaterials

The efficiency of the decellularization protocol for ECM-based scaffolds arguably has the most significant impact on the immune response to the material. Implantation of inadequately decellularized materials that retain residual xenogeneic cellular components, including DNA, mitochondria and cell membrane remnants, is associated with a potent pro-inflammatory reaction and unfavorable downstream remodeling outcome [123,124]. The adverse response to cellular debris is dose dependent [123] and although the exact threshold determining adequate removal is not defined suggested criteria have been established as 1) less than 50ng dsDNA per mg of dry weight ECM, 2) DNA fragment length less than 200bp and 3) absence of positive DAPI or hematoxylin staining upon histologic evaluation [155]. The decellularization protocol must also remove xenogeneic antigens to avoid an adverse immune response. Dalgliesh et al. recently established that removal of at least 92% of lipophilic antigens is required to obviate an unfavorable graft-specific humoral immune response [156].

The composition of the ECM varies with factors of the source tissue, including the species, anatomical location, and age of the donor, which can in turn alter the host immune and remodeling response. Confounding variables such as different processing protocols required for each species or source tissue anatomical location render systematic comparison of the immune response nearly impossible. In general the immune response to ECM-based scaffolds from different species is similar [111,112], likely due to high cross-species conservation of major ECM components including collagens, laminin, fibronectin and glycosaminoglycans. The source tissue anatomic location has been shown to influence the activation state of macrophages *in vitro* [143,147,157], as well as the overall population of infiltrating immune cells *in vivo* [148]. Additionally, ECM derived from young animals is associated with a more favorable anti-inflammatory macrophage phenotype both *in vitro* [158] and *in vivo* [159] as compared to equivalent ECM prepared from an older source.

Chemical crosslinking is commonly used as a method to increase the mechanical strength and slow down the degradation of ECM-based materials. There are certain applications in which crosslinking is warranted, however this processing step is generally associated with more detrimental effects than positive. The broad cytotoxicity and pro-inflammatory nature of glutaraldehyde, the most commonly used chemical crosslinking agent, is well established [160]. Alternative crosslinkers have been investigated primarily as an attempt to minimize cytotoxic effects, however even ECM bioscaffolds that are crosslinked with “superior” mechanisms are still associated with a pro-inflammatory immune response [161]. Inhibition of the degradation process and therefore alteration of the release profile of bioactive byproducts such as growth factors, matricryptic peptides and MBV is thought to be the primary contributor to the unfavorable host response to crosslinked naturally occurring materials.

2.3 Matrix Bound Nanovesicles Recapitulate Anti-Inflammatory Effects

The identification of lipid bound extracellular vesicles embedded within the ECM, termed matrix-bound nanovesicles (MBV) in 2016 provided new mechanistic insight into the bioactive and immunomodulatory properties of ECM-based materials [152]. MBV have been shown to largely recapitulate the effects of the whole ECM on macrophage phenotype *in vitro*. Specifically, exposure of murine bone marrow-derived macrophages to isolated MBV alone induced expression of genes and proteins associated with an anti-inflammatory M2-like phenotype [151]. MBV also downregulate pro-inflammatory cytokine expression in microglia, the resident macrophage of the brain and spinal cord [162]. Though the exact mechanisms of MBV-mediated immunomodulation have not yet been elucidated, multiple studies have revealed the potential contribution of their potent miRNA, lipid and protein cargo [151,163]. Due to the close association of MBV with fibers of the ECM, it is presumed that these vesicles are released during matrix turnover and remodeling events and therefore their bioactivity would be inhibited by processing factors that prevent matrix degradation such as chemical crosslinking.

3.0 Significance

The host immune response to a biomaterial, and specifically the phenotype of responding macrophages, is already well-recognized as a determinant of downstream outcome in other anatomic locations [111]. More specifically, M1-like macrophages produce pro-inflammatory mediators, secrete nitric oxide, and are associated with chronic inflammation and a poor downstream outcome. On the other hand, anti-inflammatory M2-like macrophages act to promote tissue repair and are associated with generally more favorable outcomes. In the context of prosthetic heart valves, two recent studies showed that the M1-like macrophage response to glutaraldehyde fixed bioprosthetic valves (BHV) was accompanied with robust calcification [77,80]. Alternatively, stimulation of an anti-inflammatory M2-like phenotype by incorporation of a functionalized coating on the bioprosthetic was associated with resistance to calcification [77,80].

To date, there is no clinically approved therapeutic to prevent SVD of BHV. Some *in vivo* [73] and clinical data [164] has indicated improved outcomes with immunosuppressive treatment, but adverse effects associated with immunosuppression have prevented further investigation. A systemically delivered immunomodulatory therapeutic that could be used to shift the immune response to currently available bioprosthetic valves represents a novel strategy to prevent bioprosthetic valve failure.

Emerging evidence suggests that MBV are liberated during degradation of the ECM scaffold at which point they can exert bioactive effects on adjacent cells. Importantly, MBV have been shown to contain potent effector molecules that can directly activate macrophages towards a pro-remodeling M2-like phenotype [151,152]. It is plausible that this immunomodulatory property

of MBV could resolve the pro-inflammatory response associated with degradation of BHV to extend their functional lifetime. The present work attempts to better characterize MBV and determine their efficacy as a prophylactic for SVD.

Early published work describing MBV has established their bioactive and immunomodulatory properties *in vitro* [151,163] and following local delivery *in vivo* [162,165]. The present research is innovative in that it expands our understanding of MBV in two major ways: first, by completing an in depth characterization of the MBV to establish them as a novel subpopulation of extracellular vesicle, and second, by broadening the clinical application of MBV as a systemically delivered bioactive modality.

The ultimate goal of the present study is to develop a therapeutic to mitigate failure of currently available bioprosthetic tissue valves. Current strategies to improve outcomes associated with prosthetic heart valve implantation generally include novel anti-calcification treatments [166], alternative functionalization [80], or entirely new material components [34]. However, these methods are all incompatible with current commercially available BHV and would therefore face significant regulatory hurdles and likely slow widespread adoption in the field. A pharmacologic approach designed to modulate cellular processes, and in particular the immune response, associated with failure of contemporary valve substitutes is therefore an innovative tactic.

4.0 Central Hypothesis and Specific Aims

4.1 Central Hypothesis

The present study hypothesizes that MBV are a unique class of extracellular vesicles that can modulate cellular processes via an interleukin-33 (IL-33) dependent mechanism to alleviate fibrosis and calcification of a bioprosthetic valve material primarily via macrophage-mediated effects.

4.2 Specific Aims

4.2.1 Specific Aim 1

Compare the structure and composition of MBV to other types of extracellular vesicles, including fluid exosomes and calcifying matrix vesicles.

Hypothesis 1: Matrix bound nanovesicles represent a distinct subset of extracellular vesicles with cargo that varies with tissue source and microenvironment.

Rationale: Other categories of extracellular vesicles such as exosomes found in bodily fluids and calcifying matrix vesicles within mineralizing tissue have distinguishing features including protein markers, function, and biogenesis [167]. However, defining characteristics of

MBV derived from soft tissue ECM have not yet been established. Since the ECM varies in composition with each organ [168,169] as well as during disease [170,171], it is hypothesized that the composition of ECM-derived MBV will also change with source cell and disease state [151,152].

4.2.2 Specific Aim 2

Determine the direct and indirect (macrophage-mediated) effect of MBV upon macrophage activation, fibrosis, and mineralization *in vitro*.

Sub Aim 2.1: Determine the contribution of IL-33 cargo to MBV mediated effects upon macrophage phenotype and fibroblast behavior.

Hypothesis 2: Exposure to IL-33⁺ MBV, but not IL-33⁻ MBV, will mitigate pro-inflammatory activation of macrophages. IL-33⁺ MBV will limit myofibroblast activation and mineralization of fibroblasts, primarily via indirect effects of an anti-inflammatory macrophage secretome induced by IL-33⁺ MBV.

Rationale: ECM degradation products alleviate a pro-inflammatory phenotype of macrophages *in vitro* [147], and MBV largely recapitulate ECM effects on macrophages [151]. IL-33 cargo is required for MBV to induce an anti-inflammatory phenotype in naïve macrophages [163]. The secreted products of anti-inflammatory macrophages, such as those stimulated by IL-33⁺ MBV [151,163], are associated with decreased ECM production by fibroblasts [172] and are protective against calcification [71,173].

4.2.3 Specific Aim 3

Evaluate the ability of systemic MBV administration to modulate the host immune response and calcification outcome to implanted glutaraldehyde-fixed bovine pericardium (gluBP) in a preclinical rodent model.

Hypothesis 3: Intravenous (IV) administration of IL-33⁺ MBV will modulate the host response towards an anti-inflammatory state and thereby mitigate immune-driven calcification of implanted gluBP.

Rationale: Preliminary data suggest that systemic IV administration of MBV can modulate macrophage phenotype to alleviate inflammation in a model of arthritis and following implantation of a surgical mesh. Though there has been little investigation of therapeutic prevention of immune-driven SVD, steroids have shown potential for limiting SVD by suppressing the immune response [73,164]. The effect of immunomodulation, rather than immunosuppression, has yet to be evaluated in a pre-clinical setting. The present study examines the macrophage phenotype and calcification response following implantation of prosthetic heart valve materials and IV administration of MBV in a rodent subcutaneous implant model.

5.0 Matrix Bound Nanovesicles Represent a Distinct Subset of Extracellular Vesicle³

5.1 Introduction

The International Society of Extracellular Vesicles defines “extracellular vesicles” (EV) as “particles naturally released from the cell that are delimited by a lipid bilayer and cannot replicate” [174]. EV are produced by essentially all cell types and contain proteins, lipids, and nucleic acids derived from the parent cell, and serve the primary function of cell-to-cell communication [175,176]. It is plausible that EV exported into a provisional bone matrix vs. a body fluid such as blood vs. a soft tissue extracellular matrix (ECM) would each have a distinctive biogenesis, lipid membrane composition, and intraluminal cargo.

A variety of names have been used to distinguish subgroups of EV, including exosomes, matrix vesicles, microvesicles, and apoptotic bodies, among others [167,177]. Despite numerous studies that characterize the size, composition, biogenesis, and biologic functions of EV harvested from a broad range of source tissues, there is no consensus regarding specific markers to distinguish different subpopulations [174,176,178].

Some of the earliest descriptions of EV were published in 1967 when membrane bound, nano-sized vesicles were identified within growth plate cartilage and bone by ultrastructural imaging [179–181]. These structures, coined “matrix vesicles”, were subsequently shown to be derived from mineral forming cells (e.g. osteoblasts) where they function as a nucleation site for

³ Portions of this chapter have been adapted from the following publication:
G.S. Hussey, C.P. Molina, **M.C. Cramer**, Y.Y. Tyurina, V.A. Tyurin, Y.C. Lee, S.O. El-Mossier, M.H. Murdock, P.S. Timashev, V.E. Kagan, S.F. Badylak, Lipidomics and RNA sequencing reveal a novel subpopulation of nanovesicle within extracellular matrix biomaterials, *Sci. Adv.* 6 (2020) 1–14.

hydroxyapatite crystal formation [167,182]. As such, these calcifying matrix vesicles are enriched for proteins such as annexins and tissue non-specific alkaline phosphatase (TNAP), and can often contain amorphous calcium phosphate mineral [177].

The term “exosome” was first used to describe a subpopulation of EV isolated from normal and neoplastic cells *in vitro* in 1981 [183]. Work by Johnstone investigating the biogenesis of these EV showed that “exosome” specifically refers to EV of endosomal origin that are released by fusion of multi-vesicular bodies with the cell membrane [184]. Subsequent studies have shown that exosomes exist exclusively within the liquid-phase, including all body fluids and the conditioned media of cells *in vitro* [176,185].

In 2016, a subpopulation of EV embedded within the extracellular matrix was identified and termed matrix-bound nanovesicles (MBV) [152]. Unlike exosomes present in body fluids and calcifying matrix vesicles present within mineralizing tissues, MBV are present within the ECM of non-mineralizing soft tissues, such as the heart, urinary bladder, dermis, skeletal muscle, and small intestinal submucosa [152,163]. The biologic effects (i.e., bioactivity) of MBV include anti-inflammatory immunomodulation, stem cell differentiation, and collagen deposition, among others [151,152,162,163]. The intraluminal cargo of MBV includes lipid, protein, miRNA and other signaling molecules [151,152,163,186], but an in depth characterization of their defining characteristics relative to EV present within bone matrix and within a fluid medium has not been described.

The first objective of the present study was to compare these three distinct subpopulations of EV, namely calcifying matrix vesicles (cMV), MBV and exosomes (Exo) by physical characteristics, protein markers commonly associated with Exo and cMV subpopulations, lipid composition, and miRNA cargo of each subpopulation. To more thoroughly characterize MBV as

a unique subpopulation of EV, we also determined if MBV differ from fluid-phase exosomes from a given cell type, if MBV vary with cell source, and if MBV cargo changes with the disease state of the source tissue.

5.2 Materials and Methods

5.2.1 Overview of Experimental Design

A panel of parameters were used to characterize both the structure and composition of MBV and other extracellular vesicles including size, surface markers, protein and miRNA cargo, and lipid membrane composition. Specific Aim 1 was designed to characterize MBV and determine if they represent a distinct subset of extracellular vesicles by answering a series of questions. The specific questions as well as the samples and planned endpoints to answer each are summarized in Table 2.

5.2.1 Source of Vesicle Subtypes

Question 1- MBV, exosomes, and cMV: MBV were isolated from C57BL/6 mouse skeletal muscle. Quadriceps muscle was first decellularized with 0.02% trypsin and 0.05% EDTA and disinfected with 0.01% peracetic acid prior to enzymatic digestion with Liberase TH in buffer (50mM Tris pH 7.5, 5mM CaCl₂, 150mM NaCl) at 37°C overnight to release MBV from the ECM.

cMV were isolated from 17IIA pre-odontoblast cells as previously described [187]. Briefly, osteogenic differentiation of 17IIA cells was induced with 10 mM Na–Pi buffer (pH 7.4) and 50 µg/ml ascorbic acid for 24 hr. The matrix deposited by 17IIA cells was enzymatically digested with 1mg/ml collagenase IA in buffer for 2 hr at 37°C to release the cMV.

Exo were isolated from C57BL/6 mouse plasma obtained from Innovative Research (Novi, MI). The plasma was first centrifuged at 3,000xg for 15min to remove cells and cellular debris and exosomes were isolated using the ExoQuick™ Exosome Precipitation Solution (System Biosciences) according to the manufacturer’s instructions.

Table 2. Summary of experimental design for Specific Aim 1.

| Question | Samples | Evaluated endpoints |
|--|--|--|
| Are MBV distinct from exosomes and calcifying matrix vesicles? | <ol style="list-style-type: none"> 1. Mouse muscle MBV 2. Mouse plasma exosomes 3. Mouse 17IIA cell-produced cMV | Vesicle size, TEM, surface protein markers, cytokine cargo, miRNA sequencing, lipidomic analysis |
| Do MBV differ from fluid vesicles of a given cell type? | <ol style="list-style-type: none"> 1. 3T3 cell-derived MBV 2. 3T3 cell-derived fluid vesicles | Vesicle size, surface protein markers, miRNA sequencing, lipidomic analysis |
| Do MBV vary with cell source? | MBV derived from: <ol style="list-style-type: none"> 1. Bone marrow-derived stem cells 2. Adipose-derived stem cells 3. Umbilical cord stem cells | Vesicle size, miRNA sequencing |
| Do MBV change with disease? | MBV derived from: <ol style="list-style-type: none"> 1. Human non-failing heart tissue 2. Human failing heart tissue | Vesicle size, cytokine cargo, RNA sequencing |

Question 2- MBV and fluid vesicles from a single cell type: Murine NIH 3T3 fibroblast cells were seeded onto a 75-cm² cell culture flask at a cell density of 3500 cells/cm² and cultured in Dulbecco's modified Eagle's medium (DMEM) supplemented with exosome-depleted FBS [188], 1% penicillin-streptomycin, and ascorbic acid 2-phosphate (Sigma-Aldrich) at a final concentration of 50 μ M for 7 days to allow deposition of ECM onto the tissue culture plate. At day 7, the supernatant from cultured 3T3 fibroblast cells was collected, and the culture plates were washed three times with phosphate-buffered saline (PBS), decellularized using 0.5% Triton in 20 mM ammonium hydroxide for 5 min, and then rinsed three times with ultra- pure H₂O. The decellularized ECM was enzymatically digested with Liberase DL for 1 hour at 37°C.

Question 3- MBV produced by distinct cell sources: Human bone marrow-derived stem cells (BMSC), human adipose-derived stem cells (ASC), and human umbilical cord stem cells (UCSC) ECM plates were provided by StemBioSys (San Antonio, TX) and prepared according to a published protocol [189]. Briefly, human BMSC, human ASC, or human UCSC were seeded onto a 75-cm² cell culture flask coated with human fibronectin (1 hour at 37°C) at a cell density of 3500 cells/cm² and cultured in α -minimum essential medium (α -MEM) supplemented with 20% fetal bovine serum (FBS) and 1% penicillin- streptomycin for 14 days. The medium was refreshed the day after initial seeding and then every 3 days. At day 7, ascorbic acid 2-phosphate (Sigma-Aldrich) was added to the medium at a final concentration of 50 μ M. At day 14, plates were decellularized using 0.5% Triton in 20 mM ammonium hydroxide for 5 min and rinsed two times with Hanks' balanced salt solution containing both calcium and magnesium (HBSS +/+) and once with ultrapure H₂O.

Question 4- MBV from healthy and diseased tissue ECM: Through the Human Cardiac Tissue Bank bio-specimen study (IRB# 0404033), de-identified human left ventricle tissue specimens from 1) non-ischemic failing hearts (failing, N = 6) and 2) non-failing, non-ischemic hearts (healthy, N = 6) were obtained. The patient characteristics are included in **Table 3**. Tissue samples were washed in sterile PBS and then enzymatically digested with Liberase TH at 37°C overnight.

Table 3. Patient characteristics of human left ventricle tissue samples.

| Group | Age | Sex | Group | Age | Sex |
|--------------|------------|------------|--------------|------------|------------|
| Healthy | 43 | M | Failing | 66 | M |
| Healthy | 13 | M | Failing | 67 | M |
| Healthy | 33 | M | Failing | 56 | M |
| Healthy | 28 | M | Failing | 50 | M |
| Healthy | 37 | M | Failing | 54 | M |
| Healthy | 59 | M | Failing | 55 | M |

5.2.2 Isolation of Vesicles

After appropriate preparation as described above, samples were subjected to centrifugation at 500xg for 10min, 2,500xg for 20min, and 10,000xg for 30 min to remove cellular and matrix debris, and the supernatant passed through a 0.22 µm filter. The clarified supernatant was then centrifuged at 100,000xg (Beckman Coulter Optima L-90K Ultracentrifuge) at 4°C for 70 min to pellet the vesicles. All vesicles were resuspended in 1X PBS, aliquoted, and stored at -20°C until use.

5.2.3 Transmission Electron Microscopy

Transmission electron microscopy (TEM) imaging was conducted on vesicles loaded on carbon-coated grids and fixed in 4% paraformaldehyde as previously described [152]. Grids were imaged at 80 kV with a JEOL 1210 TEM with a high-resolution Advanced Microscopy Techniques digital camera.

5.2.4 Nanoparticle Tracking Analysis

Vesicle size and concentration were measured using a NanoSight (NS300) instrument equipped with fast video capture and particle-tracking software. Samples were diluted with particle-free water and dispensed at a constant flow rate using a syringe pump. Measurements were performed from three captures of 45 s each sample. Data are presented as concentration versus particle size for each of the evaluated samples.

5.2.5 RNA Isolation and miRNA-Sequencing

Total RNA was isolated from vesicle samples using the miRNeasy Mini Kit (Qiagen) according to the manufacturer's instructions. Before RNA isolation, samples were treated with ribonuclease A (10 ug/ml) at 37°C for 30 min to degrade any contaminating RNA. The concentration of RNA was determined by NanoDrop spectrophotometer, and its quality was determined by Agilent Bioanalyzer 2100 (Agilent Technologies). The miRNA library preparation was initiated following the manufacturer's instructions. Briefly, mature miRNAs were ligated to adapters on their 3' and 5' ends. The ligated miRNAs were then reverse-transcribed to

complementary DNA (cDNA) using a RT primer with unique molecular indices. The cDNA was then cleaned up to remove adapter primers, followed by amplification of the library with a universal forward primer and one of 48 reverse primers that assign a sample index. Next-generation sequencing of vesicle miRNA cargo was performed and bioinformatic analysis was used to determine the differentially expressed miRNA between groups.

5.2.6 Characterization of Vesicle Proteins

The expression of protein markers commonly associated with exosomes was evaluated using the Exo-Check™ Exosome Antibody Array (System Biosciences) with 50ug of protein as measured by Micro BCA™ protein assay kit (Thermo Fisher Scientific). The cytokine content was determined using the Proteome Profiler XL Cytokine Array (R&D Systems) according to the manufacturer's instructions. Prior to evaluation using the cytokine array, MBV were lysed with 1% Triton X-100 in the presence of protease and phosphatase inhibitors to expose surface, membrane, and luminal cargo proteins and a loading of 200ug total protein was used. The relative level of each protein was quantified using ImageJ.

For western blot analysis, samples were mixed with 2× Laemmli buffer (R&D Systems) containing 5% beta mercaptoethanol (Sigma-Aldrich), resolved on a 4 to 20% gradient SDS–polyacrylamide gel electrophoresis (Bio-Rad), and then transferred onto a polyvinylidene difluoride membrane. Membranes were incubated overnight with the following primary antibodies: rabbit anti-CD63, rabbit anti-CD81, rabbit anti-CD9, and rabbit anti-Hsp70, at 1:1000 dilution (System Biosciences) to evaluate expression of common exosome-associated markers, or rabbit anti-annexin V, and goat anti-tissue non-specific alkaline phosphatase (TNAP) to evaluate expression of common cMV associated markers. Membranes were washed three times for 15 min

each before and after they were incubated with the appropriate secondary antibody. The washed membranes were exposed to substrate and then visualized using a ChemiDoc Touch instrument (Bio-Rad). Silver staining of gels was performed using the Silver Stain Plus Kit (Bio-Rad) according to the manufacturer's instruction and visualized using a ChemiDoc Touch instrument (Bio-Rad).

5.2.7 Lipidomic Analysis of Phospholipids

Lipids were extracted from the vesicle samples. Mass spectrometry analysis of phospholipids and lysophospholipids was performed as previously described [190]. The lipids identified in each sample were categorized by class to determine differences in the overall composition of each group.

5.2.8 Statistical Analysis

A one-way or two-way analysis of variance (ANOVA) and post-hoc analysis with Tukey correction determined significant comparisons between groups. All statistical analysis was completed with GraphPad Prism. Data is presented as mean +/- standard error of the mean (SEM). *P < 0.05, **P < 0.01, ***P < .001.

5.3 Results

5.3.1 MBV are Distinct from Exosomes and Calcifying Matrix Vesicles

5.3.1.1 Vesicles Have Similar Physical Characteristics

The physical characteristics of cMV, Exo, and MBV were determined using TEM and Nanosight analysis. Visualization of vesicle morphology by TEM showed no distinctive differences between groups (Figure 1A). Quantitation of vesicle size distribution by Nanosight showed that cMV range in size from approximately 80 – 450nm, Exo range from 50 – 250nm, and MBV range from 75 – 500nm (Figure 1B). Comparison of the mode diameter for each vesicle subtype showed that cMV are significantly larger than both Exo and MBV (Figure 1C). Exo also have a significantly smaller mode diameter compared to MBV.

5.3.1.2 Vesicles Have Unique Protein Signatures

An antibody array for a panel of protein markers that have been associated with exosomes [175] was used as a first metric to characterize vesicle associated-proteins of each group (Figure 2A). Overall, there was low relative expression of all exosome marker proteins in MBV, whereas the expression of these same marker proteins showed no significant differences between cMV and Exo. The expression of annexin V and tissue non-specific alkaline phosphatase (ALP), two proteins commonly associated with cMV, were evaluated by western blot (Figure 2B). cMV had the highest expression of annexin V, Exo had intermediate expression, and MBV had minimal expression. Only cMV were found to express ALP by western blot analysis.

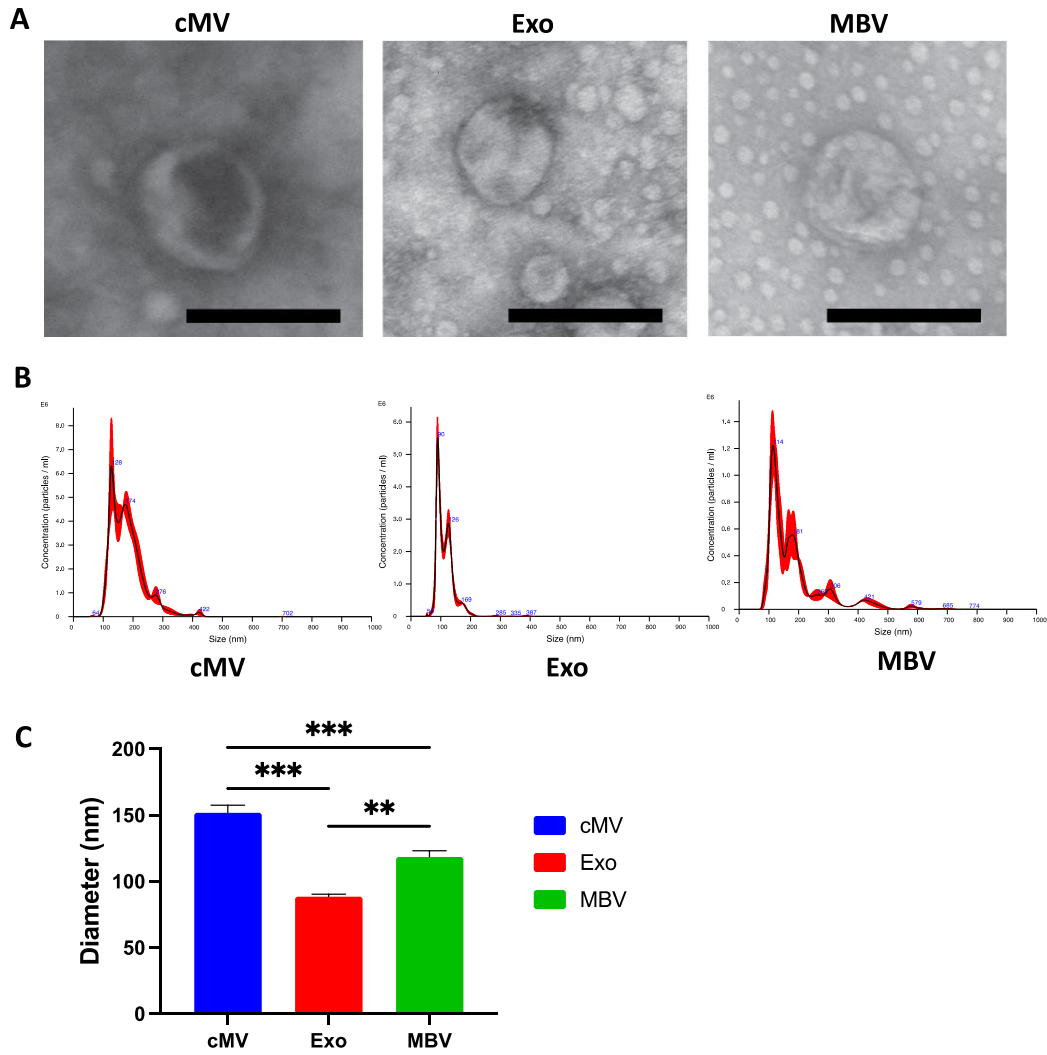


Figure 1. cMV, Exo and MBV have similar physical characteristics.

(A) Transmission electron microscope images of cMV, Exo, and MBV. Scale bars 200nm. (B) Representative size distribution plots and (B) the mode diameter of cMV, Exo, and MBV as determined by Nanosight nanoparticle tracking analysis. All values represent mean \pm SEM (N = 12).

The cytokine cargo of cMV, Exo, and MBV was characterized using a mouse cytokine array for 111 different target proteins. Principal component analysis (PCA) was used to compare and visualize the results of the cytokine array (Figure 2C). The PCA showed high similarity within replicates of each vesicle type but distinct differences between the three vesicle types. The cytokines nearest to each vesicle type contributed most strongly to the distinction of that vesicle type. cMV had significantly higher expression of osteoprogenitorin and osteopontin while Exo expressed adiponectin, epidermal growth factor (EGF) and pentraxin 2 (Figure 2D). Of the cytokines evaluated, MBV were most closely aligned with myeloperoxidase.

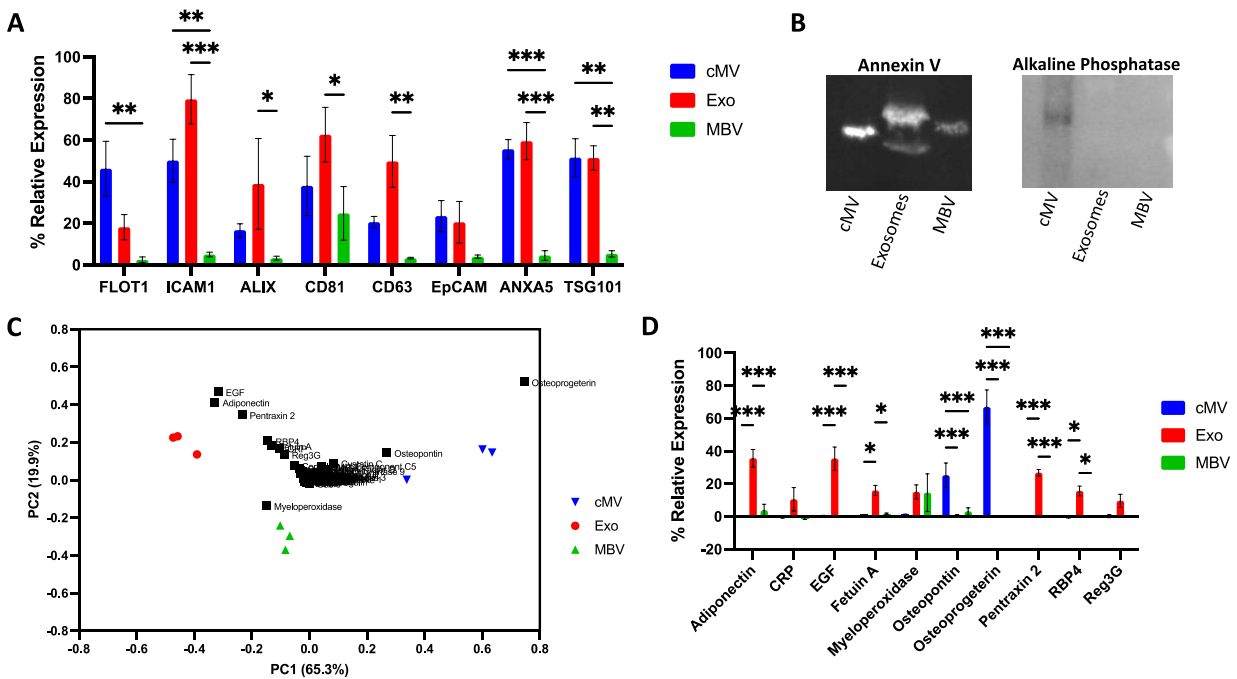


Figure 2. cMV, Exo and MBV have distinct vesicle-associated proteins.

(A) Quantification of the relative expression of 8 markers commonly associated with exosomes as measured by Exo-Check immunoblot array. (B) Western blot of annexin V and tissue non-specific alkaline phosphatase (TNAP). (C) Principal component analysis comparing the cytokine cargo of cMV (blue), Exo (red), and MBV (green). (D) Quantification of the top 10 differentially expressed cytokines as determined by immunoblot array. All values represent mean \pm SEM (N = 3).

5.3.1.3 Vesicles Have Distinctive Lipid Composition

Lipidomic analysis was used to compare the lipid composition of cMV, Exo, and MBV. Over 1370 individual lipid species were detected across the three vesicle types, with these species belonging to 38 subclasses. Volcano plots were used to visualize the individual lipid species that showed significantly different expression between each vesicle type (Figure 3A). Pairwise comparisons showed distinctions in the lipid composition of MBV compared to both cMV and Exo. Quantitatively, 165 lipid species were significantly different when comparing MBV vs. cMV, and 110 species were different between MBV vs. Exo. Across all detected lipids, cMV and Exo showed similar compositions with only 14 differentially expressed species (Figure 3A).

Given the established role of phospholipids and lysophospholipids (LPLs) in vesicle biology and bioactivity [191,192], we further characterized the overall content of these major classes. Pie plots also showed the similar lipid composition of cMV and Exo across the classes phosphatidylcholines (PC), phosphatidylethanolamines (PE), phosphatidylglycerols (PG), phosphatidylinositols (PI), phosphatidylserines (PS) and sphingolipids (SL) (Figure 3B). The phospholipids of both cMV and Exo primarily consisted of PS and SL. Relative to the other two vesicles, MBV were enriched in PC, PE and PI.

The content of lysophosphatidylcholine (LPC), lysophosphatidylethanolamine (LPE), and lysophosphatidylglycerol (LPG) were significantly different between all three vesicle types (Figure 3C). LPG was the dominant LPL class in cMV, Exo had nearly equal proportions of LPG and LPC, and MBV were enriched in LPC. MBV also had a higher content of LPE compared to both cMV and Exo (Figure 3C).

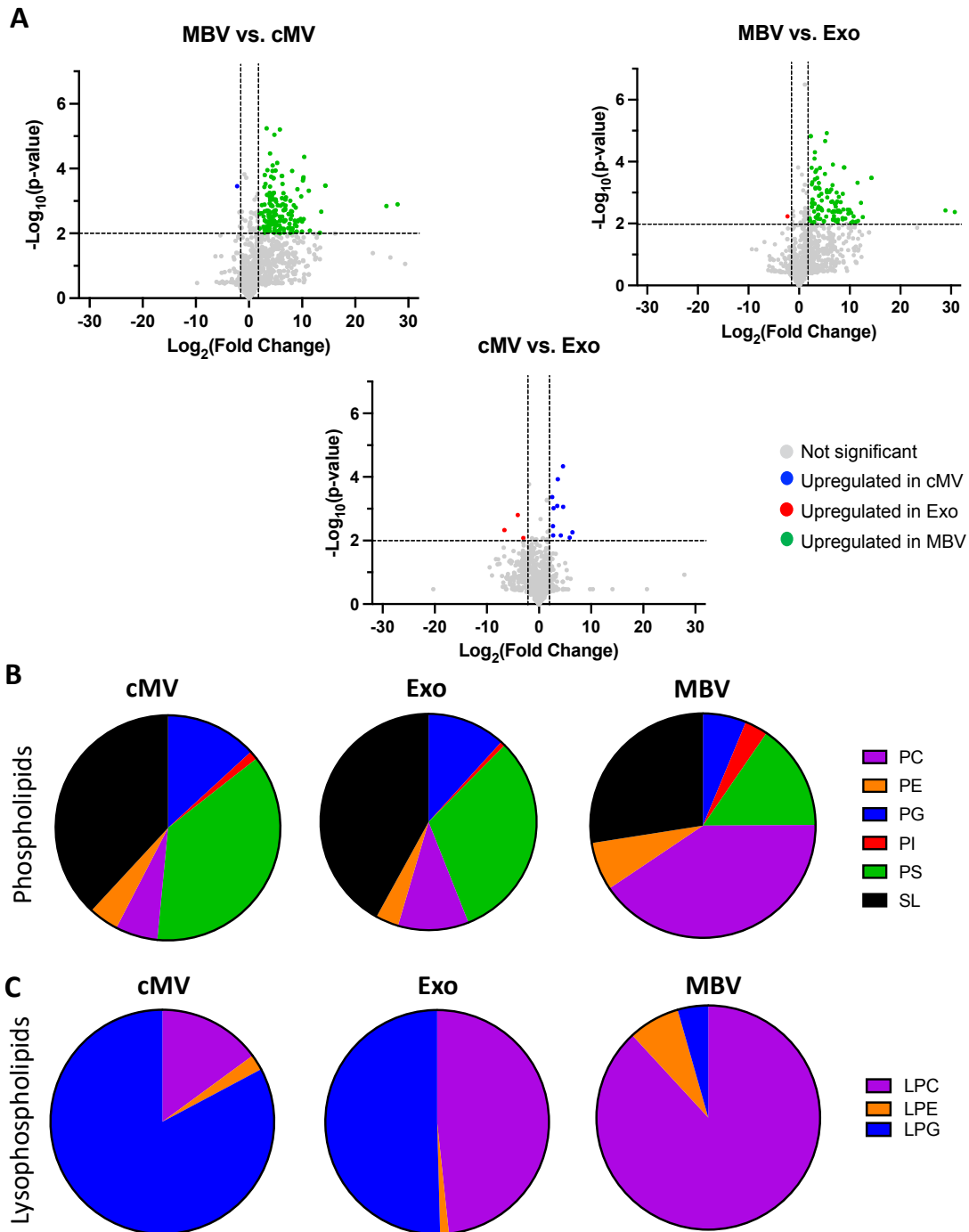


Figure 3. Lipid composition of cMV and Exo are distinct from MBV.

(A) Volcano plots showing the differential expression of individual lipid species in pairwise comparisons of cMV, Exo, and MBV. The criteria for significance were a two-fold difference in $\log_2(\text{fold change})$ with a P value < 0.05 .

Pie plots showing the total content of (B) major phospholipids and (C) lysophospholipids. Data are presented as percentage of total detected lipids. (N = 6)

5.3.1.4 Vesicle Subtypes Have Distinct miRNA Cargo

Next-generation sequencing was used to compare the miRNA cargo of cMV, Exo and MBV. A heatmap with hierarchical clustering based on Spearman's correlation distance was used to visualize the overall similarities in miRNA profile of each vesicle subtype (Figure 4A). In general, the miRNA cargo of Exo was more similar to cMV. MBV miRNA cargo had large differences compared to that of Exo, but was more similar to cMV. As evidenced by the Spearman's correlation coefficients, the miRNA within Exo was very homogenous across the biologic replicates while the cMV and MBV replicates showed more variability. A heat map was also used to show differential expression of individual miRNA species for each sample (Figure 4B). Exo had more highly expressed miRNA than cMV and MBV.

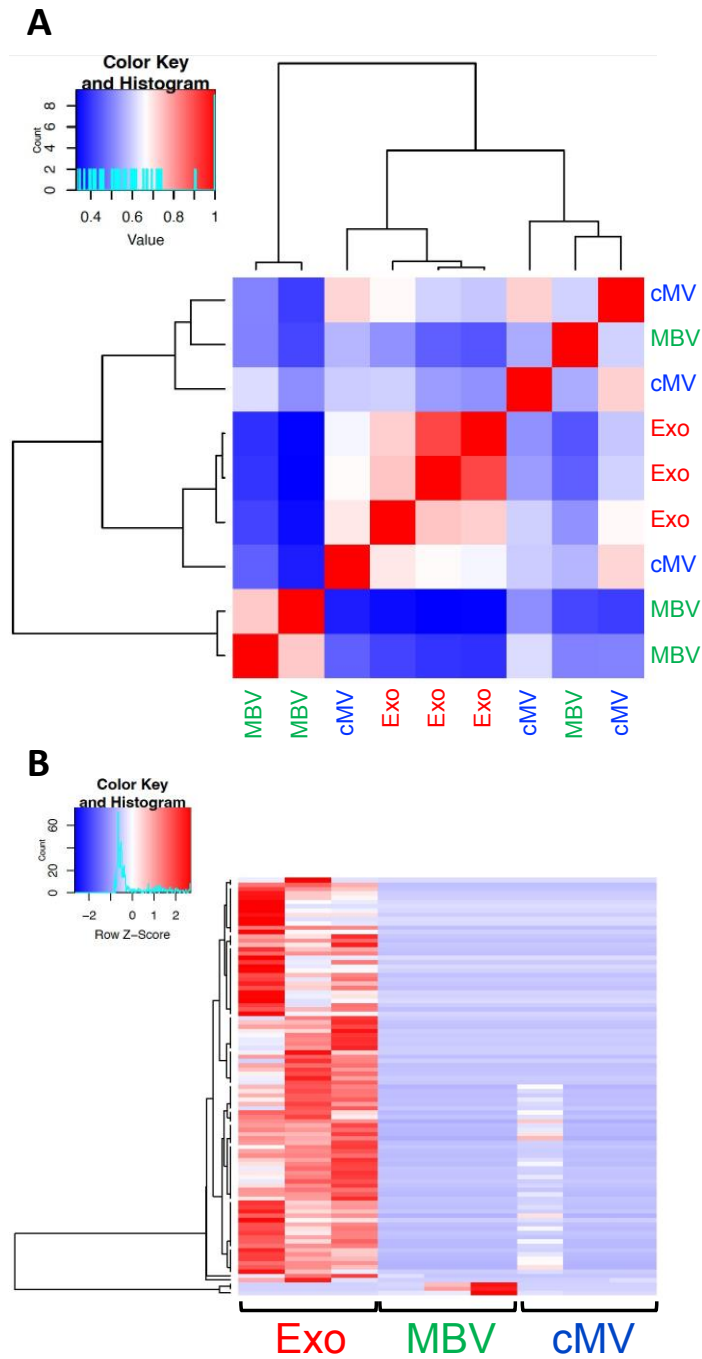


Figure 4. miRNA cargo of cMV, Exo, and MBV are distinct.

(A) Hierarchically clustered heatmap depicting Spearman's correlation distances calculated pair-wise for all samples. (B) Specific expression of individual miRNA species depicted as a heat map based on Z-score.

(N = 3)

5.3.2 MBV are Distinct from Exosomes of a Given Cell Type

5.3.2.1 3T3-derived MBV and Liquid-Phase Exo Have Similar Sizes

TEM imaging of liquid-phase EV (Exo) harvested from the cell culture supernatant (Figure 5A) and MBV isolated from decellularized ECM (Figure 5B) showed that these two populations of vesicles shared a similar morphology. Moreover, nanoparticle tracking analysis (NTA) distribution plots showed similar vesicle size of both liquid-phase EV and MBV, with the majority of vesicles having a diameter of <200 nm (Figure 5C).

5.3.2.2 3T3-derived MBV and Exosomes Have Unique Protein Markers

To determine whether MBV contained markers commonly attributed to exosomes, immunoblot analysis was performed for CD63, CD81, CD9, and Hsp70 [193]. Results showed that, in contrast to liquid-phase EV, the MBV had a marked decrease in CD63, CD81, and CD9 (Figure 6A). Furthermore, silver staining of electrophoretically separated proteins showed that MBV contained protein cargo that was distinctly different than the liquid-phase EV (Figure 6B), suggesting that MBV may be a unique subpopulation of nanovesicle.

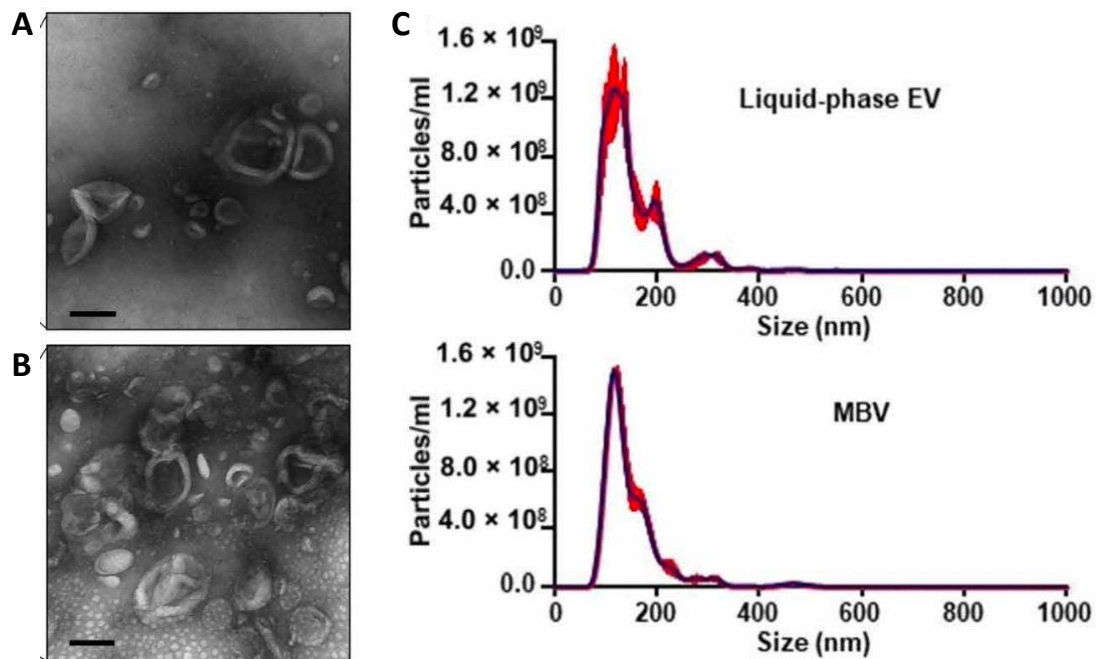


Figure 5. MBV and liquid-phase EV from 3T3 cells have similar physical characteristics.

TEM of liquid-phase EV (A) and MBV (B) isolated from the 3T3 fibroblast cell culture model. Scale bars, 100 nm. (C) Size distribution plots from NTA of liquid-phase EV (top) and MBV (bottom) isolated from the 3T3 fibroblast cell culture.

5.3.2.3 3T3-derived MBV and Exosomes Have Unique Lipid Composition

Liquid chromatography-mass spectrometry (LC-MS)-based global lipidomics analysis was performed to comparatively evaluate the phospholipid composition of MBV and liquid-phase EV compared to their 3T3 fibroblast parent cells. Nine major phospholipid classes were detected in all three types of samples, with the total number of detected molecular species of 536 distributed between the following major classes: bis-monoacylglycerophosphate (BMP), 59 species; phosphatidylglycerol (PG), 37 species; cardiolipin (CL), 117 species; phosphatidylinositol (PI), 33 species; phosphatidylethanolamine (PE), 102 species; phosphatidylserine (PS), 45 species; phosphatidic acid (PA), 26 species; phosphatidylcholine (PC), 107 species; and sphingomyelin

(SM), 10 species. There were significant differences in molecular speciation of these phospholipids and their relative contents between liquid-phase EV and MBV. Quantitatively, MBV were enriched in PI, PS, PG, and BMP (Figure 7A). In contrast, the content of PE, PA, and SM was higher in liquid-phase EV. PC was a predominant phospholipid in cells and liquid-phase EV. The content of a unique mitochondrial phospholipid, CL, was significantly lower in liquid-phase EV compared to MBV and parent cells (Figure 7A).

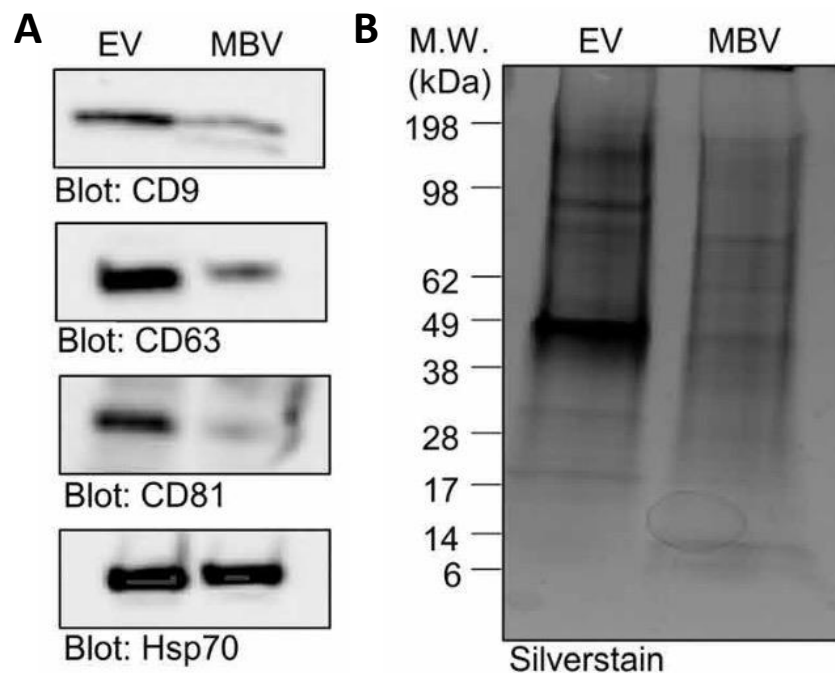


Figure 6. MBV and liquid-phase EV from 3T3 cells have unique protein markers.

(A) Immunoblot analysis of CD9, CD63, CD81, and Hsp70 expression levels in liquid-phase EV and MBV. (B) Silverstain analysis of electrophoretically separated proteins in liquid-phase EV and MBV. M.W., molecular weight.

5.3.2.4 3T3-derived MBV and Exosomes Have Unique Lipid Composition

Liquid chromatography-mass spectrometry (LC-MS)-based global lipidomics analysis was performed to comparatively evaluate the phospholipid composition of MBV and liquid-phase EV compared to their 3T3 fibroblast parent cells. Nine major phospholipid classes were detected in all three types of samples, with the total number of detected molecular species of 536 distributed between the following major classes: bis-monoacylglycerophosphate (BMP), 59 species; phosphatidylglycerol (PG), 37 species; cardiolipin (CL), 117 species; phosphatidylinositol (PI), 33 species; phosphatidylethanolamine (PE), 102 species; phosphatidylserine (PS), 45 species; phosphatidic acid (PA), 26 species; phosphatidylcholine (PC), 107 species; and sphingomyelin (SM), 10 species. There were significant differences in molecular speciation of these phospholipids and their relative contents between liquid-phase EV and MBV. Quantitatively, MBV were enriched in PI, PS, PG, and BMP (Figure 7A). In contrast, the content of PE, PA, and SM was higher in liquid-phase EV. PC was a predominant phospholipid in cells and liquid-phase EV. The content of a unique mitochondrial phospholipid, CL, was significantly lower in liquid-phase EV compared to MBV and parent cells (Figure 7A).

LC-MS analysis showed that lysophospholipids (LPLs) were present in all three types of samples, albeit with their total content in MBV and liquid-phase EV being 1.7 to 1.8 times greater compared to the parent cells. More specifically, seven classes of LPL have been identified: lysophosphatidylethanolamine (LPE), lysophosphatidylcholine (LPC), lysophosphatidylserine (LPS), lysophosphoinositol (LPI), lysophosphatidic acid (LPA), lysophosphatidylglycerol (LPG), and monolysocardiolipin (mCL). MBVs were enriched in LPE, LPA, and LPG compared to parent cells (Figure 7B). The content of LPI and mCL was significantly lower in MBV and liquid-phase EV versus cells. The contents of LPA and LPG were found to be significantly higher in MBV

compared to EV. The levels of mCL and LPI in MBV were 3 and 6.3 times higher than in EV but 3.3 and 1.9 times lower compared to cells. No significant changes in the contents of LPE, LPC, and LPS between MBV and EV were found (Figure 7B).

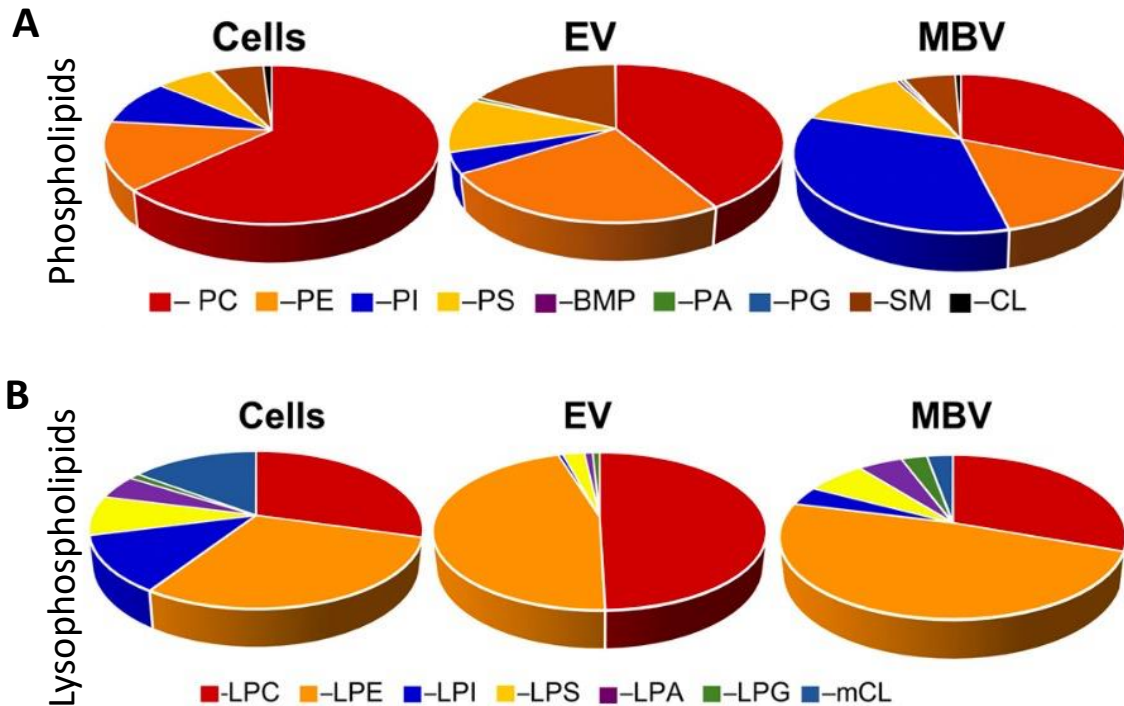


Figure 7. Lipidomic analysis reveals distinct lipid composition of 3T3 cells, MBV and liquid-phase EV.

(A) Pie plots showing the total content of major phospholipids. Data are presented as percentage of total phospholipids. (B) Pie plots showing the total content of major LPL. Data are presented as percentage of total LPL.

(N = 3)

5.3.2.5 3T3-derived MBV and Exosomes Have Unique miRNA Cargo

Comprehensive next-generation RNA-sequencing (RNA-seq) was used to catalog differentially expressed miRNA in MBV and liquid-phase EV relative to the 3T3 fibroblast parent cell from which these vesicles were derived. The analysis was focused on differential miRNA

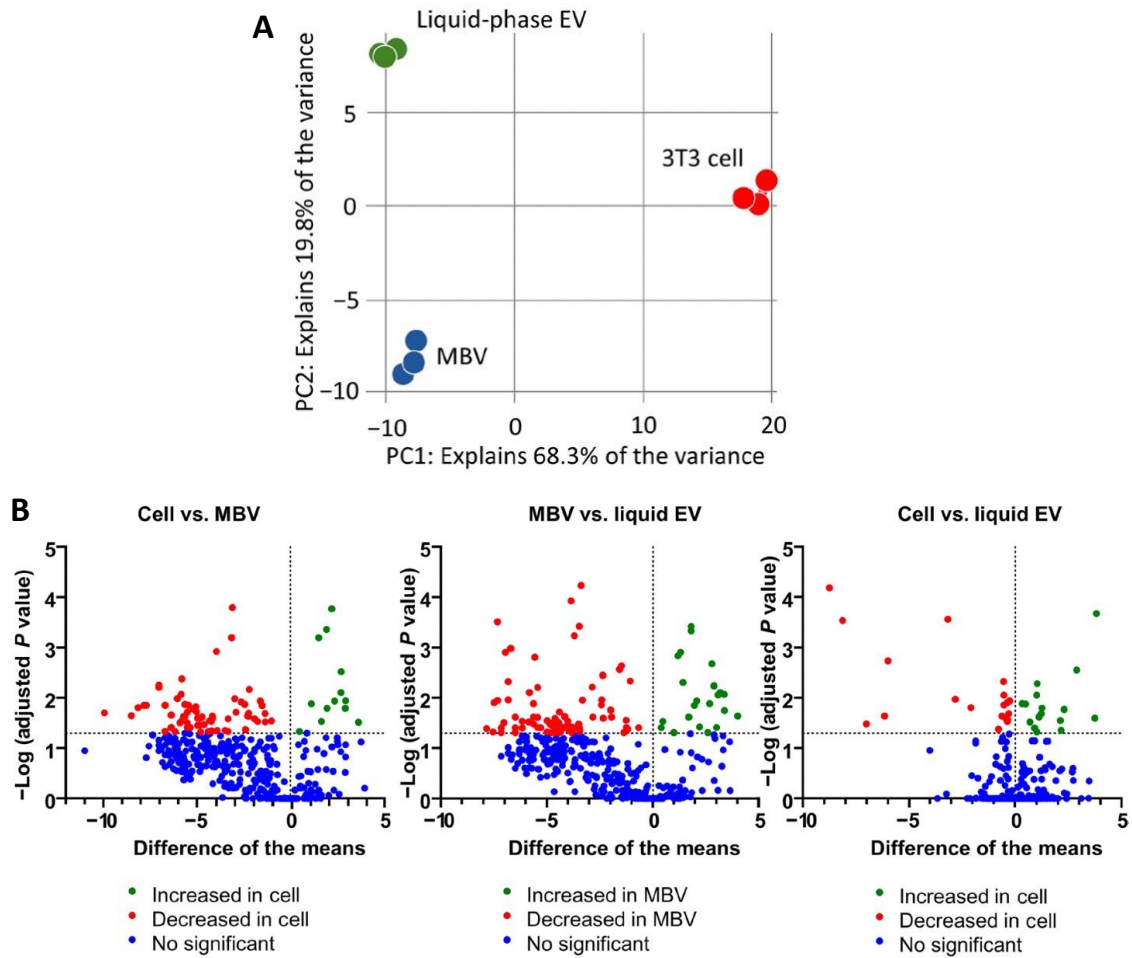


Figure 8. miRNA cargo is selectively packaged into liquid-phase EV and MBV.

(A) Principal components analysis (PCA) comparing liquid-phase EV (green), MBV (blue), and cellular (red) RNA-seq datasets. (B) Volcano plot showing the differential expression of miRNAs in liquid-phase EV, MBV, and the parental cells. The inclusion criteria were a twofold difference of log₂ (fold change) in either direction with a P value of <0.05. Each dot represents a specific miRNA transcript; green dots to the right of the vertical dashed line correspond to a relative increase in expression level, and red dots to the left correspond to a relative decrease in expression level. Blue dots indicate miRNA with no significant change in expression level. (N = 3)

signatures by conducting next-generation sequencing of miRNA libraries generated from the parental cellular RNA, the liquid-phase EV, and the MBV isolates (n = 3 per group). Principal components analysis (PCA) showed that within respective groups, the replicate miRNA profiles clustered close to one another (Figure 8A). However, extensive differences in miRNA content were observed between the parental cell and the liquid-phase EV and MBV isolates. Overall, 28 (50.91%) miRNAs were found to be differentially expressed in MBV compared to liquid-phase EV by at least twofold (Figure 8B). In addition, respective liquid-phase EV or MBV and the parental cellular miRNA profiles were clearly distinct (Figure 8A and B).

5.3.1 MBV Vary with Cell Source

5.3.1.1 Cell Source Does Not Affect MBV Size

Nanoparticle tracking analysis was first used to determine the size of MBV from distinct cellular origins. BMSC-, ASC-, and UCSC-derived MBV showed similar size distribution plots, with the majority of vesicles having a diameter of <200 nm (Figure 9).

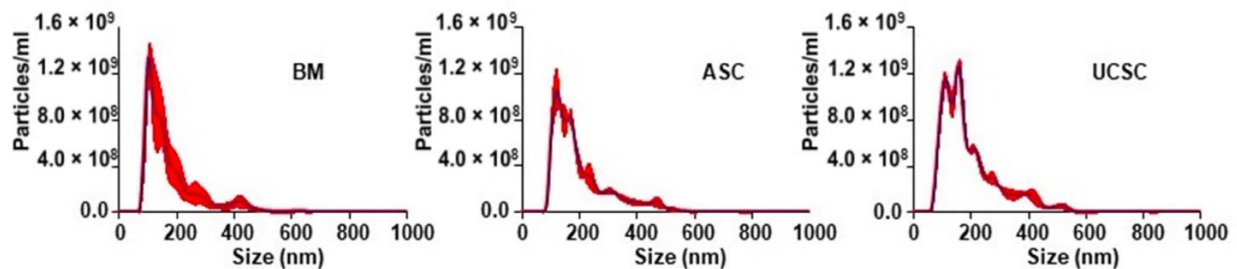


Figure 9. MBV from unique cellular origins are similar in size.

Size distribution plots from NTA of MBV isolated from BMSC, ASC, and UCSC decellularized culture plates.

5.3.1.2 MBV miRNA Cargo Varies with Cell Source

We next sought to determine whether MBV miRNA cargo is unique to the cellular origin. We characterized and compared the miRNA composition of MBV isolated from ECM produced *in vitro* by BMSC, ASC, or UCSC isolated from different human donors using next-generation sequencing methods. miRNA libraries were generated from the samples (BMSC, n = 3 human donors; ASC, n = 3 human donors; UCSC, n = 3 human donors) and subjected to miRNA sequencing. PCA showed that samples clustered primarily by the cell type from which they were derived (Figure 10A). Of note, despite the use of three separate human donors for each cell type used to generate the MBV samples, the PCA showed a high degree of homogeneity in the miRNA profile within the respective groups (Figure 10A). In addition, volcano plots showed that fewer miRNAs were found differentially expressed between BMSC- and UCSC- derived MBV than between BMSC-ASC and UCSC-ASC (Figure 10B).

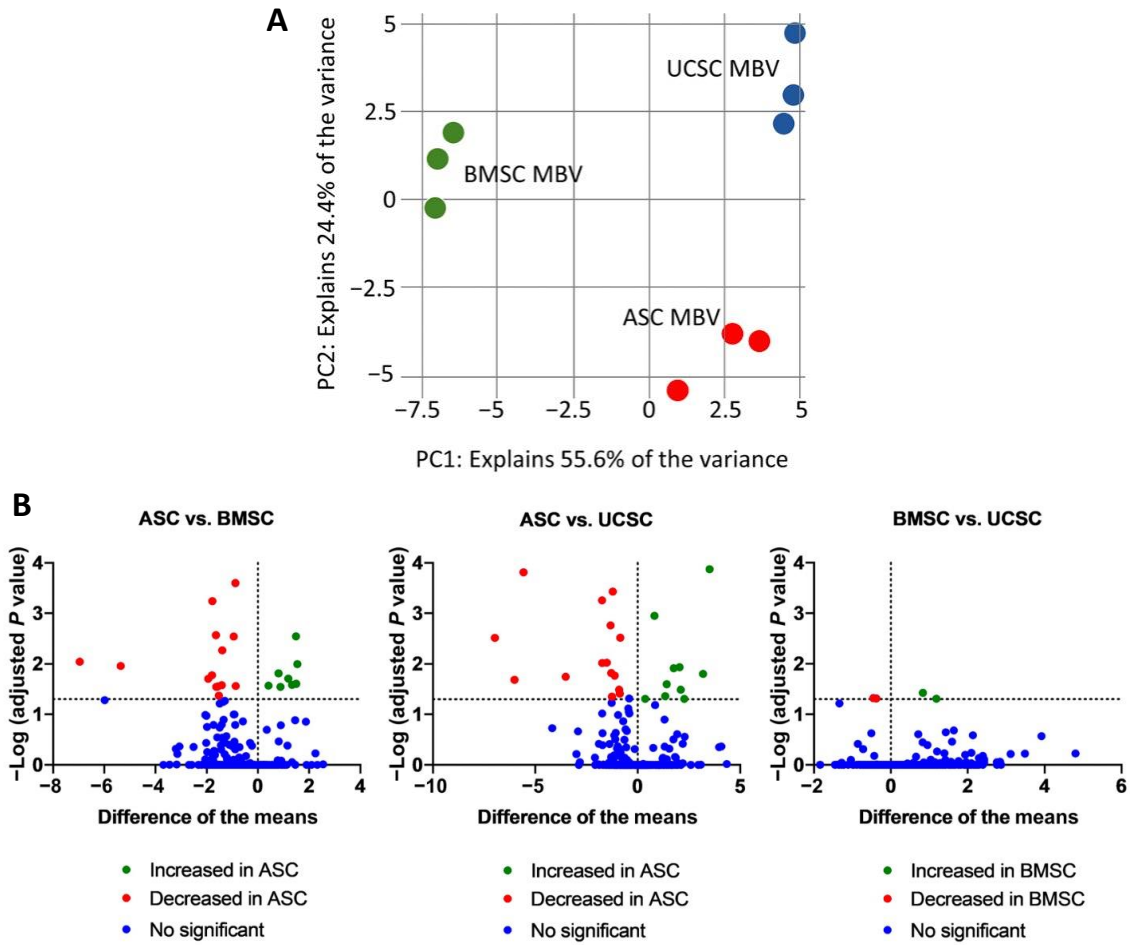


Figure 10. MBV miRNA content varies with cell source.

(A) PCA comparing BMSC MBV (green), UCSC MBV (blue), and ASC MBV (red) RNA-seq datasets. (B) Volcano plot showing the differential expression of miRNAs in BMSC-, ASC-, and UCSC-derived MBV. The inclusion criterion was a twofold difference of \log_2 (fold change) in either direction with a P value of <0.05 . Each dot represents a specific miRNA transcript; green dots to the right of the vertical dashed line correspond to a relative increase in expression level, and red dots to the left correspond to a relative decrease in expression level. Blue dots indicate miRNA with no significant change in expression level. (N = 3)

5.3.2 MBV Change with Disease

5.3.2.1 MBV Size and Abundance are Similar with Heart Disease

Nanosight particle tracking analysis was used to determine the size distribution of MBV isolated from healthy and failing left ventricular tissue. Vesicles from both healthy and failing hearts ranged in size from approximately 75 – 300 nm, consistent with the size of other MBV populations (Figure 11A) [152,186]. Comparison of the mode diameter across vesicles isolated from all patients showed a significantly larger diameter in MBV from failing hearts, but the difference was small (114 nm in healthy vs. 135 nm in failing) (Figure 11B). The MBV yield per starting tissue weight was calculated to determine the relative abundance of MBV in healthy and failing hearts. There was no difference in the MBV abundance during disease (Figure 11C).

5.3.2.2 MBV Protein Cargo Changes with Disease

An immunoblot array for 111 different cytokines was used to determine if the protein cargo of MBV varies with disease state. Visualization of the percent relative expression of all cytokines evaluated using a heat map showed distinct differences in the protein profiles of MBV from healthy and failing hearts (Figure 12A). Quantification of some of the top differentially expressed cytokines showed significantly increased expression of apolipoprotein A-1 in MBV from patients with heart failure and of C-reactive protein in MBV from healthy patients (Figure 12B).

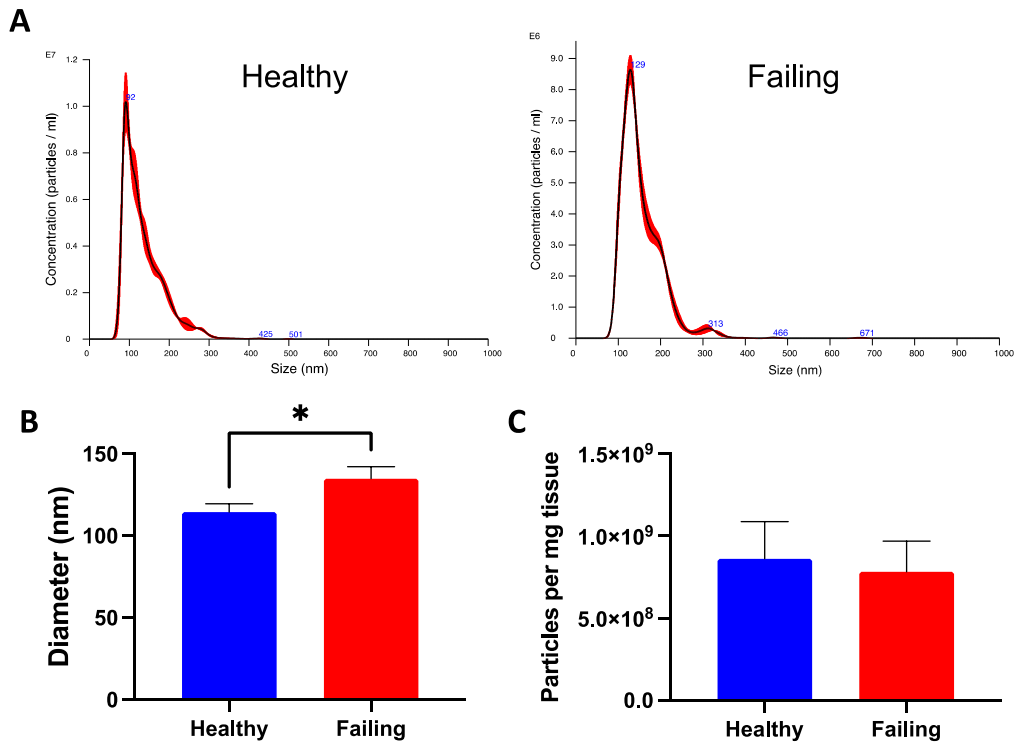


Figure 11. MBV size and abundance are similar with heart disease.

(A) Representative size distribution plots from nanoparticle tracking analysis. (B) Mode MBV diameter across MBV isolated from all patients. (C) Quantification of the MBV particle yield per weight of starting tissue. All values represent mean \pm SEM (N = 6)

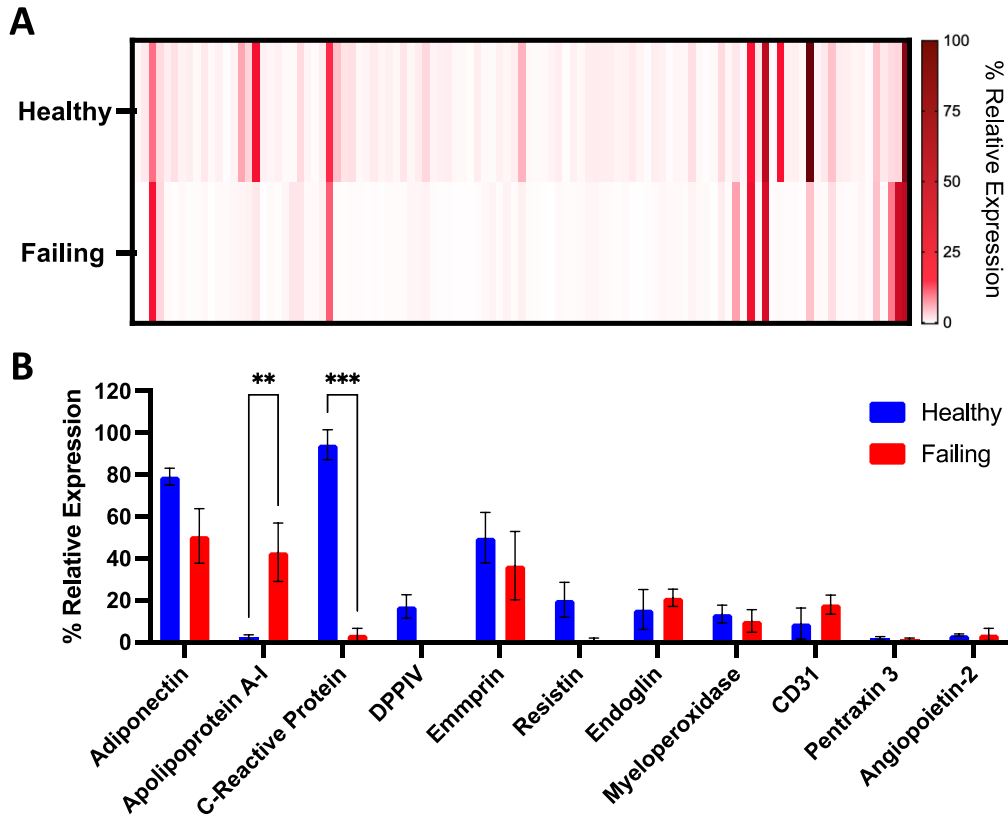


Figure 12. MBV protein cargo changes with disease state.

Quantification of an immunoblot array of 111 different cytokines. (A) Heat map depicting the relative expression of all cytokines measured. (B) Quantification of the top 11 differentially expressed cytokines shows significant differences in protein cargo between MBV from healthy and failing hearts.

All values represent mean \pm SEM (N = 4)

5.3.2.3 MBV miRNA Cargo Changes with Disease

Next generation sequencing was used to characterize differentially expressed miRNA contained within MBV from healthy and failing human hearts. A total of 687 unique miRNA were detected within the samples. Of the detected miRNA, 5% (34/687) had significantly different expression between healthy and failing MBV. A volcano plot of the differentially expressed miRNA showed that the majority of the significant miRNA were upregulated in MBV from healthy patients and only 3 miRNA had higher expression in failing MBV (Figure 13).

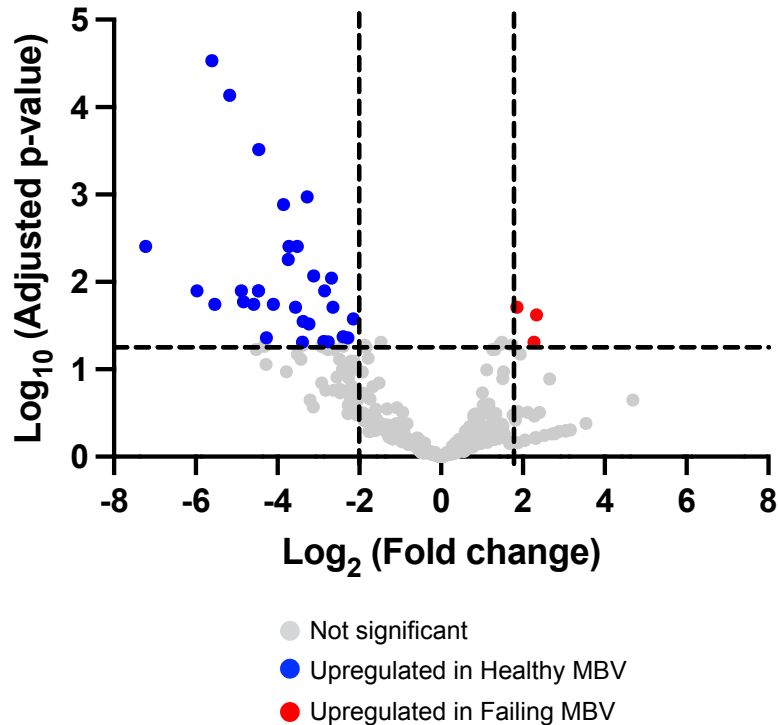


Figure 13. miRNA cargo of MBV changes with disease state.

Volcano plot of expressed miRNA in diseased vs. healthy MBV. The x-axis represents the log₂ conversion of the fold change and the y-axis represents the log₁₀ conversion of the p-value. miRNA with significant differential expression are in blue and red. (N = 6)

Some of the top differentially regulated miRNA are shown in Table 4, with miRNA enriched within failing MBV in red and those enriched in healthy MBV shown in blue. Ingenuity Pathway Analysis (IPA) of miRNA cargo showed their involvement in inflammatory diseases, organ abnormalities and dysfunction, cardiovascular system development and function, and cardiotoxicity pathways (Figure 14). Further, 149 of the detected miRNAs have known targets to 294 mRNAs involved in Cardiovascular Signaling pathways.

Table 4. miRNA name, fold change, and p-value for a subset of the top differentially expressed miRNA.
miRNA in red are upregulated in failing MBV and miRNA in blue are upregulated in healthy MBV.

| Name | Fold Change | P-value |
|-------------|-------------|----------|
| miR-335-5p | 5.05 | 2.38E-02 |
| miR-654-3p | 4.84 | 4.92E-02 |
| miR-100-5p | 3.61 | 1.95E-02 |
| miR-223-3p | -4.42 | 2.65E-02 |
| miR-4516 | -4.86 | 4.38E-02 |
| miR-185-3p | -9.37 | 3.04E-02 |
| miR-4508 | -9.70 | 1.07E-03 |
| miR-1260b | -10.37 | 2.82E-02 |
| miR-378i | -13.19 | 3.93E-03 |
| miR-378a-3p | -13.31 | 5.52E-03 |
| miR-619-5p | -14.46 | 1.30E-03 |
| miR-490-5p | -17.22 | 1.81E-02 |
| miR-206 | -19.34 | 4.38E-02 |

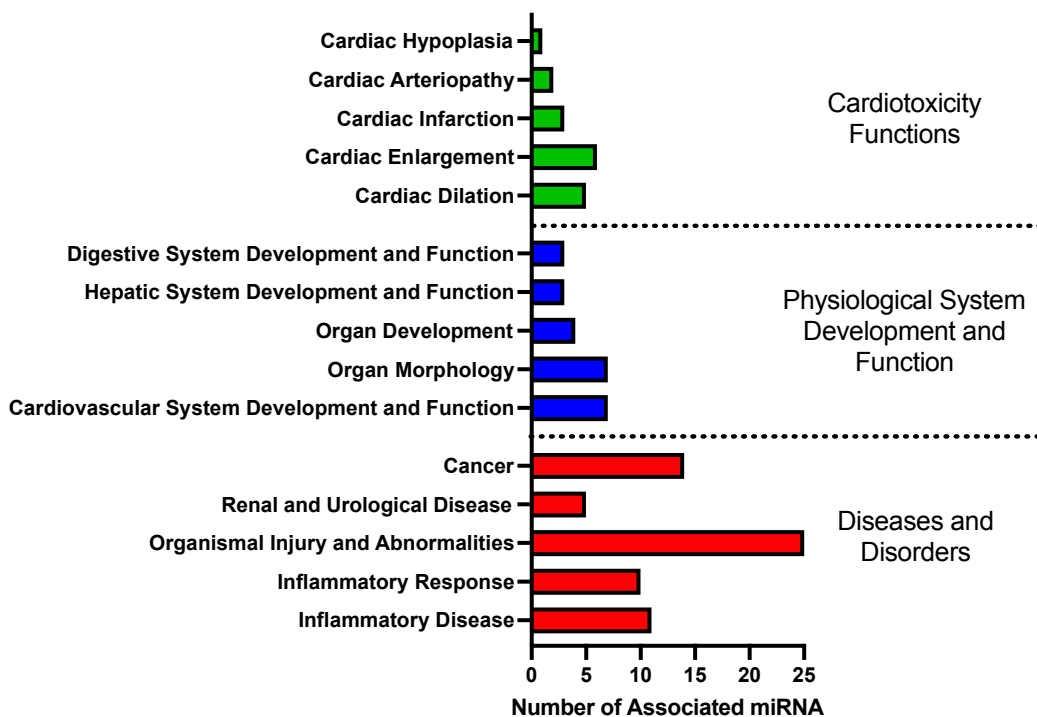


Figure 14. Top pathways regulated by healthy vs. failing MBV miRNA cargo.

Top diseases and biological functions, physiological system development and function, and cardiotoxicity functions associated with healthy vs. failing MBV miRNA cargo as determined by IPA analysis.

5.4 Discussion

The heterogenous population of EV has generally been categorized into subpopulations based on size, biogenesis, and biochemical composition. Exo (30-250nm) [177], cMV (30-400nm) [194], and MBV (50-400nm) [152] share significant overlap in size, and therefore this characteristic alone is of minimal value in distinguishing the subclass of EV. In addition to size, numerous studies have shown that Exo and cMV have similar protein and lipid composition [195–197], however, MBV have yet to be included in these comparative studies. The present study first compared the size, physical characteristics, protein, lipid, and miRNA composition of murine

cMV, Exo and MBV. Although the three types of EV have similar size and physical characteristics, the other measured criteria showed distinguishing features of the EV, especially MBV. Differences in protein markers and lipid composition were most marked with MBV, while the compositional differences between cMV and Exo were more modest. The small differences between Exo and cMV based on protein and lipid composition suggests that these two classes of EV are more similar to each other than different from each other.

EV are commonly associated with proteins having a broad range of functions including membrane organization (e.g. tetraspanins CD81, CD63, and Flotilin 1), chaperone activity (e.g. HSP70), cell adhesion (ICAM, EpCAM), intracellular trafficking (annexins), and biogenesis factors (e.g. ALIX and TSG101) [175,193]. Enrichment of these proteins was once considered the benchmark for classification as exosomes, but subsequent studies have shown expression in other subpopulations of EV, including cMV [196,197]. As expected, evaluation of a panel of these exosome-associated proteins showed high expression levels in plasma-derived Exo and cMV samples. MBV derived from 3T3-cell deposited ECM *in vitro* also showed lower expression of these panels relative to fluid-phase Exo isolated from the same cell type. Consistent with previous studies [152,186], MBV showed low expression of proteins commonly attributed to exosomes, supporting the concept that MBV are a distinctly separate subpopulation of EV. In this part of the study, MBV from skeletal muscle were most closely associated with myeloperoxidase which was also detectable in heart and intestine MBV [163]. Though myeloperoxidase is most commonly thought of as an antimicrobial peroxidase produced by leukocytes, it can also be produced by fibroblasts and direct collagen synthesis suggesting a role for this cargo protein in MBV function [198,199]. The minimal levels of proteins associated with the endosomal origin of exosomes, such as CD63, CD81 and TSG101 [177] in MBV, suggests a different biogenesis pathway.

cMV expression of mineralization-promoting proteins such as Annexin V and TNAP is essential for their function as a nucleation site for bone formation [200–204]. Consistent with a role in bone formation, cMV were also enriched in proteins associated with bone metabolism and regulation of mineralization: osteoprotegerin [205] and osteopontin [206,207]. Plasma Exo expressed similar levels of Annexin V to cMV but were devoid of TNAP, the other cMV marker evaluated. Annexin V has previously been cited as a marker of exosomes, cMV, and generic small EV, which consistent with the equivalent expression of Annexin V found in Exo and cMV samples in the present study [178]. The low expression of Annexin V and absence of TNAP in MBV signifies both the uniqueness of the MBV subpopulation and the importance of tissue source in dictating characteristics of each EV subpopulation. That is, the ECM of mineralizing tissues contain mineralization-competent cMV, while MBV found within the ECM of non-mineralizing skeletal muscle tissue are devoid of common pro-mineralization proteins.

Similarly, differences in lipid membrane composition and miRNA cargo between Exo, cMV, and skeletal muscle MBV suggest their divergent physiologic functions. Previous studies have shown that cMV are enriched in acidic phospholipids such as PS [208–210], which is consistent with findings of the present study. PS has a high affinity for calcium ions so is thought to support a stable calcium phosphate-phospholipid complex, specifically when PS is present in the inner leaflet [208,211]. MBV membranes on the other hand are enriched in PC, PI, PE, LPC, and LPE—lipid precursors to metabolites with roles in macrophage recruitment and immunomodulation [186,212–215]. These differences in membrane lipid composition and cargo all support the concept that cells have evolved distinctive intracellular pathways, methods for EV export, and physiologic functions for these three EV subpopulations.

In the second aspect of the present study, we found that MBV isolated from the ECM of 3T3 fibroblasts contained a differential miRNA and lipid signature compared with liquid-phase EV and with the parent cell. Recent studies have shown that polarized cells differentially secrete distinct exosomes to the apical and basolateral sides [216] and specific miRNA motifs are involved in exosome sorting and export [217]. The studies herein are suggestive of a similar scenario for MBV in which molecular sorting occurs during vesicle biogenesis and export to specifically distribute miRNA and lipids to vesicles destined for solid-phase vs. liquid-phase extracellular locations.

The lipid composition of MBV and Exo isolated from murine skeletal muscle and plasma, respectively, differed from that observed in MBV and liquid-phase EV (Exo) isolated from murine 3T3 cells *in vitro*. One notable difference was the enrichment of cardiolipin (CL) in 3T3 MBV compared to liquid-phase Exo. Because CL is a unique mitochondria-specific phospholipid localized predominantly in the inner mitochondrial membrane [218], this finding represents a possible link of the MBV biogenesis with the mitochondrial compartment of cells. It has been shown that ether lipids, PE, and PC plasmalogens can facilitate membrane fusion [219] and increase membrane thickness of EV [220,221] and therefore may play a role in nanovesicle uptake by cells. The present study also found that high levels of LPL, hydrolytic metabolites of phospholipids that are bioactive signaling molecules that modulate a variety of physiological responses, including macrophage activation [222], inflammation and fibrosis [223], tissue repair and remodeling [224], and wound healing [225], are a characteristic feature of 3T3-derived MBV. As LPL may act as fusogenic lipids facilitating the transfer of the vesicular contents into cellular targets, this important role of LPL found in MBV should be further explored.

Results from the third aspect of the present study show that MBV isolated from ECM produced *in vitro* by BMSC, ASC, and UCSC derived from different human donors contained a distinctive miRNA signature specific to the cell source. In addition, fewer miRNAs were found differentially expressed between BMSC- and UCSC-derived MBV than between BMSC-ASC and UCSC-ASC, a finding that may be attributed to tissue-specific differentiation potentials of ASC [226]. These findings further underline the cell-specific features of MBV miRNA profiles, which were not significantly affected by the intrinsic variability of donors.

Similarly, the MBV isolated from left ventricles of healthy patients or patients with heart failure showed disease-state dependent changes in the protein and miRNA cargo with high consistency across donors. Significant differences observed in MBV composition with disease across a broad range of ages and pathologies and the established involvement of identified miRNA targets in inflammatory and cardiovascular signaling pathways suggests their ubiquitous importance in progression of heart disease. The distinct cargo components identified between healthy and failing heart MBV suggest pleiotropic effects of MBV on disease progression. For example, MBV isolated from healthy patients had significantly higher levels of C-reactive protein which is increased systemically in both ischemic and nonischemic heart failure and failing hearts had increased levels of the atheroprotective protein apolipoprotein A-1 [227–230]. The contradictory expression of these proteins during heart failure when associated with MBV versus systemically signifies a departure of novel MBV signaling mechanisms from previously established pathways. Of note, MBV isolated from healthy intestinal ECM were also found to contain C-reactive protein which suggests an essential role of this protein in MBV bioactivity and function [163]. Conversely, healthy heart MBV were associated with increased miRNA cargo that support cardiovascular health and failing heart MBV miRNA likely contributes to disease

progression. For example, healthy MBV are enriched for miR-206 which protects against myocardial injury [231] and silences mRNA encoding ADAR and IGF-1 receptor, two proteins associated with heart disease [232,233]. On the other hand, failing MBV have increased miR-335 which silences proteins that regulate cardiac cell contractility and cardiac regeneration, such as paxillin and c-kit [234,235]. Therefore, the specific mechanisms by which MBV contribute to heart failure remains to be elucidated.

One limitation of the first part of the present study is that the plasma derived Exo and skeletal muscle derived MBV represent a heterogenous population of vesicles produced by a range of cell types, while the cMV were produced by a single cell type *in vitro*. In order to eliminate species-specific differences between the populations in this study, it was necessary to use this established *in vitro* model to obtain cMV of mouse origin [187]. While previous studies have shown that some MBV properties (e.g. protein and miRNA cargo) may vary slightly based on tissue source [151], the majority of their cargo as well as their effects on macrophage phenotype are similar among MBV source tissues tested to date.

A limitation of the second aspect of the study is the use of a single cell line to evaluate differences in cargo of liquid-phase EV and MBV produced *in vitro*. The 3T3 fibroblast cell line used in the present study was chosen because it is a well-characterized and widely used cell line in biologic research. Furthermore, results from the RNA-seq and lipidomic analyses showed that multiple replicates of MBV derived from the 3T3 fibroblast model showed a high level of consistency in terms of miRNA and lipid cargo and that this cargo is significantly different from the cargo of the corresponding liquid-phase EV, which supports the fidelity of the results.

The studies evaluating differences in MBV derived from human donors are limited in that all donors were male and varied in age. Differential expression of EV miRNA has been observed in human subjects based on variables including gender [236] and age [237]. Further studies to determine sex and age-related variations in the miRNA cargo of MBV from the stem cell and heart-derived samples are warranted. The study of heart-derived MBV is further limited in that patient matching was not possible given the source and availability of the tissue. Further studies characterizing the temporal changes in MBV cargo throughout the progression of disease from healthy to failure would provide guidance on using MBV cargo as a biomarker.

6.0 The Influence of Matrix Bound Nanovesicle Associated Interleukin-33 On Macrophage Phenotype, Fibrosis and Osteogenesis⁴

6.1 Introduction

The innate immune system, especially macrophage activation, is recognized to play a determinant role in the structural and functional outcome of engineered tissues following implantation [238,239]. Macrophages are highly plastic cells that adopt different phenotypes in response to microenvironmental stimuli. In a simplified paradigm, macrophage phenotype assumes either a pro-inflammatory (M1) state or an anti-inflammatory (M2) state. However, in reality macrophage phenotype spans a spectrum between these two extremes determined by the many biophysical, biochemical, and molecular factors that constitute the local microenvironment [240].

In the context of tissue repair, the pro-inflammatory M1 macrophage phenotype is typically associated with either fibrotic scar tissue formation or a non-healing chronic inflammatory process and a poor downstream outcome [111,113]. In contrast, the anti-inflammatory M2 phenotype is generally associated with tissue repair and a more favorable functional outcome [111,113]. In the context of cardiovascular biomaterials, M1 macrophages have been associated with promoting calcification [67] while M2 macrophages are thought to be protective against it [71].

⁴ Portions of this chapter have been adapted from the following publication:

M.C. Cramer, C. Pineda Molina, G.S. Hussey, H.R. Turnquist, S.F. Badyak. The Influence of Matrix Bound Nanovesicle Associated Interleukin-33 On Macrophage Phenotype, *Tissue Engineering Part A*. Under review.

Biologic scaffolds composed of extracellular matrix (ECM) have been used in several million patients to facilitate a constructive remodeling response for multiple clinical applications [241,242]. ECM bioscaffolds, or more accurately their degradation products, direct functional remodeling of site-appropriate tissue in part by inducing an appropriately timed transition from a pro-inflammatory M1-like to an anti-inflammatory M2-like macrophage response [111,113,148]. The mechanism of this immunomodulatory activity is only partially understood, but it is known that degradation of the bioscaffold with release of signaling molecules is required [128].

The degradation of an implanted ECM scaffold by endogenous proteases produces a complex milieu of signaling molecules including growth factors, cryptic peptides, and the more recently described matrix bound nanovesicles (MBV) [152]. MBV are nanometer-sized lipid bound vesicles embedded within the fibrous structure of the ECM and released upon matrix degradation. Notably, these vesicles, along with their associated protein, lipid, and miRNA cargo, have been shown *in vitro* to recapitulate the immunomodulatory effects of the entire ECM [151]. More specifically, isolated MBV alone have been shown to direct macrophages toward an M2-like anti-inflammatory phenotype and limit fibrosis [151,165]. Although the molecular mechanism of MBV-mediated macrophage activation is not fully understood, recent work has shown that interleukin-33 (IL-33) contained within the lumen of MBV is a critical contributor [163,165]. Specifically, this IL-33 cargo is required for MBV-induced activation of macrophages toward an M2-like phenotype and this activation occurs through a noncanonical, receptor independent mechanism [163].

IL-33 is a member of the IL-1 family that has an N-terminus nuclear localization domain with a chromatin binding motif [243,244]. IL-33 is constitutively expressed in endothelial, epithelial, neuronal and stromal cells [245–249], and its expression can be augmented by

inflammation [246,250,251]. IL-33 lacks a signaling sequence and therefore has generally been regarded as an alarmin that is released following cell damage. Upon release, IL-33 activates the canonical Stimulation-2 (ST2) receptor signaling pathway in a variety of ST2⁺ immune cells to stimulate broad responses including Type I, Type II, and regulatory immune responses [247,252]. Full length IL-33 has also been shown to intrinsically regulate gene expression mediated by its N-terminal domain [246,253–256], however the nuclear function of IL-33 is specific to cell type [257,258]. If nuclear IL-33 affects immune cell gene expression has not been established.

The objective of the present study is to establish if IL-33 delivered via MBV can modulate the gene signature of macrophages following exposure to MBV, and specifically to identify genes regulated in macrophages by IL-33 cargo independent of the ST2 receptor. Given that canonical IL-33/ST2 signaling has also been associated with calcification [259,260] and fibrosis [261], the effect of MBV-associated IL-33 on fibroblast activation and mineralization were evaluated. In addition, the indirect effects of the MBV-induced macrophage secretome on modulating these processes associated with pathologic remodeling were evaluated.

6.2 Methods

6.2.1 Overview of Experimental Design

First, RNA sequencing of wildtype and *st2*^{-/-} macrophages exposed to IL-33⁺ and IL-33⁻ MBV was used to identify genes regulated by MBV-associated IL-33 via the ST2 independent signaling pathway in order to corroborate previous findings [163] and confirm the importance of IL-33 cargo.

The ability of WT and IL-33⁻ MBV to modulate multiple pathologic processes associated with bioprosthetic valve failure were then assessed *in vitro* (Figure 15). The potency of MBV-mediated effects on macrophages was determined by inducing a pro-inflammatory phenotype in macrophages and evaluating the effect of WT or IL-33⁻ MBV on alleviating the phenotype [80,147]. The direct effect of WT or IL-33⁻ MBV and the indirect effect of MBV-induced macrophage phenotype on modulating fibrosis and osteogenesis was also determined. Cardiac fibroblasts were used as the *in vitro* model system for fibrosis and calcification in this aim since valve interstitial cells primarily consist of fibroblast-like cells [262], and cardiac fibroblasts also undergo pathologic processes associated with valve failure including myofibroblast activation [263,264] and osteogenic differentiation [265].

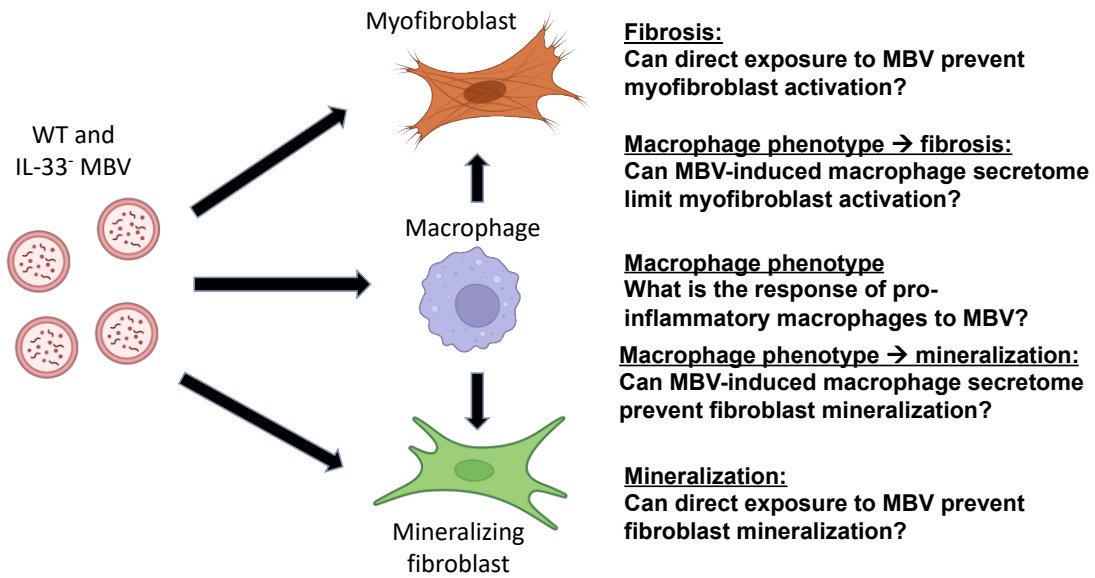


Figure 15. Schematic overview of experiments to evaluate direct and indirect effects of MBV on pathologic processes.

6.2.2 Animals

Wildtype (*wt*) C57BL/6 mice were purchased from Jackson Laboratories. *St2^{-/-}* mice obtained from Dr. Anne Sperling (University of Chicago) were originally generated on a BALB/c background [266] and backcrossed 10 times on a C57BL/6 background prior to use. C57BL/6 *il-33^{-/-}* mice were a gift from S. Nakae (University of Tokyo, Tokyo, Japan) [267]. Animal studies were performed in accordance with all regulations set by the National Institutes of Health and the Animal Welfare Act for use of animals in research.

6.2.3 Isolation of MBV

The small intestine was collected from *wt* or *il-33^{-/-}* mice and washed thoroughly in phosphate buffered saline (PBS) to remove all luminal contents. Small intestine was used as the source of MBV in this study since IL-33 is known to be abundant in mouse intestinal MBV [163]. The tissue was comminuted into 1cm pieces and enzymatically digested with 100 ng/ml Liberase TH (Roche) in buffer (50 mM Tris pH 7.5, 5 mM CaCl₂, 150 mM NaCl) for 12 hr at room temperature. The digested ECM was then subjected to centrifugation at 500 g for 10 min, 2,500 g for 20 min, and 10,000 g for 30 min to remove cell and ECM debris, and the resultant supernatant passed through a 0.22 μm filter. The clarified supernatant was then centrifuged at 100,000 g (Beckman Coulter Optima L-90K Ultracentrifuge) at 4°C for 70 min to pellet the now free nanovesicles. The MBV pellet was resuspended in 1X PBS, aliquoted, and stored at -20°C until further use.

MBV size and concentration was measured using Nanosight nanoparticle tracking analysis (Malvern Panalytical). The Brownian motion of the vesicles was used to determine the size distribution as measured across three replicates of 45 second videos for each sample. For all studies herein, the vesicle dosage was based on particle count as determined by Nanosight.

6.2.4 Isolation and Stimulation of Bone Marrow-derived Macrophages

Bone marrow-derived macrophages (BMDM) were isolated from the tibia and femur of C57BL/6 *wt* and *st2^{-/-}* mice as previously described [142]. Animals were euthanized by CO₂ inhalation and subsequent cervical dislocation in accordance with the guidelines of the American Veterinary Medical Association Panel of Euthanasia. Following euthanasia and the use of aseptic technique, the skin of the inferior legs was completely removed, and the tibia and femoral bones were isolated. Under sterile conditions, the ends of each bone were then transected, and the bone marrow flushed with medium using a 30G needle. Harvested mononuclear cells were seeded at a ratio of 2x10⁶ cells/ml and monocytes were differentiated into macrophages by culture at 37°C and 5% CO₂ for 7 days with macrophage-colony-stimulating-factor (M-CSF)-containing media (DMEM + 10% fetal bovine serum, 10% L929 supernatant, 0.1% beta-mercaptoethanol, 100 U/ml penicillin, 100 ug/ml streptomycin, 10 mM non-essential amino acids, and 10 mM hepes buffer).

Naïve macrophages isolated from *wt* or *st2^{-/-}* mice were exposed to one of the following treatments for 24hr: 1) LPS/IFN γ to derive an M1-like, pro-inflammatory macrophage phenotype, 2) IL-4 to derive an M2-like, anti-inflammatory macrophage phenotype, 3) 20ng/ml recombinant IL-33 (rIL-33), 4) 4.5x10⁹ particles/ml WT MBV, or 5) 4.5x10⁹ particles/ml IL-33⁻ MBV. After 24 hr, RNA was collected with Trizol.

6.2.5 RNA Isolation

Total RNA was extracted from stimulated macrophages with 800 μ l Trizol reagent using a cell scraper. The solution was mixed with 200 μ l chloroform, vortexed for 15 seconds and centrifuged at 12,000 g for 10 min. The aqueous phase was transferred to a new tube and the RNA precipitated with 3M sodium acetate (1/10 of the volume) and isopropanol (1 volume), followed by centrifugation at 18,000 g for 20 min. RNA was purified by washing the RNA pellet in 75% ethanol with an additional centrifugation at 18,000 g for 15 min. The RNA pellet was air dried and re-suspended in nuclease-free water. The concentration and purity were measured by NanoDrop and Agilent Bioanalyzer 2100, respectively.

6.2.6 RNA-Sequencing and Bioinformatic Analysis

Library preparation and next-generation RNA sequencing was completed by the Genomics Research Core at the University of Pittsburgh. Bioinformatic analysis was performed by Genevia Technologies (Tampere, Finland). A pipeline in TrimGalore was used to automate quality control by FastQC and adapter trimming by cutadapt. Reads with a minimum length of 35bp after trimming were used for downstream analysis. Trimmed reads were aligned to the mouse reference genome (GRCm38) and gene-level counts were obtained simultaneously. The *DESeq2* package in R [268] was used to normalize read counts and perform downstream analysis. The Core Analysis function of Ingenuity Pathway Analysis (IPA) software was used to determine the functional relevance of genes differentially regulated by IL-33 cargo.

6.2.7 qPCR Validation

To validate 16 of the top genes significantly regulated by MBV IL-33 cargo, 1000 ng of isolated RNA was converted to cDNA using the SuperScript IV First Strand Synthesis System (Invitrogen). Using a QuantStudio system machine, the qPCR was performed with the TaqMan Fast Advanced Master Mix and TaqMan Advanced Assays for mouse GPR34, Retnlg, Slco2b1, CD28, INPP5J, Klkb11, IL6, SHISA3, Nrnx2, MARCO, SYT7, IL12A, IL19, CD69, CCL4, and CSF3. Mouse hprt1 was used as the house keeping gene and fold change of WT MBV relative to IL-33⁻ MBV for each macrophage source using the $\Delta\Delta\text{Ct}$ method. A 2-way Analysis of Variance (ANOVA) was used to determine statistical significance of the $\log_2(\text{fold change})$ of WT MBV versus IL-33⁻ MBV treatment in each macrophage genotype.

6.2.8 Evaluation of MBV Effect on Inflammatory Macrophages

Two treatment schemes were used to evaluate the effect of WT and IL-33⁻ MBV on pro-inflammatory macrophages (Figure 16). In the first, macrophages were first activated to a pro-inflammatory phenotype by exposure to LPS/ IFN γ for 6 hr, washed with PBS, and then treated for 18 hr with 1) MCSF, 2) WT MBV, or 3) IL-33⁻ MBV. The second scheme simultaneously exposed macrophages to LPS/ IFN γ and WT MBV or IL-33⁻ MBV for 24 hr to determine if MBV can prevent pro-inflammatory macrophage activation. The phenotype of macrophages was evaluated by immunolabeling.

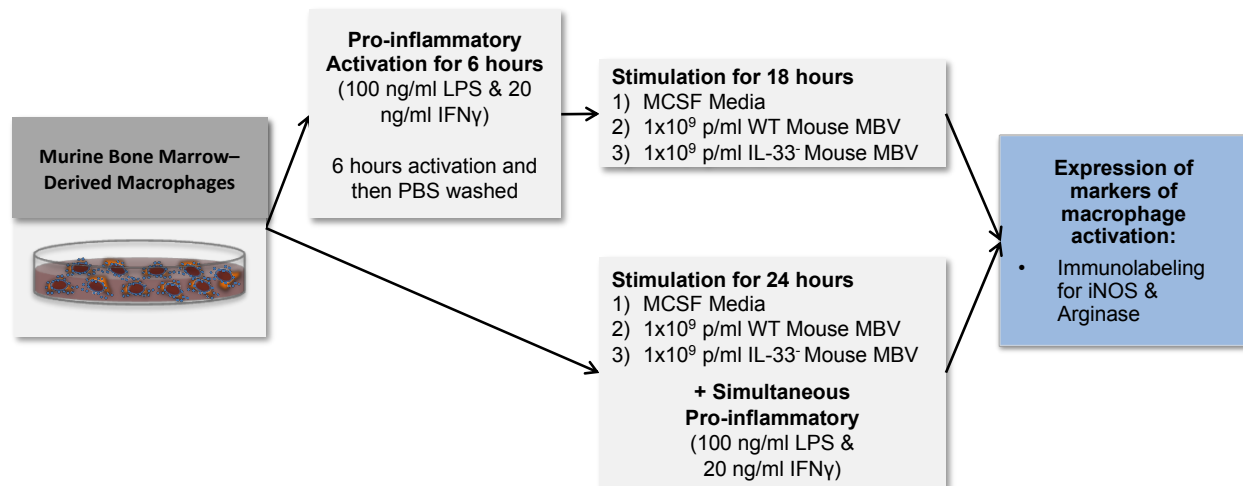


Figure 16. Schematic overview of experiments to characterize MBV effect on inflammatory macrophages.

6.2.9 Immunolabeling of Stimulated Macrophages

Primary antibodies recognizing a panel of markers associated with naïve macrophages (F4/80), pro-inflammatory (iNOS) and anti-inflammatory (Arginase) macrophage phenotype were used to characterize the macrophages. After the stimulation period, the cells were washed with PBS and fixed with 2% paraformaldehyde. Macrophages were immunolabeled as previously reported [143]. Briefly, the cells were incubated in blocking solution (PBS, 0.1% Triton-X, 0.1% Tween-20, 1% goat serum, and 0.1% bovine serum albumin) for 1 hour. The incubation with the primary antibodies was carried out for 16 hours at 4°C. The fixed cells were then washed in PBS and incubated with fluorophore-conjugated secondary antibodies for 1 hour. The cells were washed and counterstained with 4'6-diamidino-2-phenylindole (DAPI). Three images of the immunolabeled macrophages under each condition were acquired using an inverted fluorescent microscope and quantified using CellProfiler software analyzer.

6.2.10 Characterization of Fibroblast to Myfibroblast Transition

Activation of cardiac fibroblasts to myofibroblasts was induced with exposure to angiotensin II [269,270] (Figure 17). Primary rat cardiac fibroblasts were exposed to one of the following treatments in DMEM with 0.5% FBS: 1) no treatment control, 2) 1uM Ang II, 3) 1uM Ang II + WT MBV, or 4) 1uM Ang II + IL-33⁻ MBV to determine the direct effect of MBV on fibroblast activation. To evaluate the indirect macrophage-mediated effects, fibroblasts were treated with a 1:1 mixture of DMEM + 0.5% PBS and conditioned media from macrophages treated with: 1) MCSF, 2) LPS/ IFN γ as an M1-like macrophage control, 3) IL-4 as an M2-like macrophage control, 4) WT MBV, or 5) IL-33⁻ MBV. After 48hr, the activation state was determined by immunolabeling for collagen I and α SMA. Protein expression was quantified using CellProfiler.

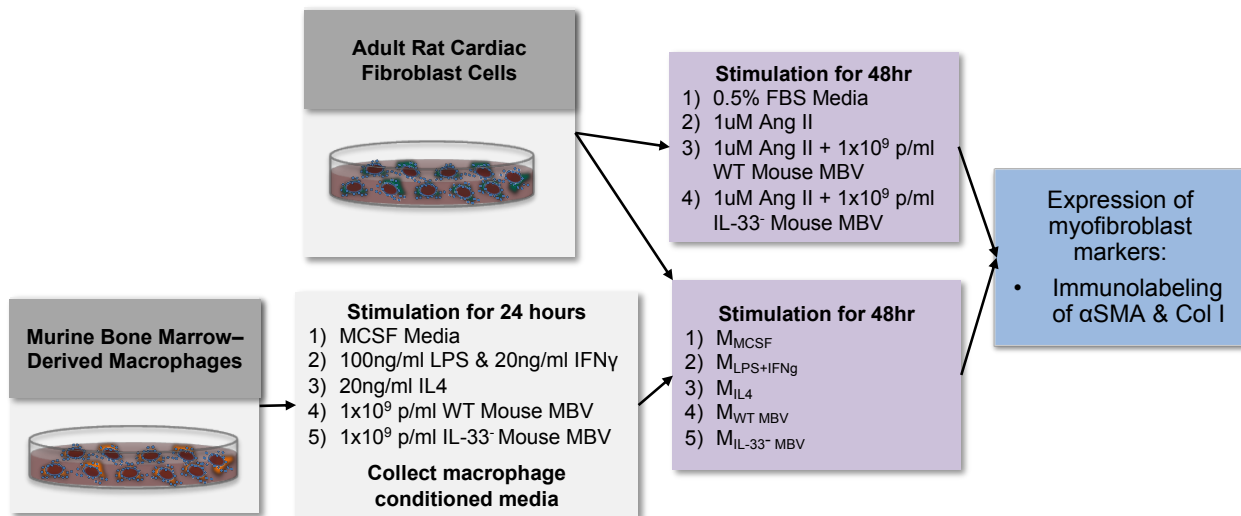


Figure 17. Schematic overview of experiments to evaluate myfibroblast activation.

6.2.11 Characterization of Osteogenic Differentiation of Fibroblasts

Osteogenic differentiation of cardiac fibroblasts was induced based on a previously published method [271], with minor modifications (Figure 18). Primary rat cardiac fibroblasts were treated with one of the following in α MEM + 10% exosome-free FBS: 1) no treatment control, 2) osteogenic supplements (OS, 50 μ M L-ascorbic acid, 10nM dexamethasone, 3mM sodium phosphate), 3) OS + WT MBV, 4) OS + IL-33⁻ MBV to determine the direct effect of MBV on fibroblast osteogenesis. A 1:1 mixture of α MEM + 10% exosome-free FBS and conditioned media from macrophages treated with: 1) MCSF, 2) LPS/ IFN γ as an M1-like macrophage control, 3) IL-4 as an M2-like macrophage control, 4) WT MBV, or 5) IL-33⁻ MBV was used to determine the indirect effect of macrophage immunomodulation. Fibroblasts were maintained for 3, 5, or 7 days. Osteogenesis was evaluated by gene expression (ENPP1, OCN, ALP, Runx2, OSX), alizarin red staining, and calcium quantification.

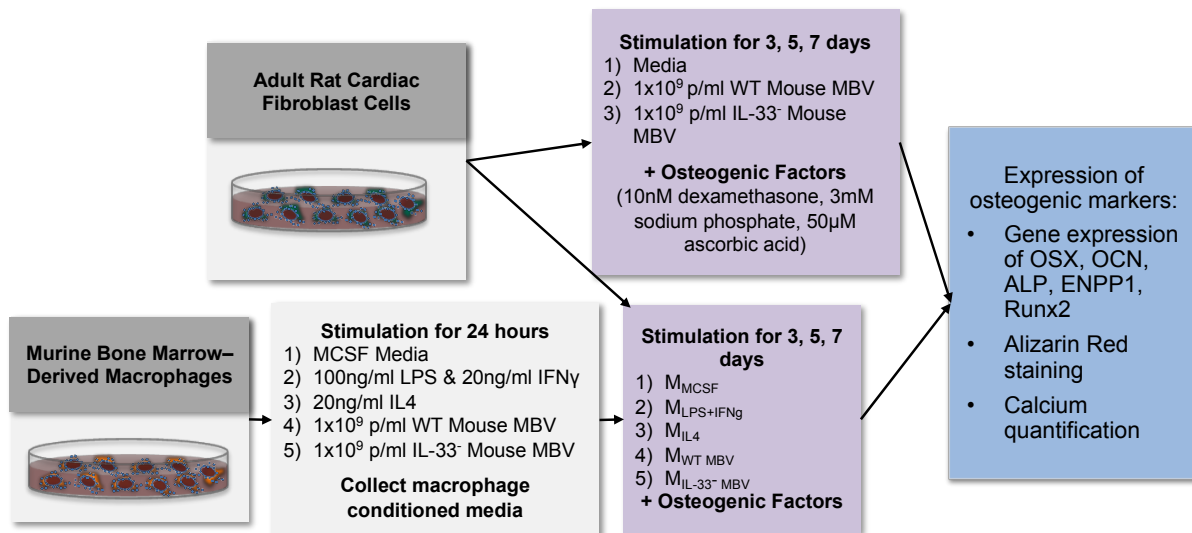


Figure 18. Schematic overview of experiments to evaluate MBV effects on osteogenesis.

6.2.12 Statistical Analysis

A two-way analysis of variance (ANOVA) was used to determine statistical significance ($p < 0.5$) of the treatments for each cell type. Post-hoc analysis with either Tukey or Sidak correction determined significant comparisons between groups. All statistical analysis was completed with GraphPad Prism. Data is presented as mean \pm standard error of the mean (SEM).

6.3 Results

6.3.1 MBV are Internalized by Macrophages and Deliver IL-33 to the Nucleus

Previous work demonstrated that exposure of macrophages to IL-33⁺ MBV resulted in a pro-remodeling phenotype, although the molecular mechanism was not established [163]. Given its localization in the lumen of MBV, IL-33 was used as an indicator to confirm internalization of MBV cargo by macrophages. Western blot of *il-33*^{-/-} macrophages exposed to IL-33⁺ MBV, but not IL-33⁻ MBV, showed intracellular IL-33 expression by 1hr after treatment that increased in intensity at 6 and 24 hr (Figure 19A). To further determine the subcellular localization, cytosolic and nuclear fractions of *il-33*^{-/-} macrophages were extracted following exposure to IL-33⁺ MBV. Intracellular IL-33 was again detected at 1hr, with the majority of IL-33 within the cytosolic extract. At 6 and 24hr after treatment, IL-33 was increasingly present within the nuclear fraction indicating translocation to the nucleus following delivery by MBV (Figure 19B). The nuclear localization of IL-33 following delivery by MBV suggests that IL-33 may directly bind DNA to direct macrophage activation.

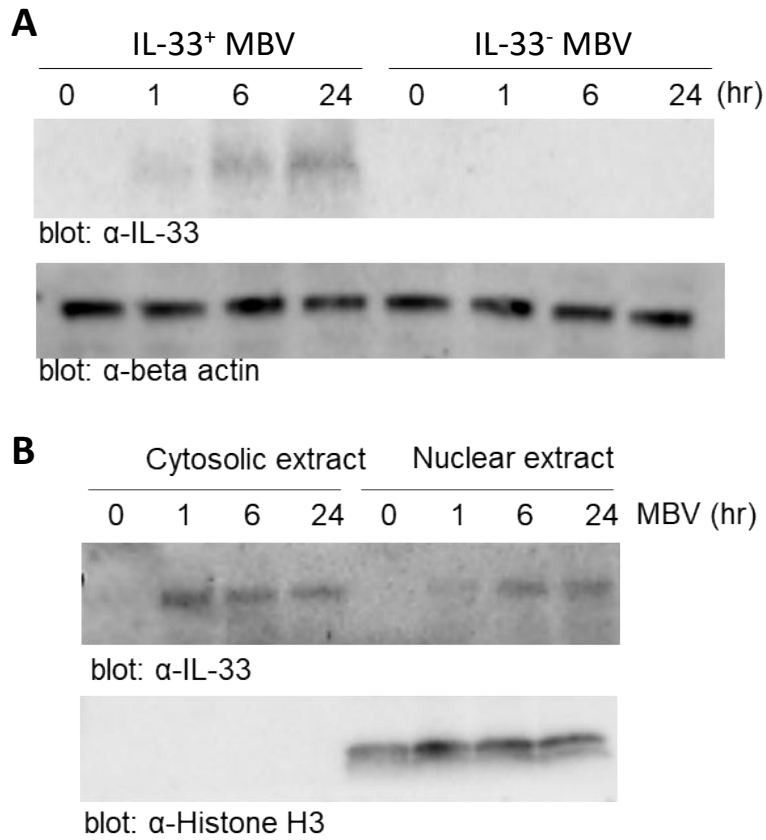


Figure 19. IL-33 translocates to the nucleus after uptake into macrophages.

(A) Bone marrow derived macrophages from *il-33*^{-/-} mice were treated with IL-33⁺ or IL-33⁻ MBV for 0, 1, 6, or 24hr. Cell lysates were analyzed for expression of IL-33 using an immunoblot. (B) Cytosolic and nuclear fractions were extracted from *il-33*^{-/-} macrophages following exposure to IL-33⁺ MBV. Subcellular localization of IL-33 was evaluated with immunoblot and fraction purity was confirmed with Histone H3.

6.3.2 MBV Alter Gene Expression in Macrophages Independently of ST2 Receptor

Next generation RNA-sequencing was used to determine the transcriptomic signature of macrophages following exposure to MBV. Macrophages with (*wt*) and without (*st2^{-/-}*) ST2 receptor were exposed to MBV with (WT) or without IL-33 cargo (IL-33⁻) to determine the genes specifically regulated by ST2-independent signaling by MBV-associated IL-33. Treatment with rIL-33 was also included to identify MBV-specific effects. The number of differentially expressed genes (DEGs), defined as ± 2 -fold change and $p < 0.05$, determined by RNA sequencing analysis for each treatment group are shown in Table 5. Exposure of macrophages to MBV resulted in over 2000 DEGs relative to naïve untreated macrophages, regardless of the macrophage genotype or the IL-33 content of the MBV. Visualization by both principal component analysis (PCA) (Figure 20A) and Pearson's correlation analysis (Figure 20B) showed separation of clusters according to group. The first principal component represented 61% of the variance between samples and showed strong separation based on treatment. The second principal component separated samples according to the genotype of the macrophages (*wt* vs. *st2^{-/-}*), but only represented 11% of the variance of the samples indicating minor contribution of the ST2 receptor to the overall macrophage response. Along the first principal axis, there is a significant effect of MBV treatment compared to naïve untreated macrophages as well as a distinct contribution of MBV IL-33 cargo. In *st2^{-/-}* macrophages the non-treated and recombinant IL-33 treated samples formed two mixed clusters indicating no significant differences between these groups, and the effect of rIL-33 on *wt* macrophages was limited compared to MBV. A Venn diagram was used to compare the genes up and down regulated by WT MBV in *wt* and *st2^{-/-}* macrophages (Figure 20C). Significant overlap in MBV-regulated genes further establishes the ST2 receptor independence of MBV signaling.

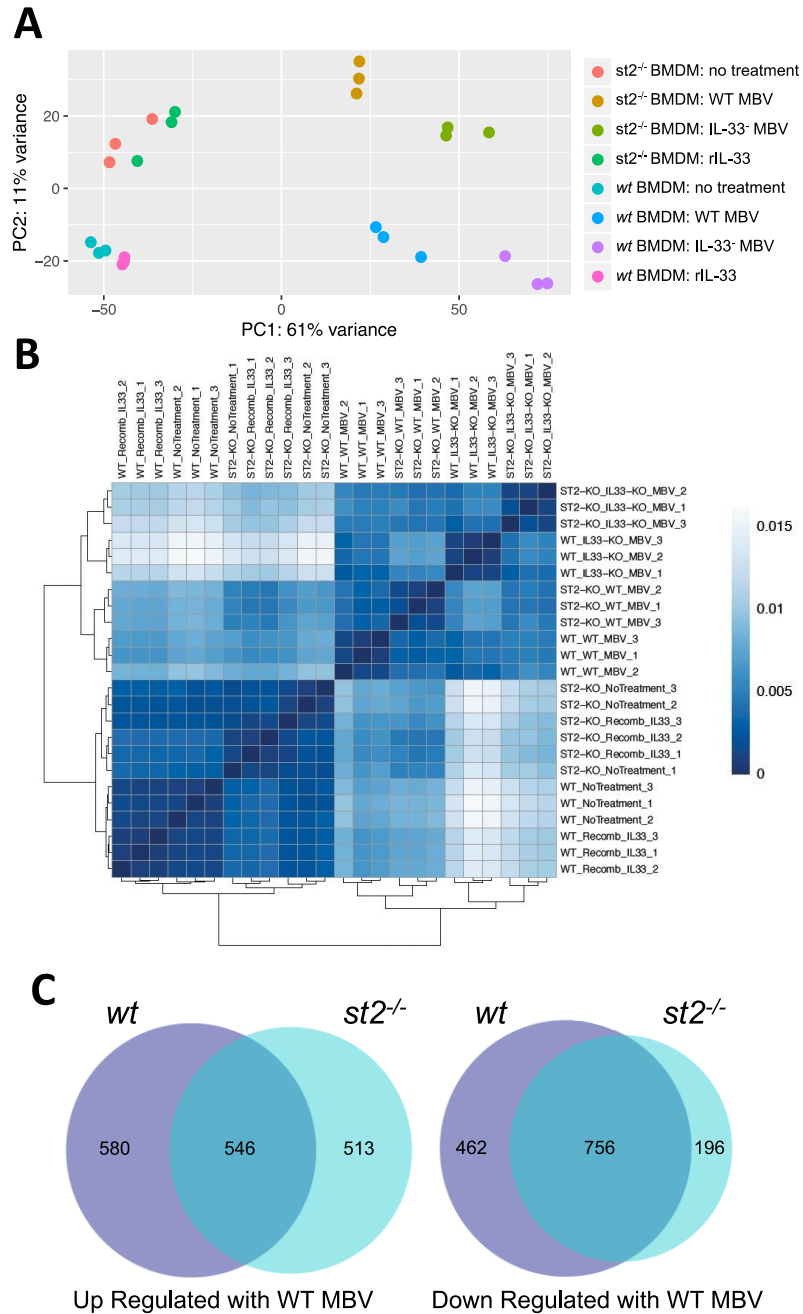


Figure 20. MBV IL-33-induced gene expression in macrophages is independent of ST2 receptor.

(A) Presentation of results of Principal Component Analysis (PCA). The first principal component (x-axis) represents 61% of the variance in the data and the second principal component (y-axis) explains 11% of the variance. (B) Hierarchically clustered heatmap depicting Pearson's correlation distances calculated pair-wise for all samples. (C) Venn diagram comparing up or downregulated genes by WT MBV in *wt* versus *st2*^{-/-} macrophages.

Table 5. Number of differentially expressed genes (DEGs) with $p < 0.05$ between each treatment group.

| Genotype | Comparison | Number of DEGs |
|---------------------------|---|-----------------------|
| <i>wt</i> | WT MBV vs. no treatment | 2344 |
| <i>wt</i> | IL-33 ⁻ MBV vs. no treatment | 4289 |
| <i>wt</i> | rIL-33 vs. no treatment | 74 |
| <i>wt</i> | WT MBV vs. IL-33 ⁻ MBV | 1202 |
| <i>st2</i> ^{-/-} | WT MBV vs. no treatment | 2011 |
| <i>st2</i> ^{-/-} | IL-33 ⁻ MBV vs. no treatment | 3862 |
| <i>st2</i> ^{-/-} | rIL-33 vs. no treatment | 25 |
| <i>st2</i> ^{-/-} | WT MBV vs. IL-33 ⁻ MBV | 1514 |
| Treatment | Comparison | Number of DEGs |
| WT MBV | <i>wt</i> BMDM vs. <i>st2</i> ^{-/-} BMDM | 438 |
| IL-33 ⁻ MBV | <i>wt</i> BMDM vs. <i>st2</i> ^{-/-} BMDM | 1315 |
| rIL-33 | <i>wt</i> BMDM vs. <i>st2</i> ^{-/-} BMDM | 55 |

6.3.3 IL-33 Cargo within MBV Differentially Regulates Gene Expression in Macrophages

Exposure of macrophages to WT MBV and IL-33⁻ MBV enabled identification of genes specifically regulated by MBV-associated IL-33. In total, WT MBV vs. IL-33⁻ MBV treatment resulted in 1202 and 1514 DEGs in *wt* and *st2*^{-/-} macrophages, respectively, suggesting the significance of IL-33 cargo in regulating macrophage activation (Table 5).

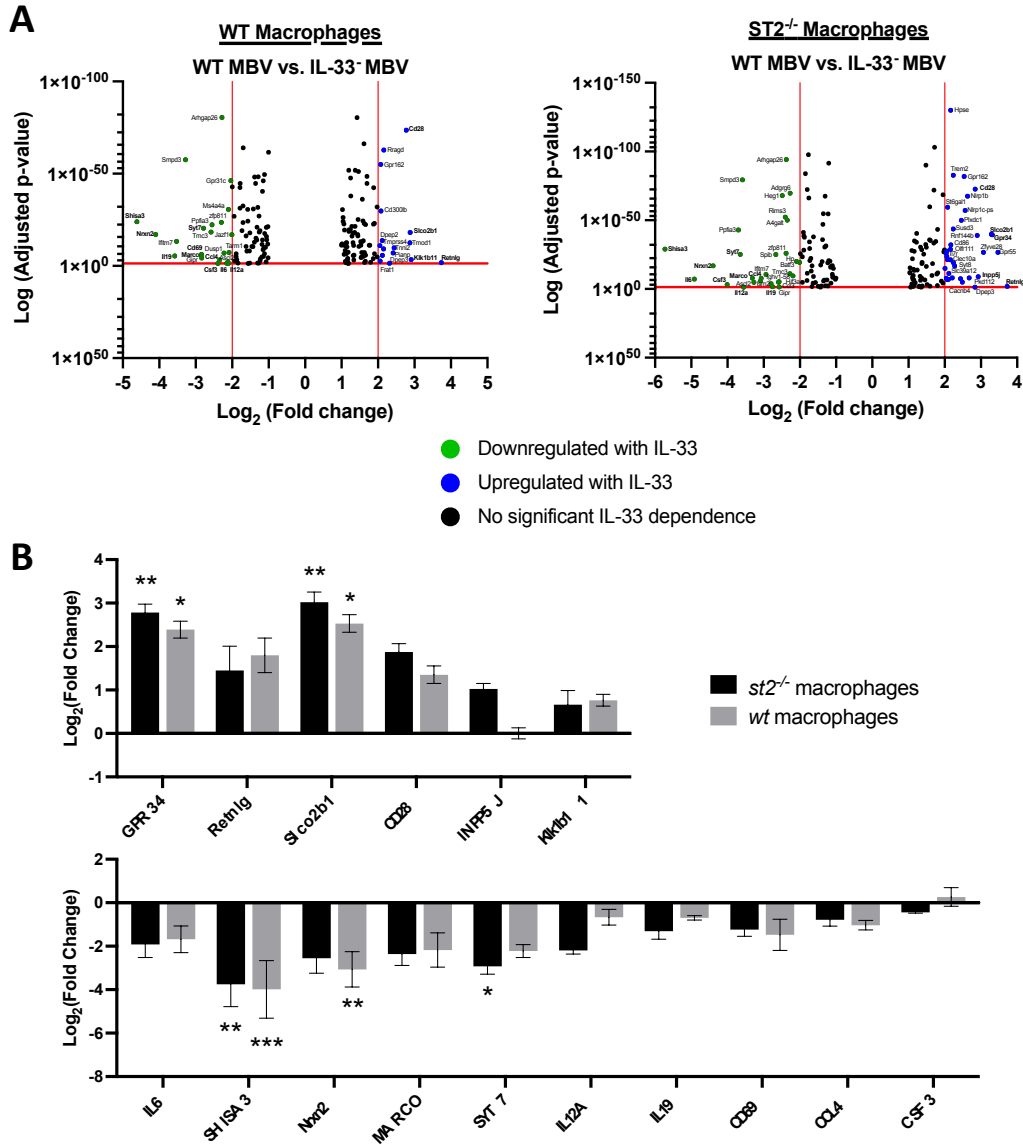


Figure 21. IL-33 content differentially regulates gene expression in macrophages.

(A) Volcano plot of regulated genes in *wt* (left) or *st2^{-/-}* (right) macrophages with the x-axis representing the log₂ conversion of the fold change and the y-axis representing the log₁₀ conversion of the adjusted p-value. Genes that are significantly downregulated with the presence of IL-33 cargo are depicted in green and genes that are significantly upregulated with IL-33 cargo are depicted in blue. Genes that have no significant dependence on IL-33 are shown in black. (B) A subset of 16 genes that are regulated by MBV IL-33 content were validated by qPCR. The log₂(fold change) of gene expression following WT MBV treatment relative to IL-33⁻ MBV treatment in *wt* and *st2^{-/-}* macrophages is shown. All values represent mean ± SEM (N = 3)

Volcano plots of WT vs. IL-33⁻ MBV in *wt* and *st2^{-/-}* macrophages show the genes that are specifically up or down regulated by IL-33 cargo within the MBV (Figure 21A). Validation by qPCR for 6 of the top upregulated and 10 of the top downregulated DEGs of interest confirmed results of the sequencing study and further demonstrated a similar response to IL-33 cargo in macrophages with and without the ST2 receptor (Figure 21B). Genes upregulated in the presence of IL-33 cargo are generally associated with pro-remodeling (M2-like) activity in macrophages while those downregulated are associated with pro-inflammatory (M1-like) effects (Table 6). These results suggest the importance of IL-33 cargo in MBV-mediated promotion of an anti-inflammatory M2-like phenotype in macrophages.

Table 6. Top regulated genes are associated with anti-inflammatory activation of macrophages.

| Gene | Gene Name | Description | IL-33 Trend |
|---------|--|--|-----------------|
| GPR34 | G protein-coupled receptor 34 | Upregulated in IL-4 stimulated M2 macrophages [272] | up with IL-33 |
| RETNLG | Resistin-like gamma, FIZZ-3 | Expressed by alternatively activated M2 macrophages [273] | up with IL-33 |
| SLCO2B1 | Solute carrier organic anion transporter 2B1 | Generally associated with tissue resident macrophages [274] | up with IL-33 |
| CD28 | CD28 antigen | Increased expression in M2-like macrophages and associated with reduced T-cell stimulatory activity [275] | up with IL-33 |
| INPP5J | Inositol polyphosphate 5-phosphatase J | Lipid phosphatase that is a negative regulator of PI3K/AKT signaling [276] | up with IL-33 |
| KLK1B11 | Kallikrein 1-related peptidase b11 | Significantly upregulated by IL-4 in tissue resident macrophages [277] | up with IL-33 |
| IL6 | Interleukin 6 | Pleiotropic cytokine with a role in both resolving acute phase inflammation and stimulating pathological chronic inflammation [278] | down with IL-33 |
| SHISA3 | Shisa family member 3 | Antagonist of Wnt/b-catenin pathway [279], which is expressed in M2 macrophages [280]. Upregulated in kidney resident macrophages that express CD206, but are associated with renal cyst formation [281] | down with IL-33 |
| NRXN2 | Neurexin II | Monocytes have hypomethylation of the CpG site of NRXN2 in ageing [282] | down with IL-33 |
| MARCO | Macrophage receptor with collagenous structure | Class A scavenger receptor that is a marker of M1 macrophages [283] and is downregulated by IL-4 in resident macrophages [277] | down with IL-33 |
| SYT7 | Synaptotagmin VII | Involved in the ability of macrophages to engulf and take up foreign particles for phagocytic degradation [284] | down with IL-33 |
| IL12a | Interleukin 12a | Encodes the p35 chain of IL12, a pro-inflammatory cytokine that activates natural killer cells and induces differentiation of T helper 1 cells that produce IFN γ [285] | down with IL-33 |
| IL19 | Interleukin 19 | Expression of IL19 in monocytes and macrophages is induced by pro-inflammatory stimuli such as LPS [286]. Associated with pro- and anti-inflammatory effects [287] | down with IL-33 |
| CD69 | CD69 antigen | Increased in macrophages following stimulation with LPS, IFN γ and TNF α [288]. Exerts pro-inflammatory function in disease pathogenesis [289] | down with IL-33 |
| CCL4 | C-C motif chemokine ligand 4 | Chemotactic factor for macrophages in the tumor microenvironment [290]. Expressed by M1 macrophages and inhibited by M2 macrophages [137] | down with IL-33 |
| CSF3 | Colony stimulating factor 3 | Encodes for granulocyte colony stimulating factor, a member of the IL6 family that stimulates the survival, proliferation and differentiation of neutrophils [291] | down with IL-33 |

6.3.4 MBV-associated IL-33 Regulates Pathways of the Inflammatory Response

The core analysis function in IPA software (Qiagen) was used to identify the top diseases, canonical pathways, and signaling networks that are associated with DEGs induced by IL-33 cargo within MBV (Figure 22). The top diseases and pathways showed a strong association of IL-33 with the inflammatory response and cell-to-cell signaling. The full list of the top canonical pathways regulated by IL-33 cargo is shown in Figure 22B. Of note, many of the genes regulated by IL-33⁺ MBV have an established role in pathways of T cell differentiation, cellular communication of both the innate and adaptive immune systems, and involvement in autoimmune diseases. Analysis of predicted upstream regulators identified activation of the anti-inflammatory IL10RA pathway and downregulation of pro-inflammatory regulators such as NFκB and TNFα by IL-33⁺ MBV regulated genes (Figure 22C). The repeated association of DEGs stimulated by IL-33 cargo signaling to the inflammatory response highlights the importance of this cargo protein in directing the immune reaction to MBV.



Figure 22. Top pathways regulated by MBV-associated IL-33 are related to the inflammatory response. (A) Top diseases and biological functions, (B) significant canonical signaling pathways, and (C) predicted upstream regulators by WT MBV vs. IL-33⁻ MBV as determined by IPA analysis.

6.3.5 IL-33⁺ MBV can Alleviate and Prevent Pro-inflammatory Activation of Macrophages

Given the ability of MBV to modulate the phenotype of naïve macrophages, the effect of MBV on pro-inflammatory macrophages was also investigated using two different treatment schemes (Figure 16). To determine if MBV can alleviate a pro-inflammatory phenotype of activated macrophages, bone marrow derived macrophages were first stimulated to a pro-inflammatory M1-like phenotype with exposure to LPS and IFN γ for 6hr. The pro-inflammatory stimuli were then removed, and the pre-activated macrophages were exposed to WT or IL-33⁻ MBV for 18 hours. Quantification of the resulting macrophage phenotype with immunolabeling showed that exposure to WT MBV significantly decreased the percentage of M1-like iNOS⁺ cells relative to media and IL-33⁻ MBV (Figure 23).

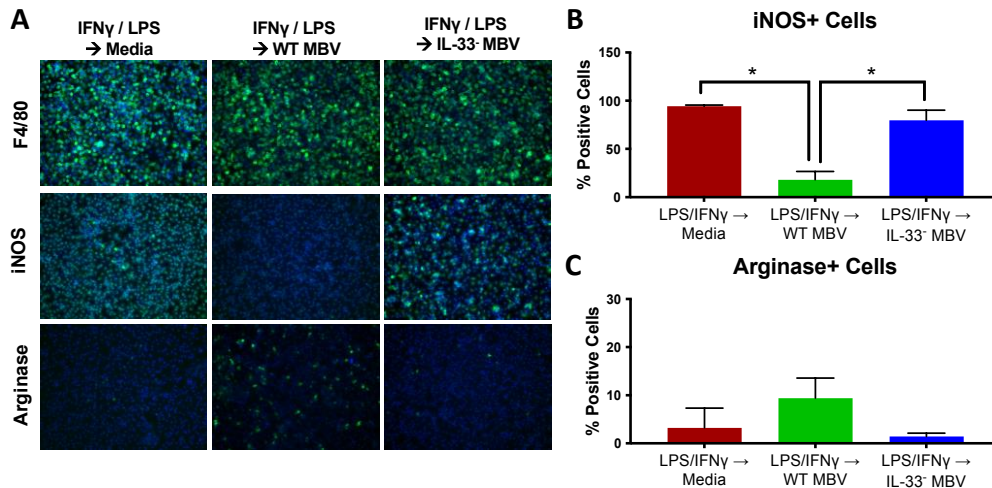


Figure 23. MBV containing IL-33 alleviate a pro-inflammatory macrophage phenotype.

Bone marrow-derived macrophages from wildtype mice were activated toward a pro-inflammatory phenotype with IFN γ /LPS for 6 hours followed by treatment with media, WT MBV or IL-33⁻ MBV for 18 hours. (A) Representative images of F4/80, iNOS and Arginase immunolabeling. Quantification of the percentage of (B) iNOS positive and (C) Arginase positive nuclei as determined with CellProfiler. All values represent mean \pm SEM (N = 3)

In the second treatment scheme, the ability of MBV to prevent pro-inflammatory macrophage activation was evaluated using simultaneous exposure of macrophages to LPS/IFN γ and MBV. The presence of WT MBV not only mitigated iNOS expression but also increased the expression of M2-like macrophage marker Arginase (Figure 24). These results suggest that WT MBV, but not IL-33⁻ MBV, are able to both alleviate and prevent pro-inflammatory activation of macrophages *in vitro*.

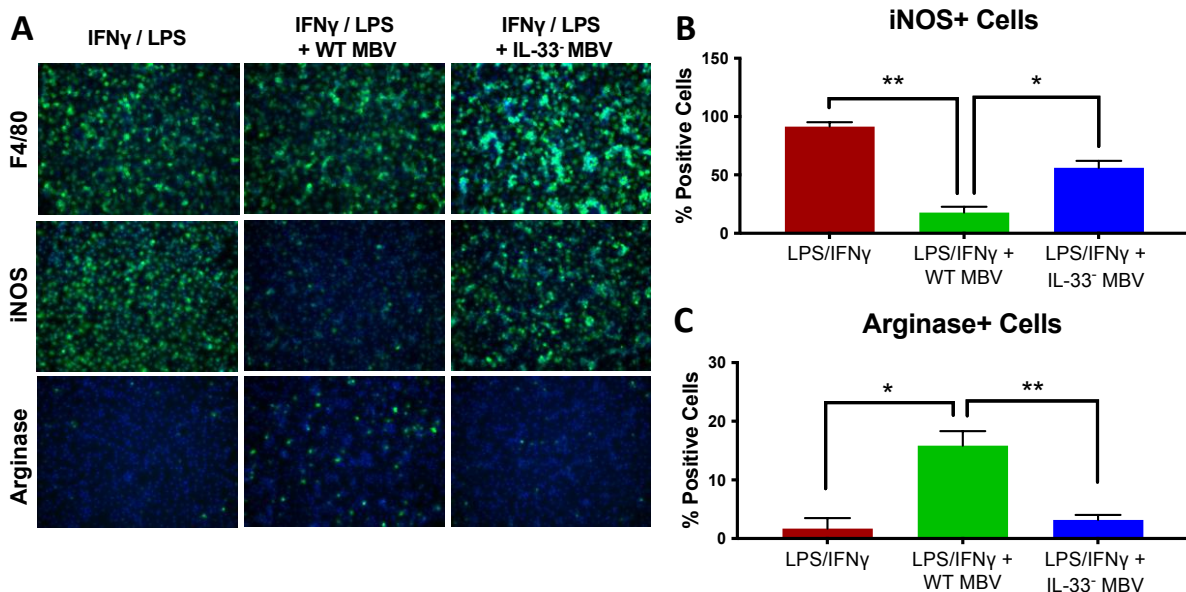


Figure 24. MBV containing IL-33 can prevent pro-inflammatory macrophage activation.

Bone marrow-derived macrophages from wildtype mice were simultaneously stimulated with pro-inflammatory activators IFN γ /LPS and media, WT MBV or IL-33⁻ MBV for 24 hours. (A) Representative images of F4/80, iNOS and Arginase immunolabeling. Quantification of the percentage of (B) iNOS positive and (C) Arginase positive nuclei as determined with CellProfiler. All values represent mean \pm SEM (N = 3)

6.3.6 MBV-Induced Macrophage Secretome Limits Myofibroblast Activation

The ability of MBV to affect the activation of fibroblasts to myofibroblasts was next evaluated both directly and indirectly (i.e., through macrophage mediated effects) (Figure 17). To determine direct effects of MBV on fibroblasts, a myofibroblast-like phenotype was induced with 500nM Angiotensin (Ang) II, and cells were simultaneously stimulated with either WT or IL-33⁻ MBV. Immunolabeling for Collagen I and α SMA were used as indicators myofibroblast activation (Figure 25A). Exposure to Ang II resulted in significantly more α SMA⁺ myofibroblasts compared to media alone. However, simultaneous exposure to WT or IL-33⁻ MBV did not significantly affect the expression of myofibroblast markers (Figure 25B & C).

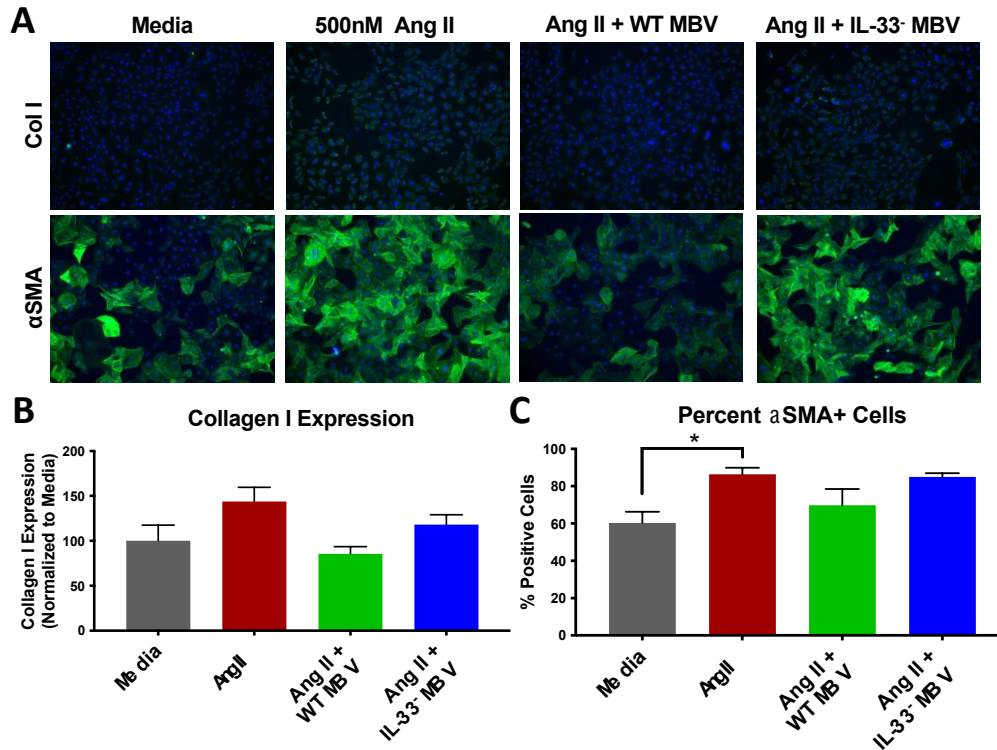


Figure 25. Direct exposure to MBV does not affect myofibroblast activation.

Cardiac fibroblasts were activated toward a myofibroblast phenotype with Angiotensin (Ang) II and simultaneously exposed to either WT or IL-33⁻ MBV. (A) Representative images of collagen I and αSMA immunolabeling. Quantification of the (B) relative intensity of Col I expression normalized to media control and (C) the percent of αSMA positive nuclei as determined by CellProfiler. All values represent mean ± SEM (N = 3)

The indirect effect of the MBV-mediated macrophage phenotype was also evaluated with Col I and αSMA expression. Exposure of fibroblasts to conditioned media from macrophages exposed to WT MBV did not affect αSMA or Col I expression relative to the conditioned media of naïve macrophages (MCSF) (Figure 26). Conversely, the macrophage secretome induced by IL-33⁻ MBV resulted in significantly more αSMA⁺ myofibroblasts relative to both naïve macrophages and WT MBV- treated macrophages. Of note, the effect of WT MBV conditioned media was equivalent to that of M2-like macrophage media, and IL-33⁻ MBV conditioned media

was consistent with M1-like macrophage media. Collagen I expression followed similar trends but did not reach significance. These results indicate that the macrophage secretome induced by WT MBV prevents myofibroblast activation *in vitro* and further corroborates the activation of macrophages toward an M2-like and M1-like phenotype by WT and IL-33⁻ MBV, respectively.

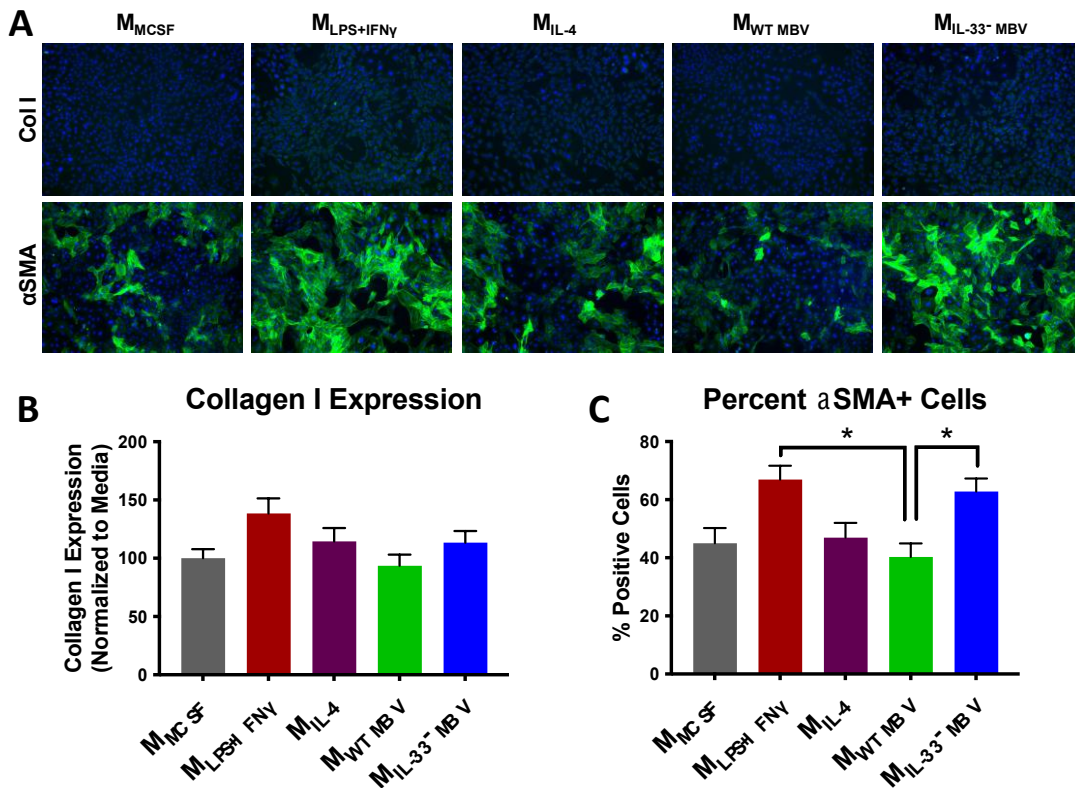


Figure 26. Macrophage secretome induced by WT MBV prevents myofibroblast activation.

Cardiac fibroblasts were exposed to conditioned media from macrophages treated with media, IFN γ /LPS, IL4, WT MBV, or IL-33⁻ MBV. (A) Representative images of collagen I and α SMA immunolabeling. Quantification of the (B) relative intensity of Col I expression normalized to media control and (C) the percent of α SMA positive nuclei as determined by CellProfiler. All values represent mean \pm SEM (N = 3)

6.3.7 MBV Directly and Indirectly Modulate Osteogenic Differentiation

Fibroblast mineralization was used as an *in vitro* model to evaluate the direct and indirect effect of MBV on osteogenic differentiation. Expression of a panel of genes commonly associated with osteogenesis were evaluated following 3, 5, or 7 days of simultaneous exposure to osteogenic media with 1×10^9 particles/ml of WT or IL-33⁻ MBV. Changes in gene expression were observed following WT and IL-33⁻ MBV treatment relative to the osteogenic media control at all time points, and the magnitude of the fold changes generally increased with time (Figure 27A). Similar trends of gene expression were observed between MBV types at all timepoints, however there was higher expression of OSX with IL-33⁻ MBV treatment relative to WT MBV treatment at both 5 and 7 days.

Alizarin red staining was used to visualize mineral deposition in the fibroblast cultures. There was no detectable alizarin positive staining in any of the treatments at day 3, but mineralization was present in all groups receiving osteogenic media by day 5 (Figure 27B & C). At 7 days, there was significantly more alizarin red when IL-33⁻ MBV were added to the media compared to osteogenic media alone and osteogenic media with WT MBV. There was no difference with the addition of WT MBV to the osteogenic media (Figure 27B & C). Quantification of the calcium content in each well was used as an additional metric for mineral deposition. The calcium content followed a similar trend as the alizarin red quantification but did not reach statistical significance between any of the groups in osteogenic media (Figure 27D).

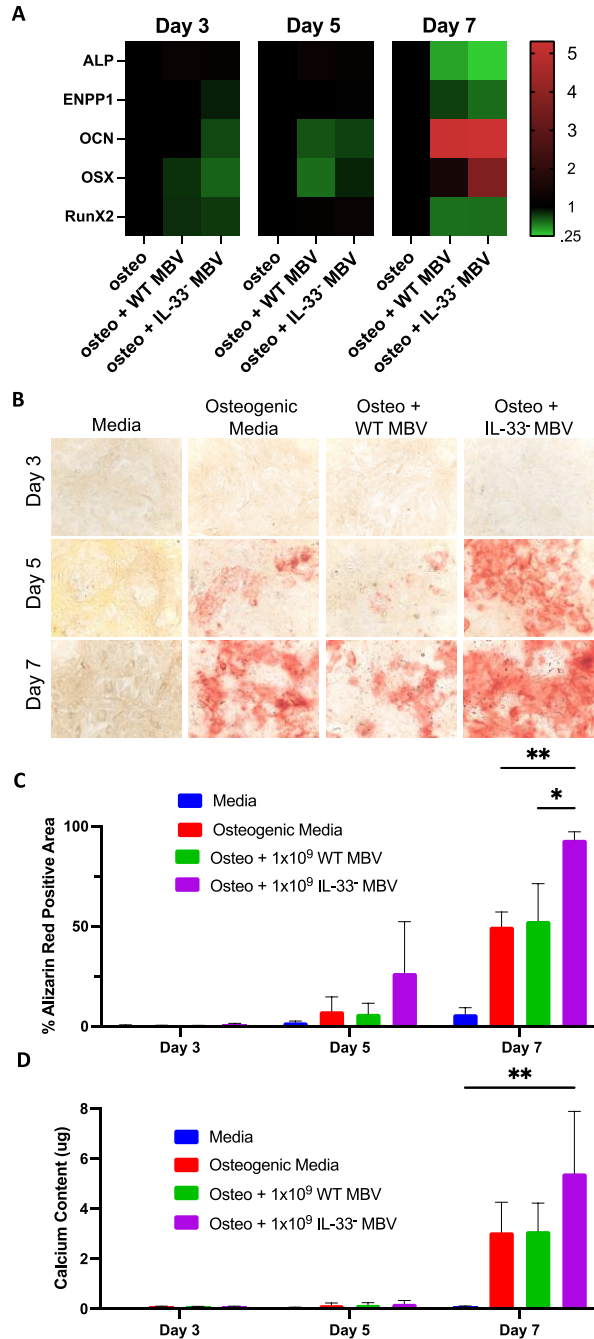


Figure 27. Direct effect of MBV on osteogenesis.

Cardiac fibroblasts were exposed to pro-osteogenic media supplements simultaneously with 1×10^9 p/ml WT or IL-33 MBV. (A) Expression of genes commonly associated with osteogenic differentiation. Represented as fold change relative to the osteogenic media control (B) Representative images of Alizarin Red staining. (C) Quantification of the percent alizarin red positive area in each well. (D) Quantification of the calcium content of each well as an indicator of mineral formation. All values represent mean \pm SEM (N = 3)

The observation of increased mineralization with IL-33⁻ MBV, but no change with WT MBV suggested that overall MBV cargo is associated with pro-mineralization effects while IL-33 cargo acts to suppress those effects. Given this finding, we performed a dose response to determine the limits of the IL-33 cargo effects, and also included recombinant IL-33 as an additional control. Alizarin red staining and calcium content were undetectable in all groups at day 3 (data not shown). Mineral deposition was present in all groups at day 5 with increasing severity at day 7 as evidenced by alizarin red staining and calcium content (Figure 28). The percent alizarin red positive area and calcium content were normalized to the osteogenic media control to observe changes based on treatment group (Figure 28B & C). At day 5, both 20ng/ml rIL-33 and a low dose of WT MBV (4.5×10^8 particles/ml) decreased mineralization, while a low dose of IL-33⁻ MBV substantially increased mineral deposition. At a higher dose (4.5×10^9 particles/ml), both WT and IL-33⁻ MBV promoted increased mineralization relative to the osteogenic media control and there was no difference based on IL-33 content. Except for increased alizarin red with 1×10^9 IL-33⁻ MBV, the differences based on treatment group were most notable at day 5, with little further changes occurring by day 7 (Figure 28B & C).

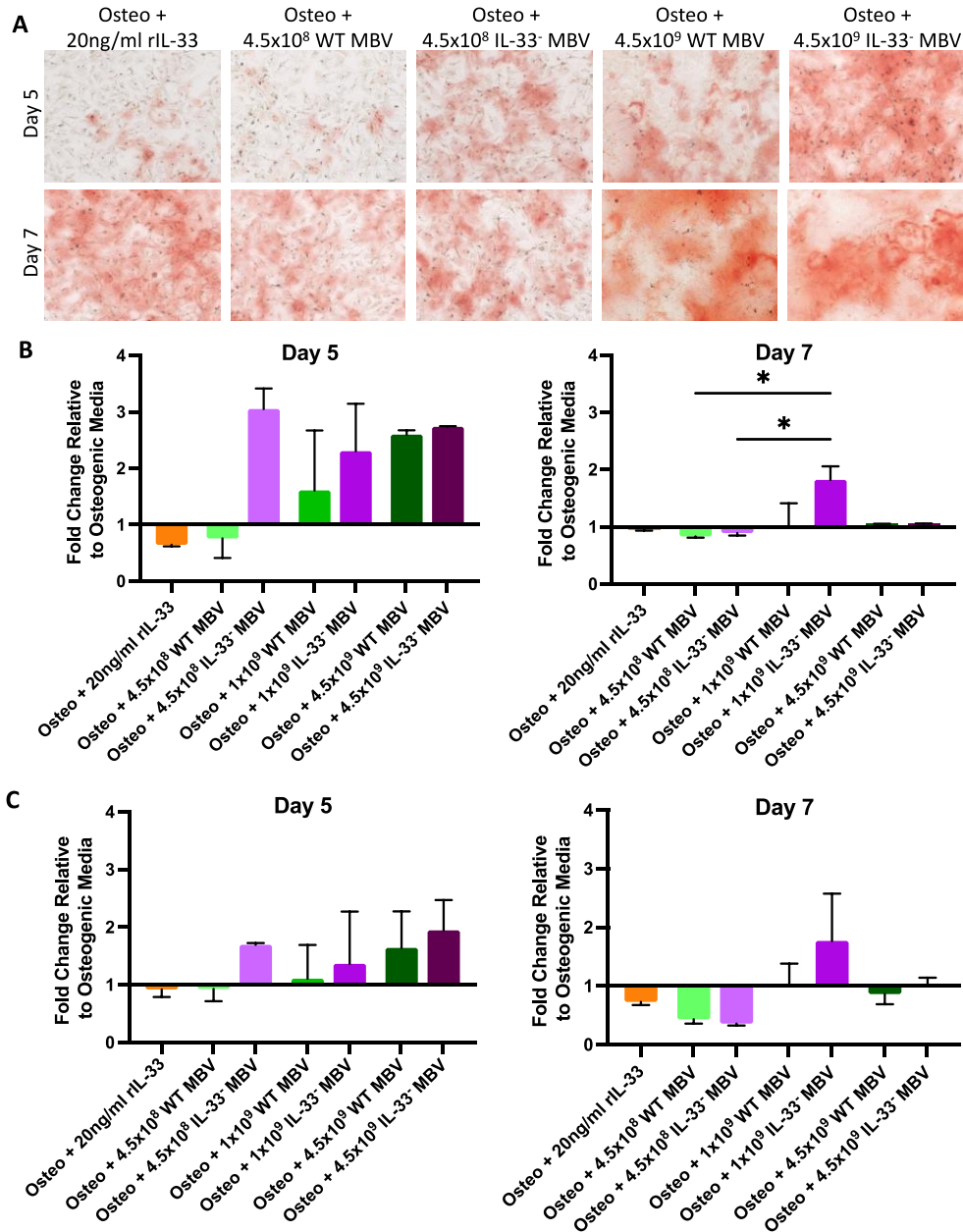


Figure 28. Dose response of direct MBV effects on osteogenesis.

Cardiac fibroblasts were exposed to pro-osteogenic media supplements simultaneously with 20ng/ml rIL-33, 4.5x10⁸ p/ml or 4.5x10⁹ p/ml of WT or IL-33⁻ MBV. (A) Representative images of Alizarin Red staining. Quantification of the fold change of the (B) percent alizarin red positive area and (C) calcium content of each well relative to the osteogenic media control. All values represent mean ± SEM (N = 3)

The indirect effect of the secreted products of MBV-stimulated macrophages on modulating osteogenic differentiation was also evaluated with gene expression, alizarin red staining, and calcium content of fibroblasts. The expression of genes commonly associated with osteogenesis did not show clear differences between any of the macrophage conditioned media groups (Figure 29A). Relative to the osteogenic media control, all macrophage conditioned medias generally promoted downregulation of ENPP1, OCN, and RunX2 at all timepoints. Alizarin red staining for mineralization showed no positive staining at 3 days in any groups. At day 5, alizarin red staining was present in the osteogenic media control, M_{MCSF}, M_{LPS/IFN γ} , and M_{IL4} groups, and the prevalence of the staining was increased at day 7 (Figure 29B & C). At all timepoints evaluated, the conditioned media from macrophages treated with either WT or IL-33⁻ MBV prevented mineral deposition. Both the percent alizarin red positive area and the calcium content of M_{WT MBV} and M_{IL-33⁻ MBV} were significantly lower than all other osteogenic groups and equivalent to the growth media control (Figure 29C & D).

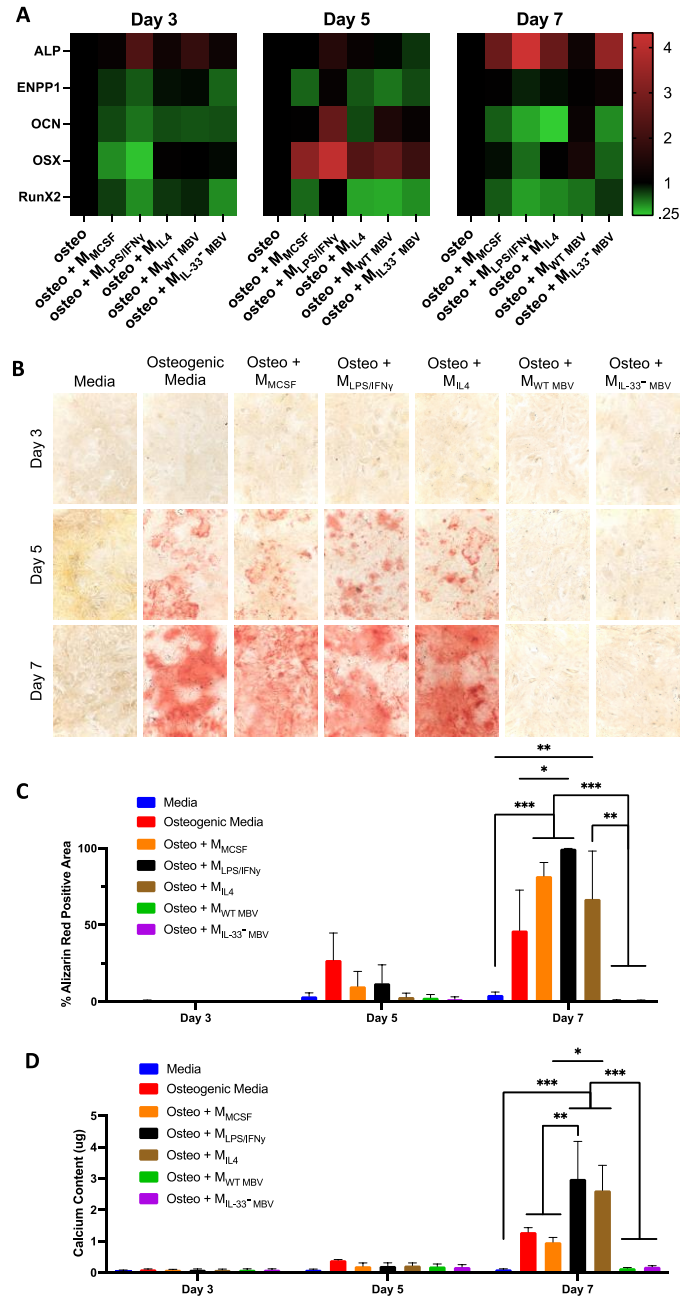


Figure 29. Indirect effect of MBV-induced macrophage secretome on osteogenesis.

Cardiac fibroblasts were exposed to conditioned media from macrophages treated with media, IFN γ /LPS, IL4, WT MBV, or IL-33⁺ MBV simultaneously with pro-osteogenic media supplements. (A) Expression of genes commonly associated with osteogenic differentiation. Represented as fold change relative to the osteogenic media control (B) Representative images of Alizarin Red staining. (C) Quantification of the percent alizarin red positive area in each well. (D) Quantification of the calcium content of each well as an indicator of mineral formation. All values represent mean \pm SEM (N = 3)

6.4 Discussion

In the present study, transcriptomic analysis was used to determine the effect of MBV associated IL-33 cargo on macrophage activation. Results show significant contribution of ST2 receptor-independent IL-33 signaling to the macrophage response to MBV. Specifically, MBV IL-33 cargo plays an important role in promoting an anti-inflammatory M2-like macrophage phenotype by up regulating M2-associated and down regulating M1-associated genes. The repertoire of IL-33 mediated genes in macrophages are broadly related to the inflammatory response and crosstalk between cells of the innate and adaptive immune systems. IL-33 cargo was also revealed as an important contributor to direct and macrophage-mediated effects of MBV on fibroblast activation and mineralization.

Implantation of an ECM bioscaffold is typically associated with a constructive remodeling outcome characterized by site appropriate tissue deposition and absence of foreign body reaction in multiple anatomical locations [81,82,84,85,109,112]. An early transition of responding immune cells toward a type 2, anti-inflammatory phenotype is now recognized as a critical determining factor of the positive downstream outcome to ECM scaffolds [111]. Though numerous constituents of the ECM contribute to the overall cellular response to bioscaffold implantation, MBV have emerged as an important, perhaps necessary, factor in directing the anti-inflammatory M2-like activation of macrophages [151,152]. Further evaluation of individual MBV components identified the determinant role of intraluminal IL-33 cargo in the MBV-mediated macrophage response. Specifically, MBV containing IL-33 produced the expected M2-like activation of bone marrow derived macrophages, and elimination of IL-33 within the MBV instead induced a pro-inflammatory phenotype [163]. Owing to the potential clinical importance of IL-33 to MBV effects, the secreted products of macrophages exposed to IL-33⁺ MBV, but not IL-33⁻ MBV,

promoted myogenesis of skeletal muscle progenitor cells *in vitro* [163]. In a mouse heart transplant model, IL-33 cargo was required for MBV to reduce the presence of pro-inflammatory macrophages and mitigate immune-driven chronic rejection of the graft [165].

Consideration of the top signaling pathways predicted by IPA to be regulated by MBV-IL-33 cargo may suggest additional or alternative contributions of IL-33 to the biologic and remodeling effects broadly associated with ECM bioscaffolds. Wolf et al. showed that ECM produced from urinary bladder matrix (UBM-ECM), known to contain IL-33⁺ MBV [163], synergized with PD-1 and PD-L1 checkpoint blockade to inhibit tumor formation by a macrophage dependent mechanism [150]. “PD-1/PD-L1 cancer immunotherapy” is among the top pathways regulated by MBV-associated IL-33 in macrophages. Exposure of LPS/IFN γ activated microglia to either UBM-ECM or UBM-MBV inhibits production of pro-inflammatory cytokines, including IL-33-regulated IL6, consistent with a role of IL-33⁺ MBV in the “neuroinflammation signaling pathway” [162]. Genes regulated by MBV-associated IL-33 direct pathways of T cell activation and immune cell phenotype, including “communication between innate and adaptive immune cells”, “cytokines mediating communication between immune cells”, “T helper cell differentiation”, and “Th1 and Th2 activation pathway”. Sadtler et al. showed that the pro-regenerative, anti-inflammatory response to ECM scaffolds requires crosstalk between innate and adaptive cells, specifically T helper 2 cells [145,148]. Overall, the connection of IL-33 signaling by MBV to known effects of ECM and MBV suggest that IL-33 may be a significant, but previously uncharacterized, contributor.

IL-33 is produced as a ~32kDa protein that lacks a signaling sequence for secretion but has an N-terminal domain containing a nuclear localization sequence and chromatin binding motif. Due to the nuclear domain, IL-33 is predominantly found within the nucleus and is constitutively

expressed by endothelial, epithelial, and fibroblast cells with little to no basal presence in hematopoietic cells including macrophages [244,292,293]. Following cell death, damage, or mechanical stress, free IL-33 is released into the extracellular space and can stimulate the canonical ST2 signaling pathway in ST2 receptor positive cells [247]. Of importance, the genes significantly regulated by MBV-associated IL-33 in macrophages are unique from previously established effects of IL-33/ST2 signaling in other cell types. For example, ST2 signaling by IL-33 increased CSF3 expression in dendritic cells [294] and adipocytes [295], CD69 expression in CD8⁺ T cells and NK cells [296,297], CCL4 in mast cells [298,299], and IL-6 expression in intestinal immune cells [300], bone marrow mast cells [298], adipocytes [295], and dendritic cells [294] : a stark contrast to the downregulation of all these genes by MBV-associated IL-33 signaling in macrophages. Canonical IL-33/ST2 signaling also decreases CD28 expression in mast cells [301] while non-canonical signaling by MBV increased the expression of this anti-inflammatory marker in macrophages. Activation of MyD88 and NF- κ B signaling cascades are also stimulated by IL-33/ST2 signaling in macrophages and other cell types [247,302], but are predicted to be inhibited by MBV-associated IL-33 signaling.

IL-33 has previously been shown to be packaged within membranous vesicles in the cytoplasm of fibroblasts [303] and within exosomes produced by Epstein-Barr Virus infected cells [304], but the bioactive effects of vesicle-associated IL-33 cargo, specifically MBV, has not been previously described. Previous work showed that encapsulation of IL-33 within the MBV lumen enables bypassing of the ST2 surface receptor to stimulate changes in macrophage phenotype [163]. Herein it is further shown that IL-33 cargo delivered by MBV localizes to the nucleus of macrophages and induces transcriptomic changes independent of the ST2 receptor. In other cell types, nuclear IL-33 binds chromatin through protein-protein interactions and acts as a

transcriptional repressor [244,253]. Full length IL-33 can bind directly to the p65 and p50 subunits of NF- κ B in HEK293 cells to dampen pro-inflammatory signaling [253]. In endothelial cells, IL-33 has also been shown to suppress transcription of the pro-inflammatory cytokine IL-6 by binding to promoter-bound proteins [305]. In the present work, IL-33 MBV cargo significantly decreased IL-6 gene expression, and IPA analysis identified NF- κ B as a predicted upstream regulator that is downregulated by the presence of IL-33 within the MBV. The present results suggest a similar mechanism of NF- κ B inhibition following IL-33 translocation to the nucleus of macrophages.

The parallels between the role of nuclear IL-33 in other cells and the response of macrophages to MBV informs a hypothesis that following uptake and translocation to the nucleus, IL-33 interacts with chromatin to diminish pro-inflammatory activities in macrophages. In this previously uncharacterized paradigm of signaling, MBV may act as a vector for nucleus-to-nucleus transport of proteins to direct cell activation. Though results shown here apply specifically to IL-33, this model of receptor-independent delivery of MBV cargo may also apply to other nuclear alarmins and cytokines lacking a signaling sequence. Future studies will explore this novel hypothesis and confirm that nuclear localization of IL-33 by way of MBV uptake in macrophages is at least partially responsible for transcriptomic regulation.

To characterize the effects of MBV and the contribution of IL-33 cargo on stromal cell phenotype, we evaluated myofibroblast activation and mineralization of cardiac fibroblasts. The effects of recombinant IL-33 on these processes have previously been studied and therefore rIL-33 was not included in the present analyses [260,261,306,307]. Direct exposure to MBV with or without IL-33 cargo had no effect on modulating the activation of fibroblasts in the presence of pro-fibrotic stimuli. On the other hand, the secreted products of stimulated macrophages did affect fibroblast to myofibroblast transition. MBV derived from porcine vocal fold lamina propria ECM

have been shown to directly inhibit TGF-beta1 induced myofibroblast activation of human vocal fold fibroblasts *in vitro* [308]. The inability of MBV to directly inhibit myofibroblast activation in the present study may be due to differences in cell source, MBV tissue source [151,152,308] and MBV isolation method [309]. Consistent with the results of the present study, IL-33 content was not expected to directly modulate fibrosis *in vitro*. IL-33 signaling inhibited cell migration and activated cytokine and chemokine expression in rat cardiac fibroblasts, but had no effect on the expression of myofibroblast markers [307].

The indirect effect of macrophage-fibroblast crosstalk has not previously been studied *in vitro*, but rIL-33 and IL-33⁺ MBV have both been shown to limit fibrosis in various models *in vivo* [165,261,306]. Though a causative role was not specifically determined, decreased fibrosis was associated with modulation of innate [165] and adaptive [261] immune responses. These studies together with the present data support a role of IL-33 dependent MBV-induced changes to macrophage phenotype in mediating myofibroblast activation.

Though direct biologic effects of MBV were not observed in the model of *in vitro* fibrosis, the same cell type was affected directly by MBV, with IL-33 dependence, in a model of mineralization. A dose dependent effect was observed with direct MBV treatment in which a low dose of WT MBV prevented mineralization, an intermediate dose had little effect on mineralization, and a high dose of WT MBV stimulated increased mineralization in cardiac fibroblasts. Conversely, IL-33⁻ MBV increased mineralization at all doses evaluated. These results suggest that the anti-osteogenic effects of IL-33 cargo dominate at lower doses but are overpowered by the pro-osteogenic effects of other MBV cargo at higher doses. Pleiotropic effects of IL-33 signaling on mineralization and osteogenesis have been reported by other groups previously [259,260,310–313]. The finding that IL-33 inhibits mineralization in rat cardiac

fibroblasts is consistent with findings by Kukolj et al. in which IL-33 treatment decreased ALP activity, Alizarin Red staining, and calcium deposition in dental pulp and periodontal ligament stem cells [260].

Identification of other cargo components that may be contributing to MBV-mediated effects on mineralization is outside the scope of the present study. Hussey et al. previously performed a cytokine array on mouse small intestine-derived WT and IL-33⁻ MBV, the same source as used herein [163]. C-reactive protein, cystatin C, and hepatocyte growth factor were among the cytokines with the highest expression levels and have reported pro-osteogenic effects [314–316]. The lipid, nucleic acid, and other protein composition of MBV also likely impact the mineralization response to MBV but have not yet been characterized for mouse intestine MBV.

The ability of the macrophage secretome induced by both WT and IL-33⁻ MBV, but not naïve, M1, or M2 macrophages, to indirectly prevent fibroblast mineralization is a novel finding. This supports an MBV-specific macrophage phenotype that occurs independently of IL-33 cargo. Multiple studies have shown that ECM scaffold-associated macrophages have an activation state that is unique from the established LPS/IFN γ or IL-4 induced phenotypes [147–149,317,318]. The present study identified specific genes regulated by IL-33 cargo in macrophages but did not characterize the universal MBV-associated macrophage phenotype. Given the dose dependent promotion of mineralization by MBV directly and the potent inhibition of mineralization indirectly, future work using co-culture, or an *in vivo* model is necessary to determine the overall effect of MBV on the mineralization response.

The finding that receptor-independent delivery of MBV-associated IL-33 is sufficient for directing an anti-inflammatory macrophage response highlights the importance of this cytokine in determining the host response and remodeling outcome to MBV and ECM. Further, understanding the importance of IL-33 signaling in macrophages activation and other cellular processes is relevant for intelligent design of the next generation of ECM-based therapies.

7.0 MBV Modulate Host Response to Implanted Bioprosthetic Tissue Valve⁵

7.1 Introduction

The success or failure of a biomaterial in the clinical setting is ultimately dependent upon the host tissue response following *in vivo* placement [319], a characteristic called *biocompatibility*. A definition for biocompatibility, widely accepted in the biomaterials and medical device communities [320,321], includes the phrase “*the ability of a material to perform with an appropriate host response in a specific application*”, a concept that has been expanded to include biologically active biomaterials [322,323].

The host immune response following implantation of a biomaterial is influenced by the physical and chemical properties of the material [319]. While cells of both the innate and adaptive immune system can contribute to the host response, the phenotype of responding macrophages is arguably the most important determinant of the downstream remodeling outcome [238,239]. Specifically, persistent pro-inflammatory (M1-like) macrophages are associated with a less favorable outcome characterized by dense fibrosis, scar tissue, and chronic inflammation [324,325]. In contrast, a rapid transition of infiltrating macrophages from an initial M1-like response to an M2-like phenotype is associated with a constructive remodeling response, characterized by a resolution of inflammation and deposition of more organized, site-appropriate tissue [111,113]. In the context of the host response to bioprosthetic heart valves, pro-

⁵ Excerpts of this chapter have been adapted from the following publication:

M.C. Cramer, J. Chang, M. Cox, H. Li, A. Serrero, M. El-Kurdi, F.J. Schoen, S.F. Badylak, Tissue response, macrophage phenotype, and intrinsic calcification induced by cardiovascular biomaterials: Can clinical regenerative potential be predicted in a rat subcutaneous implant model?, *J Biomed Mater Res Part A*. (2021) 1–12.

inflammatory M1-like macrophages and their cytokines are associated with promotion of calcification, while anti-inflammatory M2-like macrophages are thought to be protective against calcification [67,71].

The present aim used a subcutaneous rat model to investigate the *in vivo* tissue host response to a biologic scaffold composed of glutaraldehyde-fixed bovine pericardium (gluBP), which is the standard of care for valve substitutes for heart valve replacement [326]. The therapeutic effect of systemic administration of WT or IL-33⁻ MBV in modulating the host response following gluBP implantation was evaluated by multiple metrics including inflammation, neovascularization, macrophage phenotype, remodeling and calcification.

7.2 Materials and Methods

7.2.1 Overview of Experimental Design

A subcutaneous rat model was used to compare the tissue response, including macrophage phenotype, remodeling potential and calcification propensity of gluBP following administration of WT or IL-33⁻ MBV. Three week old weanling rats received dorsal subcutaneous implants of gluBP. To evaluate the therapeutic effect of MBV, animals were also administered saline, WT or IL-33⁻ MBV via tail vein injection. Each animal received a total of four material implants with two placed bilaterally on each dorsal side. The time points for evaluation were 2, 14, 21, 90 and 180 days (n=3 animals per timepoint/group). The host macrophage and calcification response to the test material was evaluated with histochemistry, immunolabeling and radiographic analysis. A schematic overview of the animal study used in Specific Aim 3 is depicted in Figure 30.

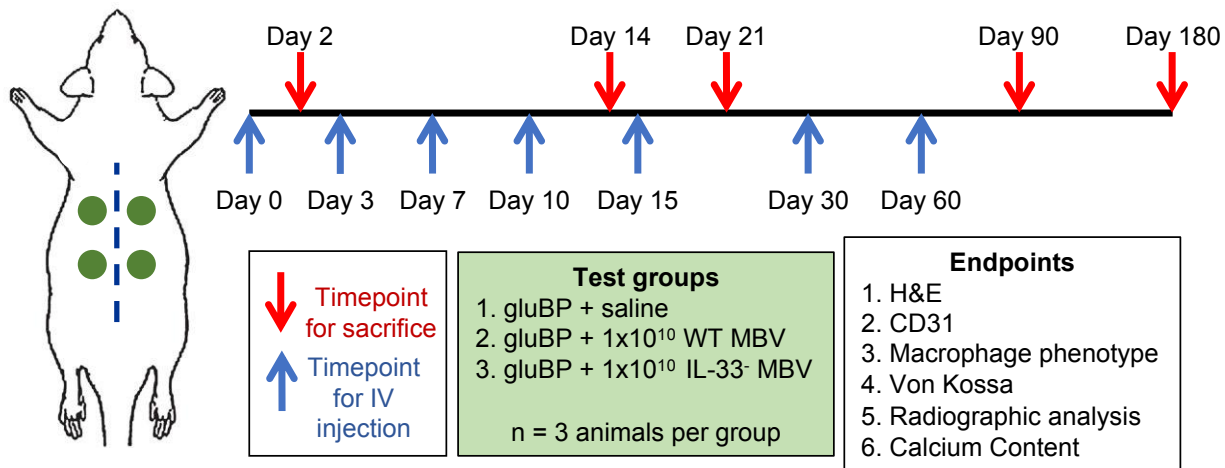


Figure 30. Overview of experimental design for Specific Aim 3.

7.2.2 Preparation of gluBP

To produce gluBP, fresh bovine pericardium was obtained from Innovative Research (Novi, MI). Pericardium was rinsed in sterile saline and then fixed in a buffered 0.625% glutaraldehyde solution (pH 7.4) for 7 days followed by storage in 0.2% glutaraldehyde until use as previously described [77]. After fixation, gluBP was cut into 8mm discs with a biopsy punch in an aseptic environment. The gluBP material was rinsed twice in sterile saline to remove residual glutaraldehyde solution prior to implantation.

7.2.3 Dorsal Subcutaneous Implantation in Rats

Animal studies were conducted in compliance with all regulations regarding the humane treatment of laboratory animals as set forth by the University of Pittsburgh's Institutional Animal Care and Use Committee. Three-week old female Sprague Dawley rats were obtained from Envigo (Indianapolis, IN). Rats were anesthetized and maintained at a surgical plane of anesthesia with 1.5-3% isoflurane in oxygen and prepared for aseptic surgical procedures. A midline incision was made on the dorsal dermis of the animal and the dermis was undermined on each side to create a pocket of sufficient size to accommodate the implants. An 8mm diameter disc of gluBP was sutured to the adjacent panniculus carnosus muscle with 7-0 Prolene. Each animal received 4 total subcutaneous implants, with two bilaterally on each dorsal side. The skin was closed with absorbable sutures. The animals were recovered from anesthesia and allowed normal ambulation and diet for the remainder of the study period. Animals were sacrificed by CO₂ asphyxiation at 2, 14, 21, 90, or 180 days after implantation. At the time of sacrifice the samples with surrounding tissue were explanted and fixed in 10% neutral buffered formalin.

7.2.4 Intravenous Injection of MBV

Rats were anesthetized with isoflurane prior to tail vein injection of MBV. Animals implanted with gluBP were injected with sterile saline, 1×10^{10} MBV particles from the small intestine of wildtype mice (WT MBV), or 1×10^{10} MBV particles *il33*^{-/-} mice (IL-33⁻ MBV). Small intestine was used as the source of MBV in this study since IL-33 is known to be abundant in mouse intestinal MBV [163]. MBV were resuspended in 100ul sterile saline and injections were administered at the time of surgery (day 0) and on post-operative days 3, 7, 10, 15, 30 and 60.

7.2.5 Histologic Evaluation

At the designated time point samples with surrounding tissue were explanted, formalin-fixed, embedded in paraffin and 5 μ m serial sections were cut. Sections were stained with either hematoxylin and eosin (H&E) or von Kossa stains according to standard procedures to visualize general morphology, cellular infiltration, and calcification. Neovascularization of the implant was evaluated by CD31 immunolabeling. Briefly, slides were deparaffinized and antigen retrieval was performed with citrate buffer (pH = 6) at 95-100°C for 20 min. Slides were treated with 3% H₂O₂ in methanol for 10 min to quench endogenous peroxidase activity prior to blocking in 1% bovine serum albumin, 2% normal horse serum, 0.1% Triton X-100 and 0.1% Tween-20 at room temperature for 1 hr. Tissue sections were incubated overnight at 4°C with rabbit monoclonal CD31 antibody (1:500, Abcam) in blocking buffer. Slides were incubated with horseradish peroxidase-conjugated (HRP) anti-rabbit IgG secondary antibody (1:200, Sigma Aldrich) at room temperature for 1 hr. Slides were developed with peroxidase substrate, 3,3'-diaminobenzadine (ImmPACT™ DAB, Vector Laboratories) followed by hematoxylin counterstaining, ethylene-xylene dehydration and mounting in non-aqueous medium.

7.2.6 Evaluation of Macrophage Phenotype

Tissue sections were deparaffinized and antigen retrieval was performed with citrate buffer prior to blocking. Tissue sections were immunolabeled with primary antibodies for pan-macrophage marker (mouse anti-CD68, 1:150, Bio-Rad Antibodies) and indicators of M1-like (rabbit anti-TNF α , 1:100, Abcam) and M2-like (goat anti-CD206, 1:100, R&D Biosystems) macrophage phenotypes and secondary antibodies goat anti-mouse HRP (1:100, Sigma Aldrich),

goat anti-rabbit HRP (1:100, Sigma Aldrich), or rabbit anti-goat HRP (1:100, Sigma Aldrich) in blocking buffer for 3 min in the microwave at mid-low power. Signal was generated with Opal Polymer HRP (Akoya Biosciences), and nuclei were visualized with DRAQ5 (Thermo Scientific) staining. Slides were imaged on the Zeiss Observer Z1 microscope with Axiocam MRc camera and a 32x objective with the FITC/TRITC/DAPI/DRAQ5 filter set. Three fields of view per slide were selected in areas of cellular infiltration into the implanted material to depict the phenotype of the resultant host response. Quantification of macrophage immunolabeling was accomplished with an image analysis algorithm in CellProfiler which verifies co-localization of positive immunolabeling with cell nuclei.

7.2.7 Radiographic Analysis

Explanted samples with surrounding tissue were fixed in formalin and then rinsed in PBS prior to radiographic analysis. Computed tomography (CT) scans were performed on tissue samples using an EPiCA VimagoTM Veterinary CT scanner (Duncan, SC). The volume of calcified tissue was calculated from CT scans using the Region of Interest function in the Horos Viewer software.

7.2.8 Quantification of Calcium Content within gluBP Implants

Following radiographic analysis, a subset of gluBP samples were cleared of surrounding tissue, thoroughly rinsed in PBS to remove residual formalin, and then washed in deionized water to remove residual salts. The washed samples were then lyophilized and weighed. Inductively-Coupled Plasma Mass Spectrometry (ICP-MS) for calcium content was performed by Huffman Hazen Laboratories (Golden, CO). Calcium content was reported as ug Calcium per mg dry weight tissue (n=3 per group).

7.2.9 Statistical Analysis

Quantitative outcomes were compared with a two-way ANOVA and post hoc Sidak test to determine differences between groups. All statistical analysis were performed using GraphPad Prism and p values <0.05 were considered statistically significant. Data is presented as mean +/- standard error of the mean (SEM).

7.3 Results

7.3.1 Cellular Infiltration

Regardless of treatment group, implantation of the gluBP stimulated a mononuclear cell response to the materials as early as 2 days post implantation, but the cells were limited to the edges of the implant adjacent to the recipient tissue (Figure 31). At 14 days post implantation, the

magnitude of the cellular response was increased in animals that received saline or IL-33⁻ MBV injections compared to those that received WT MBV. After 21 days, the cellular response to the gluBP in animals receiving saline was significantly higher than those receiving MBV derived from either WT or IL-33⁻ mice. The cellularity of WT MBV treated animals remained similar from 2 – 21 days, while the IL-33⁻ MBV treated animals had increased cellularity at 14 days followed by a decrease at 21 days. The magnitude of the cellular response was significantly diminished in all treatment groups at 90 and 180 days post implantation. Across all groups and all timepoints, the cells remained distributed primarily in those areas close to the edges with only a small number of cells deep into the material (Figure 31).

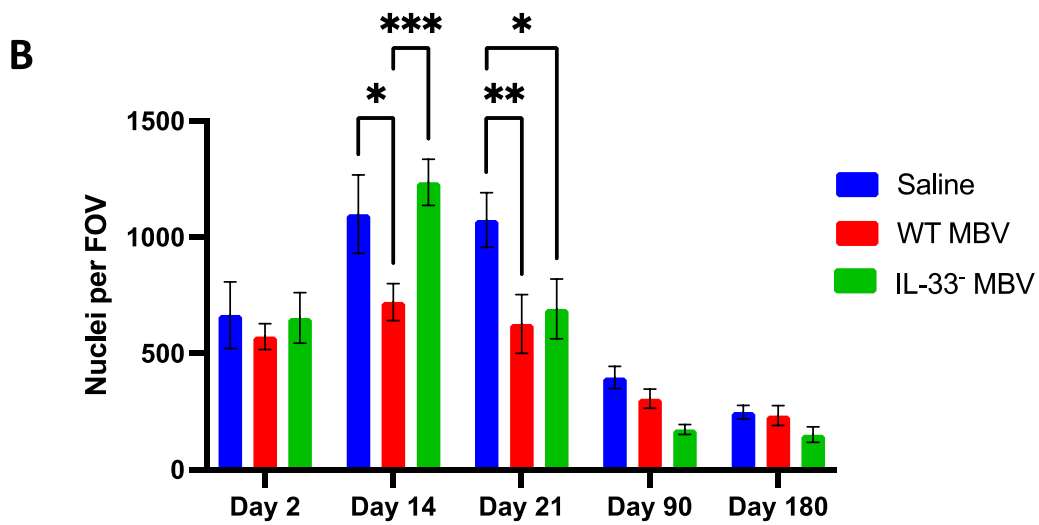
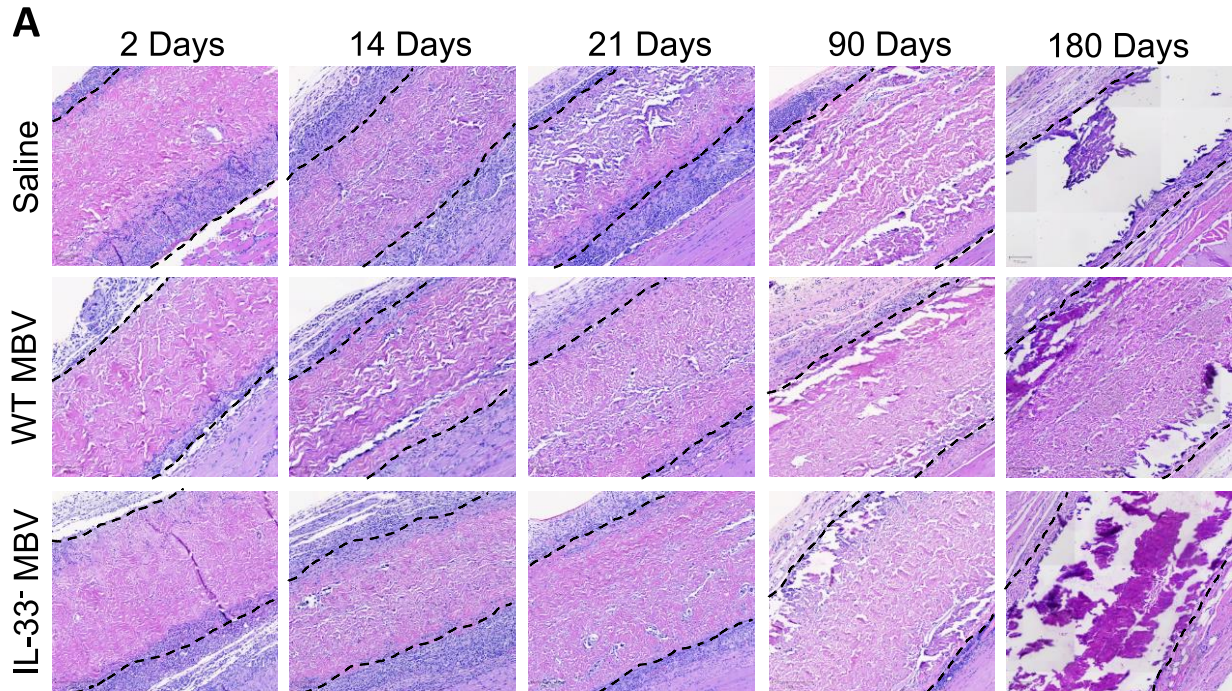


Figure 31. Cellular response to gluBP implantation.

(A) Representative images of gluBP implants with injections of saline, WT MBV, or IL-33- MBV at 2, 14, 21, 90 and 180 days stained with H&E. Dotted lines define the interface of the material. (B) Quantification of the total nuclei per field of view. All values represent mean \pm SEM (N = 3)

7.3.2 Neovascularization

Consistent with the spatial distribution of cellularity, the presence of CD31+ cells and neovasculature were only present at the interface of the gluBP material with the underlying tissue (Figure 32). There were no detectable differences between the extent of the neovascularization between any of the treatment groups at any of the timepoints.

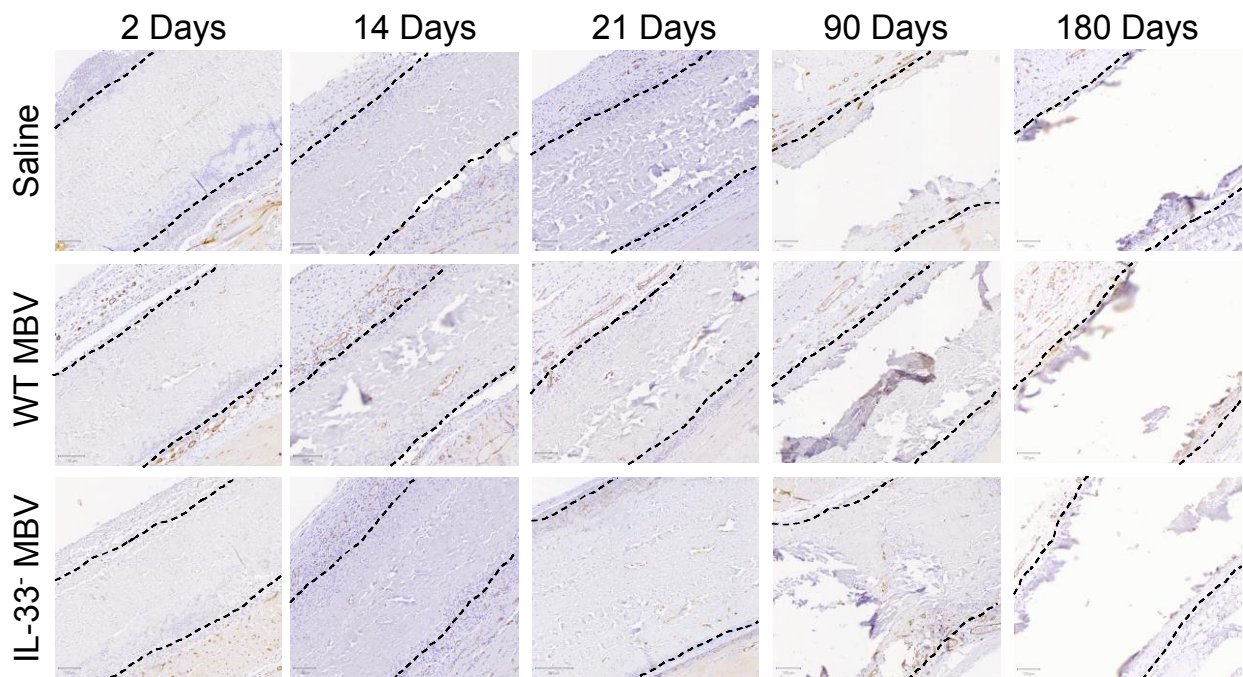


Figure 32. Endothelial cell and neovascularization response to gluBP.

Representative images of CD31 immunolabeling of gluBP implants with injections of saline, WT MBV, or IL-33⁻ MBV at 2, 14, 21, 90 and 180 days. Dotted lines define the interface of the material.

7.3.3 Macrophage Phenotype

Macrophage phenotype was evaluated by immunolabeling for CD68⁺, TNF α ⁺ and CD206⁺ cells (Figure 33A). The total numbers of CD68⁺CD206⁺ and CD68⁺TNF α ⁺ macrophages and the ratio of M2-like (CD68⁺CD206⁺) and M1-like (CD68⁺TNF α ⁺) macrophages was used to determine the dominant phenotype within the material (Figure 33B) and character of the inflammatory response (Figure 33C).

The phenotype of macrophages present at the surface of the gluBP materials changed with systemic administration of WT MBV. Intravenous injection of WT MBV stimulated a more dominant anti-inflammatory phenotype as indicated by a higher ratio of M2-like (CD68⁺CD206⁺) and M1-like (CD68⁺TNF α ⁺) macrophages relative to saline and IL-33⁻ MBV administration at days 2, 21, and 90 (Figure 33B). There was no significant difference in the M2-like to M1-like ratio between saline and IL-33⁻ MBV treatment at any timepoint, with the ratio being nearly balanced. The overall number of macrophages of either phenotype was similar across treatment groups at all timepoints. By 180 days post implantation, the magnitude of the macrophage response was diminished and there were no significant differences in the phenotype based on treatment (Figure 33C).

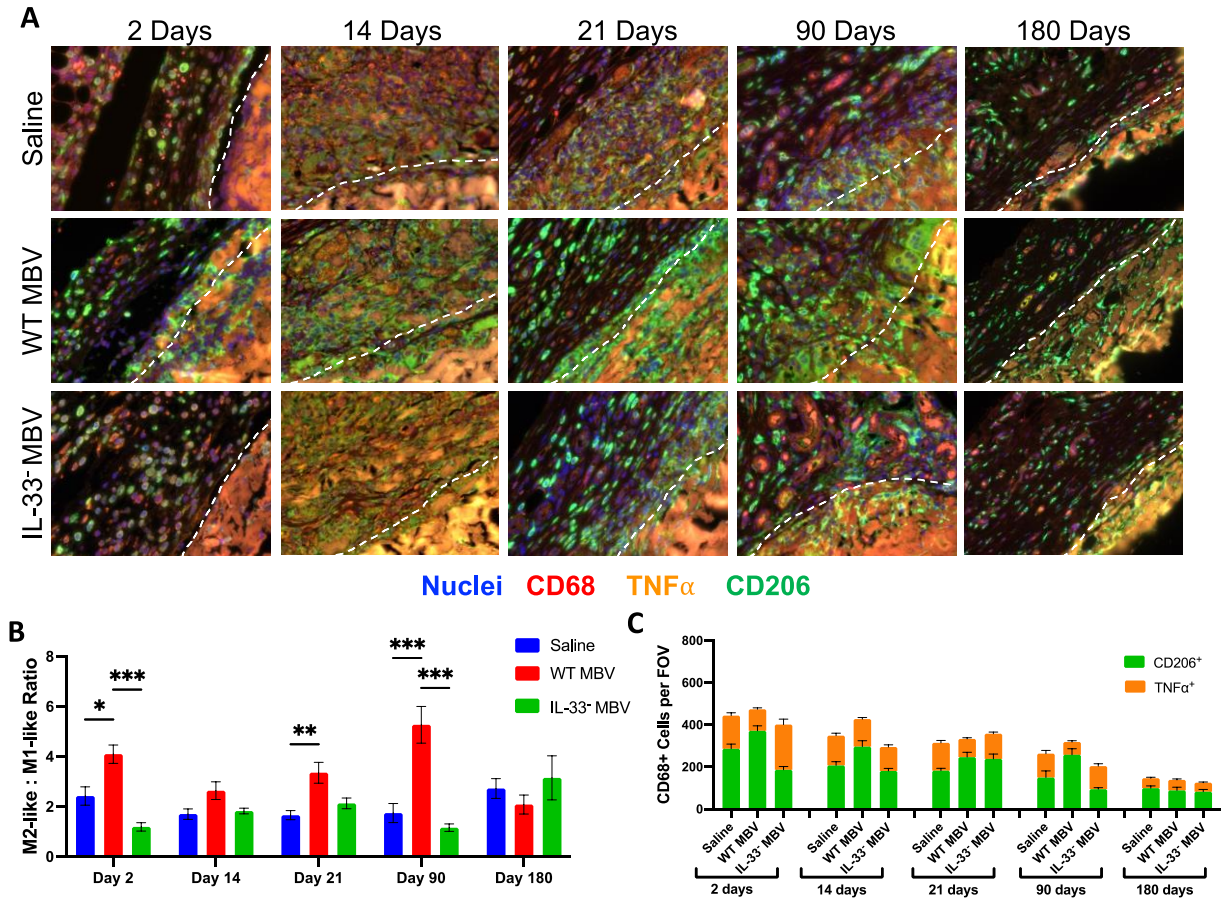


Figure 33. Macrophage response to gluBP.

(A) Representative images of immunolabeling of pan-macrophages (CD68⁺, red), pro-remodeling M2-like macrophages (CD206⁺, green) and pro-inflammatory M1-like macrophages (TNF α ⁺, orange). Dotted lines define the interface of the material. (B) Quantification of the ratio of M2-like: M1-like (CD68⁺CD206⁺: CD68⁺TNF α ⁺) macrophages. (C) Quantification of the number of CD68⁺CD206⁺ and CD68⁺TNF α ⁺ macrophages per field of view.

All values represent mean \pm SEM (N = 3)

7.3.4 Susceptibility to Calcification

Histologic evaluation with von Kossa staining showed evidence of calcification in all groups beginning at 14 days post implantation (Figure 34). The intensity of the staining increased from day 14 to day 180 regardless of treatment. At 14 and 21 days, there was some evidence of non-mineralized areas of gluBP in animals that received WT MBV whereas the full thickness of the gluBP implants appeared fully encompassed following saline and IL-33⁻ MBV treatment.

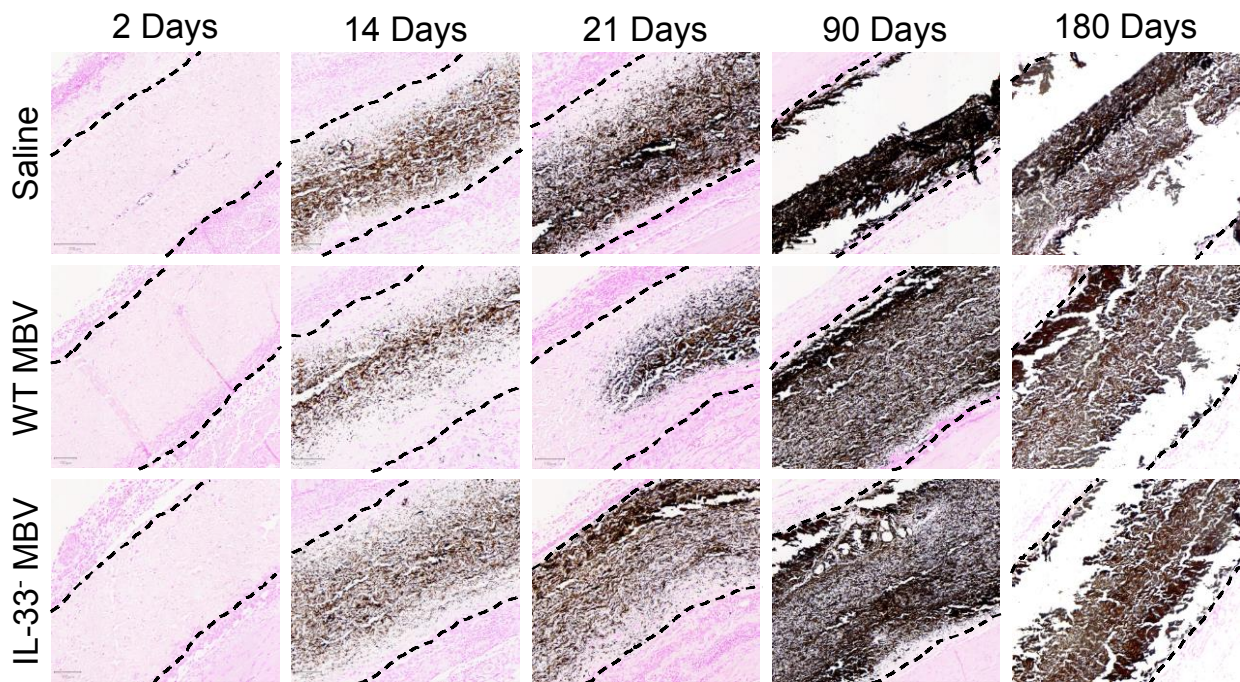


Figure 34. Histologic assessment of calcification.

Representative images of mineralization of gluBP implants observed histologically by von Kossa staining. Dotted lines define the interface of the material.

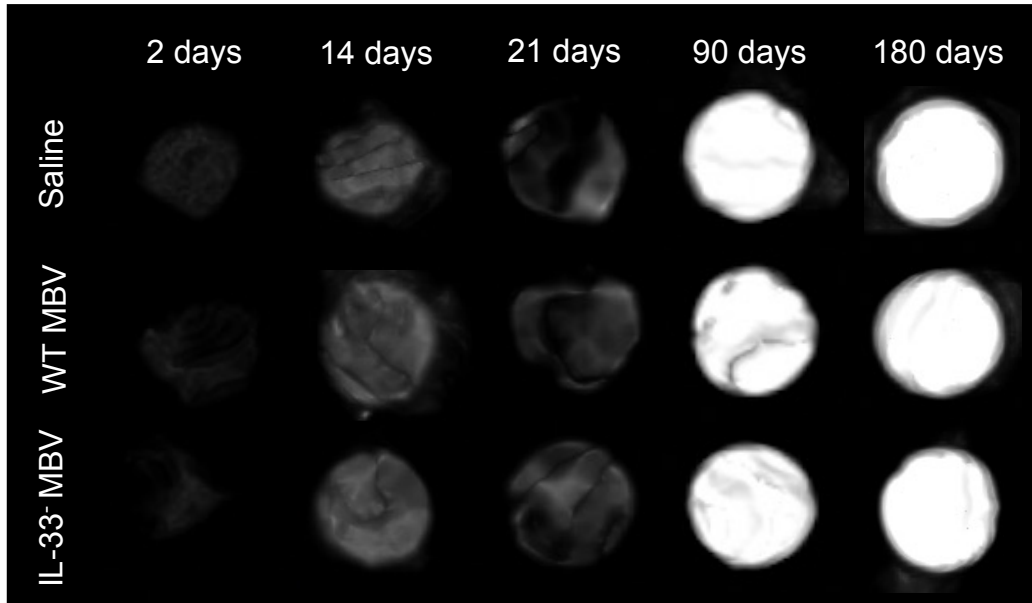
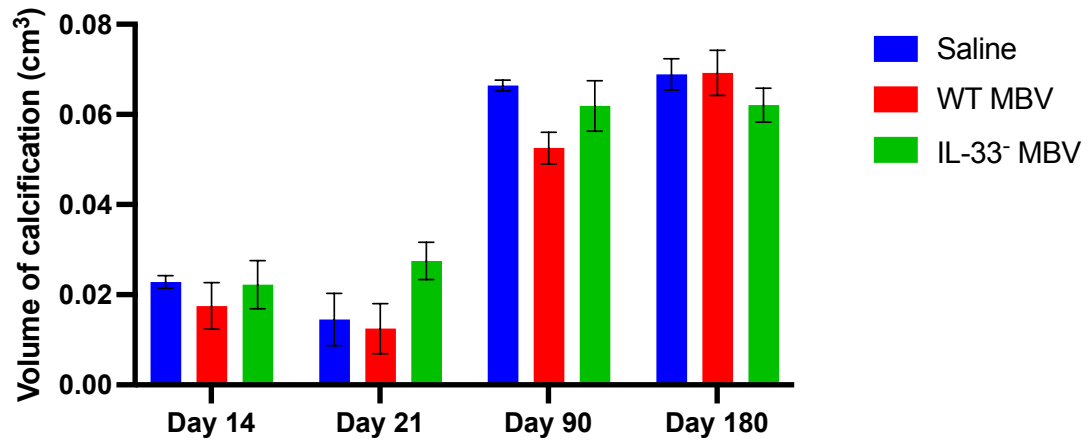
A**B**

Figure 35. Radiographic assessment of calcification.

(A) Representative images of calcification of gluBP implants with radiographic CT scans. All images displayed with the same viewing window. (B) Quantification of the volume of calcification within each test material as determined by CT analysis. All values represent mean \pm SEM (N = 3)

Consistent with the histologic evaluation, radiographic analysis with CT scanning showed mineralization in all groups at 14 days that increased in intensity throughout the remainder of the study (Figure 35). In general, the volume of calcification was lower with WT MBV versus IL-33⁻ MBV administration at days 21 and 90, however there were no statistically significant differences in the volume of calcification between any of the treatments at any timepoint (Figure 35B).

ICP-MS analysis was used to quantify the calcium content within a subset of gluBP implants as an additional metric of mineralization. No significant differences in calcium content were observed at any timepoint evaluated (Figure 36).

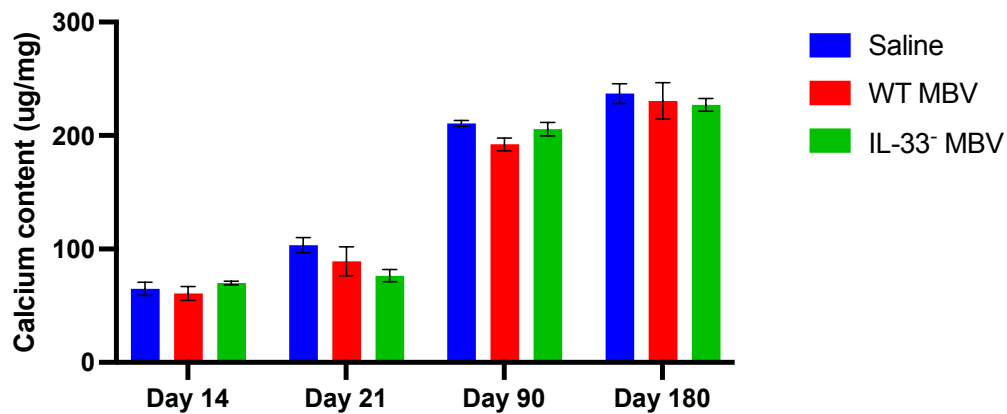


Figure 36. Calcium content of gluBP samples.

Quantification of the calcium content per dry weight of a subset of gluBP samples as determined by ICP-MS. All values represent mean \pm SEM (N = 3)

7.4 Discussion

The present aim used a subcutaneous implant model to determine the effect of WT or IL-33⁻ MBV in modulating the host remodeling, macrophage, and calcification response to implanted gluBP. Systemically administered MBV altered the magnitude and phenotype of the inflammatory response to gluBP in an IL-33 cargo-dependent manner. More specifically, WT MBV containing IL-33 cargo significantly decreased the magnitude of the cells responding locally to the gluBP and promoted an increased the ratio of anti-inflammatory M2-like to pro-inflammatory M1-like macrophages. Despite modulation of the immune response, intravenous MBV did not significantly affect neovascularization or mitigate mineralization of the material relative to administration of saline alone.

The observed temporal and spatial pattern of pro-inflammatory TNF α ⁺ macrophages to the gluBP with saline administration was consistent with that of other studies in which chemically crosslinked biologic scaffolds have been investigated [111,327]. These findings differ markedly from the anti-inflammatory macrophage phenotype associated with non-crosslinked ECM scaffolds studied previously [113,149,328]. Systemic MBV administration shifted the default macrophage response to the gluBP implant and, consistent with previous studies and the work presented in Chapter 6, intraluminal IL-33 cargo was required for this MBV-induced promotion of an anti-inflammatory macrophage phenotype [163]. The finding that immunomodulation by MBV-associated IL-33 occurs independently of the ST2 receptor is particularly crucial in the context of the heart because levels of the soluble decoy receptor (sST2) are significantly increased [79] and associated with worse prognosis [329] following implantation of bioprosthetic tissue valves, thereby limiting the efficacy of IL-33 signaling through the canonical pathway [261,306].

Calcification is the most important pathology limiting the long-term success of heart valve replacement with bioprosthetic valves [18,58]. As described in detail in Chapter 1, calcification of bioprosthetic heart valves during SVD occurs by both passive and active (immune-mediated) mechanisms [11,18,59]. The observation that WT MBV administration dampened the inflammatory response and shifted macrophages toward an M2-like phenotype but did not affect the calcification response suggests that the contribution of passive calcification outweighed the immune-mediated failure of the implant. Most commercially available bioprosthetic heart valves are treated with an anti-calcification treatment following glutaraldehyde fixation to try to limit passive calcification. The gluBP scaffold used in the present study was not decellularized prior to glutaraldehyde fixation and, unlike clinically used bioprosthetic valves, also did not undergo any anti-calcification treatment: two factors that likely exacerbated mechanisms of passive calcification [328]. Future work is necessary to determine if the immunomodulatory properties of MBV would impact the calcification response to a commercially relevant material that is less susceptible to passive failure.

The model of subcutaneous implantation in rats, as used in the present study, is well established [63,75,330,331] and generally predicts a calcification response similar to that observed in clinical specimens [75,332]. Weanling animals were used in this study because of their more active immune system [333], and rapid, robust calcification response [75]. The subcutaneous implant model is more cost effective, less technically difficult and more reliable than valve replacement in large animals [64,334]. Nevertheless, the subcutaneous implantation model used in the present study does not subject the material to continuous blood flow, blood pressure or dynamic mechanical stress which could influence the cellular and calcification response [36,335]. This model was further limited in that modulation of fibrosis or pannus formation of the implanted

gluBP material by MBV administration could not be evaluated. Given the effect of MBV on cardiac fibroblasts *in vitro* (Chapter 6), evaluation of the ability of MBV to modulate fibrotic processes *in vivo* warrants further investigation.

The present study was also limited in that only one dose of MBV and one treatment regimen was used. The MBV dose and treatment schedule used in this study were informed by previous studies performed in our laboratory evaluating the effect of systemic MBV administration in a rodent model of rheumatoid arthritis but were not optimized specifically for our model of valve calcification. Further, the effect of MBV administration may be partially dependent on the species and tissue source of the MBV. For example, MBV derived from mouse small intestinal ECM were associated with dose-dependent pro-calcific activity *in vitro* (Chapter 6) and contain cytokines with pro-mineralization properties [163]. Conversely, the mouse skeletal muscle and human heart derived MBV evaluated in Specific Aim 1 did not show substantial expression of calcific cytokines. It is therefore plausible, yet unconfirmed, that a therapeutic effect of MBV in limiting bioprosthetic heart valve mineralization could be achieved with further optimization of the model parameters.

Further work evaluating the safety of intravenous MBV administration would be necessary to pursue MBV as a therapeutic. Though no adverse effects were observed with systemic MBV in the present study, MBV biodistribution, toxicity, hemocompatibility and systemic off-target effects are all parameters that still need to be evaluated. Additionally, potential translation to the clinic would require multiple steps for large-scale manufacturing and commercialization. Development of methods for bulk MBV isolation, purification and sterilization, and identification of appropriate benchmark bioactivity assays would need to be established to minimize lot-to-lot variability and ensure reproducibility of results.

8.0 Dissertation Summary

The work presented in the present dissertation characterized matrix bound nanovesicles (MBV) as a distinct subpopulation of extracellular vesicle and evaluated the therapeutic potential of immunomodulatory MBV in mitigating immune driven bioprosthetic heart valve failure. The physical characteristics, protein cargo, and lipid composition of MBV were compared to other subpopulations of extracellular vesicle, namely exosomes (Exo) and calcifying matrix vesicles (cMV). The lipid and miRNA composition of MBV produced by 3T3 cells was also compared to the fluid-phase Exo produced by the same cell type. In order to determine how MBV change with cell source, the differences in composition of MBV produced by three different stem cells and the changes that occur in MBV during heart failure were evaluated.

The contribution of MBV cargo protein interleukin-33 (IL-33) in directing transcriptomic changes in macrophages was evaluated. The direct and indirect macrophage-mediated effect of MBV, and the contribution of IL-33 cargo, on modulating macrophage activation, fibroblast to myofibroblast and fibroblast mineralization were evaluated *in vitro*. Finally, a rat subcutaneous implant model was used to evaluate the host inflammatory, macrophage phenotype, and calcification response to a glutaraldehyde-fixed bovine pericardium (gluBP) following systemic administration of MBV with and without IL-33 cargo. The major findings of each aim are outlined below.

8.1 Major Findings

Specific Aim 1: To compare the structure and composition of MBV to other types of extracellular vesicles, including fluid exosomes and calcifying matrix vesicles.

- Despite similar size and morphology, MBV isolated from non-mineralizing soft tissue have protein, lipid, and miRNA cargo that are distinctly different from Exo and cMV
- Even when produced by a single cell type, fluid-phase Exo and solid-phase MBV have distinct cargo and composition
- Cell source type, not human donor variability, is a predominant contributor to changes in MBV miRNA cargo
- MBV cargo changes with heart failure and the resulting changes may contribute to the progression of disease

Specific Aim 2: To determine the direct and indirect (macrophage-mediated) effect of MBV upon macrophage activation, fibrosis, and mineralization *in vitro*.

Subaim 2.1: To determine the contribution of IL-33 cargo to MBV mediated effects upon macrophage phenotype and fibroblast behavior.

- MBV associated IL-33 cargo signals independently of the ST2 receptor to upregulate genes associated with anti-inflammatory M2-like macrophages and downregulate pro-inflammatory M1-like genes

- The gene expression profile induced by MBV in macrophages is related to immune cell crosstalk and other pathways that have previously been attributed to ECM bioscaffolds
- The macrophage secretome induced by IL-33⁺ MBV, but not IL-33⁻ MBV, inhibits fibroblast to myofibroblast transition
- MBV containing IL-33 are protective against fibroblast mineralization in a dose-dependent manner
- MBV-induced macrophage secreted products inhibit mineralization independently of MBV IL-33 cargo

Specific Aim 3: To evaluate the ability of systemic MBV administration to modulate the host immune response and calcification outcome to implanted gluBP in a preclinical rodent model.

- Intravenous administration of MBV dampened the magnitude of the local inflammatory response to gluBP implants
- Treatment with MBV containing IL-33 cargo shifted the phenotype of responding macrophages toward an anti-inflammatory M2-like phenotype relative to administration of saline alone
- Despite changes in the default immune response to the gluBP implant, there was no significant effect of MBV administration on preventing calcification of the material

8.2 Overall Conclusions

The work described in the present dissertation expands our understanding of MBV as a subpopulation of extracellular vesicle. Compositional differences between MBV, fluid-phase Exo and mineralizing cMV suggest unique biogenesis pathways and selective deposition of each vesicle type. Within the MBV subpopulation of vesicles, the composition varies with cell source and disease state of the tissue. *In vitro*, MBV direct macrophages toward an anti-inflammatory M2-like phenotype that is dependent on transcriptomic changes specifically regulated by IL-33 cargo within the MBV. The secretome of macrophages stimulated by MBV enact phenotypical changes in fibroblasts that modulate their activation to myofibroblasts and their susceptibility to mineralization. *In vivo*, intravenous administration of IL-33⁺ MBV dampened the local inflammatory response and shifted the phenotype of macrophages responding to implantation of gluBP toward an anti-inflammatory state. Despite modulation of the immune response to gluBP, MBV did not inhibit the calcification response to the material.

This work supports a paradigm in which MBV and their bioactive constituent components primarily target macrophages to direct an anti-inflammatory or pro-remodeling phenotype. While the direct effect of MBV on other cell types is small, the MBV-induced phenotypical changes in macrophages play a significant role in modulating other pathways associated with disease progression (Figure 37).

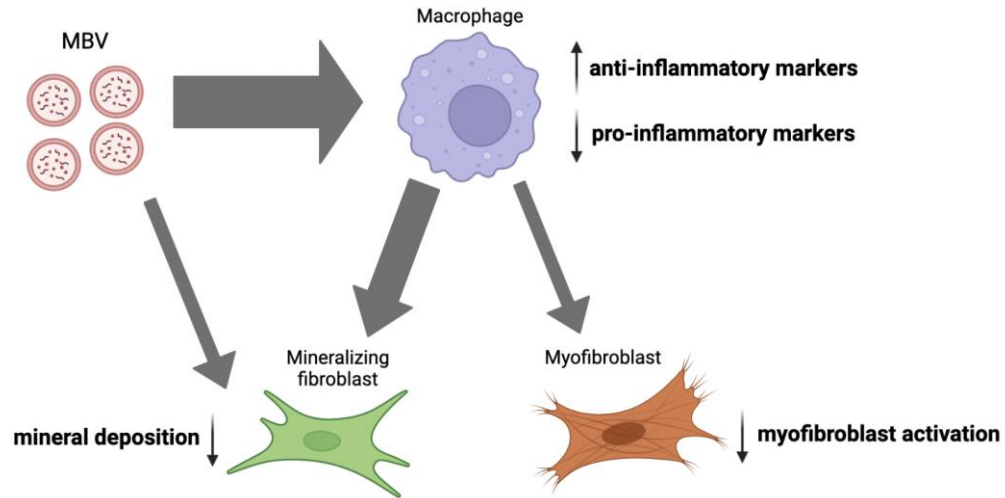


Figure 37. Schematic summary of MBV effects on cellular processes.

Results of the present study suggest that macrophages are the main target cell for MBV. The anti-inflammatory effects of MBV in macrophages result in downstream phenotypical effects of the macrophage secretome on fibroblasts. The size of the gray arrows represent the magnitude of the effect.

The results of the present work may have significant clinical implications. Exosomes harvested from biological fluids are being investigated for both diagnostic and therapeutic applications. Identification of MBV as unique from fluid-phase exosomes provides a new perspective in extracellular vesicle-based therapeutics and may guide next generation regenerative medicine solutions. The understanding of how MBV cargo, composition, and most likely bioactive effects vary with tissue source and disease state is imperative to inform the appropriate choice of MBV for the desired application as well as facilitate quality control metrics of the MBV for clinical use. The critical importance of IL-33 cargo to MBV bioactivity as evidenced throughout this work highlights the importance of MBV cargo in directing phenotypical changes and encourages development of tailored vesicles to enhance clinical results. Finally, the ability of systemic MBV administration to modulate the local host immune response expands their potential clinical application.

Bibliography

- [1] B. Iung, A. Vahanian, Epidemiology of valvular heart disease in the adult, *Nat. Rev. Cardiol.* 8 (2011) 162–172. <https://doi.org/10.1038/nrcardio.2010.202>.
- [2] J.L. D’Arcy, S. Coffey, M.A. Loudon, A. Kennedy, J. Pearson-Stuttard, J. Birks, E. Frangou, A.J. Farmer, D. Mant, J. Wilson, S.G. Myerson, B.D. Prendergast, Large-scale community echocardiographic screening reveals a major burden of undiagnosed valvular heart disease in older people: The OxVALVE Population Cohort Study, *Eur. Heart J.* 37 (2016) 3515-3522a. <https://doi.org/10.1093/eurheartj/ehw229>.
- [3] S. Virano, A. Alonso, H.J. Aparicio, E.J. Benjamin, M. Bittencourt, C.W. Callaway, A.P. Carson, A. Chamberlain, S. Cheng, F. Dellings, M.S. V Elkind, K.R. Evenson, J.F. Ferguson, D. Gupta, S. Khan, B. Kissela, K.L. Knutson, C.D. Lee, T.T. Lewis, J. Liu, M.S. Loop, P.L. Lutsey, J. Ma, J. Mackey, S. Martin, D.B. Matchar, M. Mussolino, S. Navaneethan, A.M. Perak, G. Roth, Z. Samad, G. Satou, E. Schroeder, S. Shah, C. Shay, A. Stokes, L. VanWagner, N.-Y. Wang, C. Tsao, Heart disease and stroke statistics-2021 update: A report from the American Heart Association, 2021. <https://doi.org/10.1161/CIR.0000000000000950>.
- [4] L. Musumeci, N. Jacques, A. Hego, A. Nchimi, P. Lancellotti, C. Oury, Prosthetic aortic valves: Challenges and solutions, *Front. Cardiovasc. Med.* 5 (2018) 1–5. <https://doi.org/10.3389/fcvm.2018.00046>.
- [5] C. Basso, M. Boschello, C. Perrone, A. Mecenero, A. Cera, D. Bicego, G. Thiene, E. De Dominicis, An echocardiographic survey of primary school children for bicuspid aortic valve, *Am. J. Cardiol.* 93 (2004) 661–663. <https://doi.org/10.1016/j.amjcard.2003.11.031>.
- [6] R. Danielsen, T. Aspelund, T.B. Harris, V. Gudnason, P. Sciences, The prevalence of aortic stenosis in the elderly in Iceland and predictions for the coming decades : The AGES-Reykjavík study, *Int. J. Cardiol.* 176 (2014) 916–922. <https://doi.org/10.1016/j.ijcard.2014.08.053>.The.
- [7] S.S. Qi, R.F. Kelly, R. Bianco, F.J. Schoen, Increased utilization of bioprosthetic aortic valve technology:Trends, drivers, controversies and future directions, *Expert Rev. Cardiovasc. Ther.* 19 (2021) 537–546. <https://doi.org/10.1080/14779072.2021.1924676>.
- [8] J.D. Carroll, M.J. Mack, S. Vemulapalli, H.C. Herrmann, T.G. Gleason, G. Hanzel, G.M. Deeb, V.H. Thourani, D.J. Cohen, N. Desai, A.J. Kirtane, S. Fitzgerald, J. Michaels, C. Krohn, F.A. Masoudi, R.G. Brindis, J.E. Bavaria, STS-ACC TVT registry of transcatheter aortic valve replacement, *J. Am. Coll. Cardiol.* 76 (2020) 2492–2516. <https://doi.org/10.1016/j.jacc.2020.09.595>.
- [9] G.J. Vlahakes, Mechanical heart valves, *Circulation.* 116 (2007) 1759–1760.

<https://doi.org/10.1161/CIRCULATIONAHA.107.729582>.

- [10] R. Jiménez-García, N. Perez-Farinos, J. de Miguel-Díez, V. Hernández-Barrera, M. Méndez-Bailón, I. Jimenez-Trujillo, J.M. de Miguel-Yanes, A. López-De-Andrés, National trends in utilization and in-hospital outcomes of surgical aortic valve replacements in Spain, 2001-2015, *Brazilian J. Cardiovasc. Surg.* 35 (2020) 65–74. <https://doi.org/10.21470/1678-9741-2019-0181>.
- [11] K.Y.C. Li, Bioprosthetic heart valves: Upgrading a 50-year old technology, *Front. Cardiovasc. Med.* 6 (2019) 1–6. <https://doi.org/10.3389/fcvm.2019.00047>.
- [12] A.E. Kostyunin, A.E. Yuzhalin, M.A. Rezvova, E.A. Ovcharenko, T. V. Glushkova, A.G. Kutikhin, Degeneration of bioprosthetic heart valves: Update 2020, *J. Am. Heart Assoc.* 9 (2020) e018506. <https://doi.org/10.1161/JAHA.120.018506>.
- [13] T. Bottio, G. Thiene, E. Pettenazzo, P. Ius, U. Bortolotti, G. Rizzoli, C. Valfré, D. Casarotto, M. Valente, Hancock II bioprosthesis: A glance at the microscope in mid-long-term explants, *J. Thorac. Cardiovasc. Surg.* 126 (2003) 99–105. [https://doi.org/10.1016/S0022-5223\(03\)00131-4](https://doi.org/10.1016/S0022-5223(03)00131-4).
- [14] A. Anselmi, V.G. Ruggieri, B. Lelong, E. Flecher, H. Corbineau, T. Langanay, J.P. Verhoye, A. Leguerrier, Mid-term durability of the Trifecta bioprosthesis for aortic valve replacement, *J. Thorac. Cardiovasc. Surg.* 153 (2017) 21-28.e1. <https://doi.org/10.1016/j.jtcvs.2016.07.080>.
- [15] B.S. Fyfe, F.J. Schoen, Pathological analysis of nonstented Freestyle aortic root bioprostheses treated with amino oleic acid., *Semin. Thorac. Cardiovasc. Surg.* 11 (1999) 151–156.
- [16] M. Celiento, G. Ravenni, A.D. Milano, S. Pratali, G. Sciotti, C. Nardi, U. Bortolotti, Aortic valve replacement with the medtronic mosaic bioprosthesis: A 13-year follow-up, *Ann. Thorac. Surg.* 93 (2012) 510–515. <https://doi.org/10.1016/j.athoracsur.2011.10.062>.
- [17] F.J. Schoen, R.J. Levy, H. Tam, N. Vyavahare, 2.4.5 - Pathological calcification of biomaterials, in: W.R. Wagner, S.E. Sakiyama-Elbert, G. Zhang, M. Yaszemski (Eds.), *Biomater. Sci. An Introd. to Mater. Med.*, 4th editio, Academic Press, 2020: pp. 973–994. <https://doi.org/https://doi.org/10.1016/B978-0-12-816137-1.00065-9>.
- [18] R.F. Siddiqui, J.R. Abraham, J. Butany, Bioprosthetic heart valves: Modes of failure, *Histopathology.* 55 (2009) 135–144. <https://doi.org/10.1111/j.1365-2559.2008.03190.x>.
- [19] T. Xi, J. Ma, W. Tian, X. Lei, S. Long, B. Xi, Prevention of tissue calcification on bioprosthetic heart valve by using epoxy compounds: a study of calcification tests in vitro and in vivo., *J. Biomed. Mater. Res.* 26 (1992) 1241–1251. <https://doi.org/10.1002/jbm.820260913>.
- [20] H.G. Lim, S.H. Kim, S.Y. Choi, Y.J. Kim, Anticalcification effects of decellularization, solvent, and detoxification treatment for genipin and glutaraldehyde fixation of bovine

- pericardium, *Eur. J. Cardio-Thoracic Surg.* 41 (2012) 383–390. <https://doi.org/10.1016/j.ejcts.2011.05.016>.
- [21] Y. Chang, C.C. Tsai, H.C. Liang, H.W. Sung, In vivo evaluation of cellular and acellular bovine pericardia fixed with a naturally occurring crosslinking agent (genipin), *Biomaterials*. 23 (2002) 2447–2457. [https://doi.org/10.1016/S0142-9612\(01\)00379-9](https://doi.org/10.1016/S0142-9612(01)00379-9).
- [22] D. Wang, H. Jiang, J. Li, J. Zhou, S. Hu, Mitigated calcification of glutaraldehyde-fixed bovine pericardium by tannic acid in rats, *Chin. Med. J. (Engl)*. 121 (2008) 1675–1679.
- [23] H. Tam, W. Zhang, D. Infante, N. Parchment, M. Sacks, N. Vyavahare, Fixation of bovine pericardium-based tissue biomaterial with irreversible chemistry improves biochemical and biomechanical properties, *J. Cardiovasc. Transl. Res.* 10 (2017) 194–205. <https://doi.org/10.1007/s12265-017-9733-5>.
- [24] N. Li, Y. Li, D. Gong, C. Xia, X. Liu, Z. Xu, Efficient decellularization for bovine pericardium with extracellular matrix preservation and good biocompatibility, *Interact. Cardiovasc. Thorac. Surg.* 26 (2018) 768–776. <https://doi.org/10.1093/icvts/ivx416>.
- [25] C. Collatusso, J.G. Roderjan, E.D. Vieira, F.D.A. da Costa, L. de Noronha, D. de F. Fornazari, Effect of SDS-based decelullarization in the prevention of calcification in glutaraldehyde- preserved bovine pericardium. Study in rats, *Brazilian J. Cardiovasc. Surg.* 27 (2012) 88–96. <https://doi.org/10.5935/1678-9741.20120013>.
- [26] N. Filippo, A. Paola, I. Laura, Biocompatibility evaluation criteria for novel xenograft materials: Distribution and quantification of remnant nucleic acid and alpha-Gal epitope, *J. Stem Cell Res. Ther.* 01 (2013). <https://doi.org/10.4172/2157-7633.s6-009>.
- [27] C.G.A. McGregor, H. Kogelberg, M. Vlasin, G.W. Byrne, Gal-knockout bioprostheses exhibit less immune stimulation compared to standard biological heart valves., *J. Heart Valve Dis.* 22 (2013) 383–390.
- [28] B. Rahmani, C. McGregor, G. Byrne, G. Burriesci, A durable porcine pericardial surgical bioprosthetic heart valve: a Proof of concept, *J. Cardiovasc. Transl. Res.* 12 (2019) 331–337. <https://doi.org/10.1007/s12265-019-09868-3>.
- [29] K. Mendelson, F.J. Schoen, Heart valve tissue engineering: Concepts, approaches, progress, and challenges, *Ann. Biomed. Eng.* 34 (2006) 1799–1819. <https://doi.org/10.1007/s10439-006-9163-z>.
- [30] F.J. Schoen, Heart valve tissue engineering: Quo vadis?, *Curr. Opin. Biotechnol.* 22 (2011) 698–705. <https://doi.org/10.1016/j.copbio.2011.01.004>.
- [31] T. Shinoka, C.K. Breuer, R.E. Tanel, G. Zund, T. Miura, P.X. Ma, R. Langer, J.I. Vacanti, J.E. Mayer, Tissue engineering heart valves: Valve leaflet replacement in a lamb model, *Ann. Thorac. Surg.* 60 (1995) S513–S516. [https://doi.org/10.1016/0003-4975\(95\)00733-4](https://doi.org/10.1016/0003-4975(95)00733-4).
- [32] A. Driessen-Mol, M.Y. Emmert, P.E. Dijkman, L. Frese, B. Sanders, B. Weber, N.

- Cesarovic, M. Sidler, J. Leenders, R. Jenni, J. Grünenfelder, V. Falk, F.P.T. Baaijens, S.P. Hoerstrup, Transcatheter implantation of homologous “off-the-shelf” tissue-engineered heart valves with self-repair capacity: Long-term functionality and rapid in vivo remodeling in sheep, *J. Am. Coll. Cardiol.* 63 (2014) 1320–1329. <https://doi.org/10.1016/j.jacc.2013.09.082>.
- [33] S.P. Hoerstrup, R. Sodian, S. Daebritz, J. Wang, E.A. Bacha, D.P. Martin, A.M. Moran, K.J. Guleserian, J.S. Sperling, S. Kaushal, J.P. Vacanti, F.J. Schoen, J.E.J. Mayer, Functional living trileaflet heart valves grown in vitro., *Circulation.* 102 (2000) III44-9. https://doi.org/10.1161/01.cir.102.suppl_3.iii-44.
- [34] C.V.C. Bouten, A.I.P.M. Smits, F.P.T. Baaijens, Can we grow valves inside the heart? Perspective on material-based in situ heart valve tissue engineering, *Front. Cardiovasc. Med.* 5 (2018) 1–10. <https://doi.org/10.3389/fcvm.2018.00054>.
- [35] P. Zilla, J. Brink, P. Human, D. Bezuidenhout, Prosthetic heart valves: Catering for the few, *Biomaterials.* 29 (2008) 385–406. <https://doi.org/10.1016/j.biomaterials.2007.09.033>.
- [36] J. Kluin, H. Talacua, A.I.P.M. Smits, M.Y. Emmert, M.C.P. Brugmans, E.S. Fioretta, P.E. Dijkman, S.H.M. Söntjens, R. Duijvelshoff, S. Dekker, M.W.J.T. Janssen-van den Broek, V. Lintas, A. Vink, S.P. Hoerstrup, H.M. Janssen, P.Y.W. Dankers, F.P.T. Baaijens, C.V.C. Bouten, In situ heart valve tissue engineering using a bioresorbable elastomeric implant – From material design to 12 months follow-up in sheep, *Biomaterials.* 125 (2017) 101–117. <https://doi.org/10.1016/j.biomaterials.2017.02.007>.
- [37] I. Tudorache, A. Horke, S. Cebotari, S. Sarikouch, D. Boethig, T. Breymann, P. Beerbaum, H. Bertram, M. Westhoff-Bleck, K. Theodoridis, D. Bobylev, E. Cheptanaru, A. Ciubotaru, A. Haverich, Decellularized aortic homografts for aortic valve and aorta ascendens replacement, *Eur. J. Cardio-Thoracic Surg.* 50 (2016) 89–97. <https://doi.org/10.1093/ejcts/ezw013>.
- [38] S. Sarikouch, K. Theodoridis, A. Hilfiker, D. Boethig, G. Laufer, M. Andreas, S. Cebotari, I. Tudorache, D. Bobylev, L. Neubert, K. Teiken, J.L. Robertus, D. Jonigk, P. Beerbaum, A. Haverich, A. Horke, Early insight into in vivo recellularization of cell-free allogenic heart valves, *Ann. Thorac. Surg.* 108 (2019) 581–589. <https://doi.org/10.1016/j.athoracsur.2019.02.058>.
- [39] I. Tudorache, K. Theodoridis, H. Baraki, S. Sarikouch, C. Bara, T. Meyer, K. Höffler, D. Hartung, A. Hilfiker, A. Haverich, S. Cebotari, Decellularized aortic allografts versus pulmonary autografts for aortic valve replacement in the growing sheep model: Haemodynamic and morphological results at 20 months after implantation, *Eur. J. Cardio-Thoracic Surg.* 49 (2016) 1228–1238. <https://doi.org/10.1093/ejcts/ezv362>.
- [40] L. Iop, A. Bonetti, F. Naso, S. Rizzo, S. Cagnin, R. Bianco, C. Dal Lin, P. Martini, H. Poser, P. Franci, G. Lanfranchi, R. Busetto, M. Spina, C. Basso, M. Marchini, A. Gandaglia, F. Ortolani, G. Gerosa, Decellularized allogenic heart valves demonstrate self-regeneration potential after a long-term preclinical evaluation, *PLoS One.* 9 (2014). <https://doi.org/10.1371/journal.pone.0099593>.

- [41] K. Theodoridis, I. Tudorache, A. Calistru, S. Cebotari, T. Meyer, S. Sarikouch, C. Bara, R. Brehm, A. Haverich, A. Hilfiker, Successful matrix guided tissue regeneration of decellularized pulmonary heart valve allografts in elderly sheep, *Biomaterials*. 52 (2015) 221–228. <https://doi.org/10.1016/j.biomaterials.2015.02.023>.
- [42] F. Zafar, R.B. Hinton, R.A. Moore, R.S. Baker, R. Bryant, D.A. Narmoneva, M.D. Taylor, D.L. Morales, Physiological growth, remodeling potential, and preserved function of a novel bioprosthetic tricuspid valve: Tubular bioprosthesis made of small intestinal submucosa-derived extracellular matrix, *J. Am. Coll. Cardiol.* 66 (2015) 877–888. <https://doi.org/10.1016/j.jacc.2015.06.1091>.
- [43] C.E. Ruiz, M. Iemura, S. Medie, P. Varga, W.G. Van Alstine, S. Mack, A. Deligio, N. Fearnot, U.H. Beier, D. Pavcnik, Z.M. Hijazi, M. Kiupel, Transcatheter placement of a low-profile biodegradable pulmonary valve made of small intestinal submucosa: A long-term study in a swine model, *J. Thorac. Cardiovasc. Surg.* 130 (2005) 477.e1-477.e9. <https://doi.org/10.1016/j.jtcvs.2005.04.008>.
- [44] B. Weber, J. Scherman, M.Y. Emmert, J. Gruenenfelder, R. Verbeek, M. Bracher, M. Black, J. Kortsmid, T. Franz, R. Schoenauer, L. Baumgartner, C. Brokopp, I. Agarkova, P. Wolint, G. Zund, V. Falk, P. Zilla, S.P. Hoerstrup, Injectable living marrow stromal cell-based autologous tissue engineered heart valves: First experiences with a one-step intervention in primates, *Eur. Heart J.* 32 (2011) 2830–2840. <https://doi.org/10.1093/eurheartj/ehr059>.
- [45] J.M. Reimer, Z.H. Syedain, B.H.T. Haynie, R.T. Tranquillo, Pediatric tubular pulmonary heart valve from decellularized engineered tissue tubes, *Biomaterials*. 62 (2015) 88–94. <https://doi.org/10.1016/j.biomaterials.2015.05.009>.
- [46] J. Reimer, Z. Syedain, B. Haynie, M. Lahti, J. Berry, R. Tranquillo, Implantation of a tissue-engineered tubular heart valve in growing lambs, *Ann. Biomed. Eng.* 45 (2017) 439–451. <https://doi.org/10.1007/s10439-016-1605-7>.
- [47] A.K. Capulli, M.Y. Emmert, F.S. Pasqualini, D. Kehl, E. Caliskan, J.U. Lind, S.P. Sheehy, S.J. Park, S. Ahn, B. Weber, J.A. Goss, S.P. Hoerstrup, K.K. Parker, JetValve: Rapid manufacturing of biohybrid scaffolds for biomimetic heart valve replacement, *Biomaterials*. 133 (2017) 229–241. <https://doi.org/10.1016/j.biomaterials.2017.04.033>.
- [48] G. Bennink, S. Torii, M. Brugmans, M. Cox, O. Svanidze, E. Ladich, T. Carrel, R. Virmani, A novel restorative pulmonary valved conduit in a chronic sheep model: Mid-term hemodynamic function and histologic assessment, *J. Thorac. Cardiovasc. Surg.* 155 (2018) 2591-2601.e3. <https://doi.org/10.1016/j.jtcvs.2017.12.046>.
- [49] M.Y. Emmert, B. Weber, L. Behr, S. Sammut, T. Frauenfelder, P. Wolint, J. Scherman, D. Bettex, J. Gruenenfelder, V. Falk, S.P. Hoerstrup, Transcatheter aortic valve implantation using anatomically oriented, marrow stromal cell-based, stented, tissue-engineered heart valves: Technical considerations and implications for translational cell-based heart valve concepts, *Eur. J. Cardio-Thoracic Surg.* 45 (2014) 61–68. <https://doi.org/10.1093/ejcts/ezt243>.

- [50] M. Brugmans, A. Serrero, M. Cox, O. Svanidze, F.J. Schoen, Morphology and mechanisms of a novel absorbable polymeric conduit in the pulmonary circulation of sheep, *Cardiovasc. Pathol.* 38 (2020) 31–38. <https://doi.org/10.1016/j.carpath.2018.10.008>.
- [51] Y. Miyazaki, O.I. Soliman, M. Abdelghani, A. Katsikis, C. Naz, S. Lopes, B. Warnack, M. Cox, Y. Onuma, P.W. Serruys, Acute performance of a novel restorative transcatheter aortic valve: Preclinical results, *EuroIntervention.* 13 (2017) e1410–e1417. <https://doi.org/10.4244/EIJ-D-17-00554>.
- [52] L.A. Bockeria, O. Svanidze, A. Kim, K. Shatalov, V. Makarenko, M. Cox, T. Carrel, Total cavopulmonary connection with a new bioabsorbable vascular graft: First clinical experience, *J. Thorac. Cardiovasc. Surg.* 153 (2017) 1542–1550. <https://doi.org/10.1016/j.jtcvs.2016.11.071>.
- [53] D.L. Morales, C.C. Herrington, E.A. Bacha, V.O. Morell, Z. Prodán, T. Mroczek, S. Sivalingam, M. Cox, G. Bennink, F.M. Asch, Z. Prodan, T. Mroczek, S. Sivalingam, M. Cox, G. Bennink, F.M. Asch, A novel restorative pulmonary valve conduit: Early outcomes of two clinical trials, *Front. Cardiovasc. Med.* 7 (2021) 1–9. <https://doi.org/10.3389/fcvm.2020.583360>.
- [54] D. Capodanno, A.S. Petronio, B. Prendergast, H. Eltchaninoff, A. Vahanian, T. Modine, P. Lancellotti, L. Sondergaard, P.F. Ludman, C. Tamburino, N. Piazza, J. Hancock, J. Mehilli, R.A. Byrne, A. Baumbach, A.P. Kappetein, S. Windecker, J. Bax, M. Haude, Standardized definitions of structural deterioration and valve failure in assessing long-term durability of transcatheter and surgical aortic bioprosthetic valves: A consensus statement from the European Association of Percutaneous Cardiovascular Interventions, *Eur. J. Cardio-Thoracic Surg.* 52 (2017) 408–417. <https://doi.org/10.1093/EJCTS/EZX244>.
- [55] A. Koziarz, A. Makhdom, J. Butany, M. Ouzounian, J. Chung, Modes of bioprosthetic valve failure: A narrative review, *Curr. Opin. Cardiol.* 35 (2020) 123–132. <https://doi.org/10.1097/HCO.0000000000000711>.
- [56] S. Karakoyun, M. Ozan Gürsoy, M. Yesin, M. Kalçık, M.A. Astarçioğlu, S. Gündüz, A. Emrah Oğuz, Ş. Çoban Kökten, A. Nimet Karadayı, A. Tuncer, C. Köksal, T. Gökdeniz, M. Özkan, Histopathological and immunohistochemical evaluation of pannus tissue in patients with prosthetic valve dysfunction., *J. Heart Valve Dis.* 25 (2016) 104–111.
- [57] H. Teshima, N. Hayashida, H. Yano, M. Nishimi, E. Tayama, S. Fukunaga, H. Akashi, T. Kawara, S. Aoyagi, Obstruction of St Jude medical valves in the aortic position: Histology and immunohistochemistry of pannus, *J. Thorac. Cardiovasc. Surg.* 126 (2003) 401–407. [https://doi.org/10.1016/S0022-5223\(03\)00702-5](https://doi.org/10.1016/S0022-5223(03)00702-5).
- [58] F.J. Schoen, R.J. Levy, Tissue heart valves: current challenges and future research perspectives., *J. Biomed. Mater. Res.* 47 (1999) 439–65. [https://doi.org/10.1002/\(sici\)1097-4636\(19991215\)47:4<439::aid-jbm1>3.0.co;2-o](https://doi.org/10.1002/(sici)1097-4636(19991215)47:4<439::aid-jbm1>3.0.co;2-o).
- [59] R.A. Manji, W. Lee, D.K.C. Cooper, Xenograft bioprosthetic heart valves: Past, present and future, *Int. J. Surg.* 23 (2015) 280–284. <https://doi.org/10.1016/j.ijssu.2015.07.009>.

- [60] M.J. Thubrikar, J.D. Deck, J. Aouad, S.P. Nolan, Role of mechanical stress in calcification of aortic bioprosthetic valves, *J. Thorac. Cardiovasc. Surg.* 86 (1983) 115–125. [https://doi.org/10.1016/s0022-5223\(19\)39217-7](https://doi.org/10.1016/s0022-5223(19)39217-7).
- [61] G. Golomb, F.J. Schoen, M.S. Smith, J. Linden, M. Dixon, R.J. Levy, The role of glutaraldehyde-induced cross-links in calcification of bovine pericardium used in cardiac valve bioprostheses, *Am. J. Pathol.* 127 (1987) 122–130.
- [62] M. Grabenwöger, J. Sider, F. Fitzal, C. Zelenka, U. Windberger, M. Grimm, A. Moritz, P. Böck, E. Wolner, Impact of glutaraldehyde on calcification of pericardial bioprosthetic heart valve material., *Ann. Thorac. Surg.* 62 (1996) 772–777.
- [63] B. Meuris, H. De Praetere, M. Strasly, P. Trabucco, J.C. Lai, P. Verbrugghe, P. Herijgers, A novel tissue treatment to reduce mineralization of bovine pericardial heart valves, *J. Thorac. Cardiovasc. Surg.* 156 (2018) 197–206. <https://doi.org/10.1016/j.jtcvs.2018.01.099>.
- [64] D.T. Simionescu, Prevention of calcification in bioprosthetic heart valves: Challenges and perspectives, *Expert Opin. Biol. Ther.* 4 (2004) 1971–1985. <https://doi.org/10.1517/14712598.4.12.1971>.
- [65] F.J. Schoen, R.J. Levy, Calcification of tissue heart valve substitutes: progress toward understanding and prevention., *Ann. Thorac. Surg.* 79 (2005) 1072–1080. <https://doi.org/10.1016/j.athoracsur.2004.06.033>.
- [66] M. Dahm, M. Husmann, E. Mayer, D. Prüfer, E. Groh, H. Oelert, Relevance of immunologic reactions for tissue failure of bioprosthetic heart valves, *Ann. Thorac. Surg.* 60 (1995). [https://doi.org/10.1016/0003-4975\(95\)00291-R](https://doi.org/10.1016/0003-4975(95)00291-R).
- [67] G. Li, W. Qiao, W. Zhang, F. Li, J. Shi, N. Dong, The shift of macrophages toward M1 phenotype promotes aortic valvular calcification, *J. Thorac. Cardiovasc. Surg.* 153 (2017) 1318-1327.e1. <https://doi.org/10.1016/j.jtcvs.2017.01.052>.
- [68] I. Šteiner, L. Krbal, T. Rozkoš, J. Harrer, J. Laco, Calcific aortic valve stenosis: Immunohistochemical analysis of inflammatory infiltrate, *Pathol. Res. Pract.* 208 (2012) 231–234. <https://doi.org/https://doi.org/10.1016/j.prp.2012.02.009>.
- [69] J.J. Kaden, R. Kiliç, A. Sarikoç, S. Hagl, S. Lang, U. Hoffmann, M. Brueckmann, M. Borggrefe, Tumor necrosis factor alpha promotes an osteoblast-like phenotype in human aortic valve myofibroblasts: a potential regulatory mechanism of valvular calcification., *Int. J. Mol. Med.* 16 (2005) 869–872.
- [70] Z. Yu, K. Seya, K. Daitoku, S. Motomura, I. Fukuda, K.I. Furukawa, Tumor necrosis factor- α accelerates the calcification of human aortic valve interstitial cells obtained from patients with calcific aortic valve stenosis via the BMP2-Dlx5 pathway, *J. Pharmacol. Exp. Ther.* 337 (2011) 16–23. <https://doi.org/10.1124/jpet.110.177915>.
- [71] L. Hénaut, A. Candellier, C. Boudot, M. Grissi, R. Mentaverri, G. Choukroun, M. Brazier,

- S. Kamel, Z.A. Massy, New insights into the roles of monocytes/macrophages in cardiovascular calcification associated with chronic kidney disease, *Toxins (Basel)*. 11 (2019) 1–33. <https://doi.org/10.3390/toxins11090529>.
- [72] P. Human, P. Zilla, Characterization of the immune response to valve bioprostheses and its role in primary tissue failure, *Ann. Thorac. Surg.* 71 (2001) 20–23. [https://doi.org/10.1016/S0003-4975\(01\)02492-4](https://doi.org/10.1016/S0003-4975(01)02492-4).
- [73] R.A. Manji, L.F. Zhu, N.K. Nijjar, D.C. Rayner, G.S. Korbitt, T.A. Churchill, R. V. Rajotte, A. Koshal, D.B. Ross, Glutaraldehyde-fixed bioprosthetic heart valve conduits calcify and fail from xenograft rejection, *Circulation*. 114 (2006) 318–327. <https://doi.org/10.1161/CIRCULATIONAHA.105.549311>.
- [74] P. Human, P. Zilla, The possible role of immune responses in bioprosthetic heart valve failure., *J. Heart Valve Dis.* 10 (2001) 460–466.
- [75] R.J. Levy, F.J. Schoen, J.T. Levy, A.C. Nelson, S.L. Howard, L.J. Oshry, Biologic determinants of dystrophic calcification and osteocalcin deposition in glutaraldehyde-preserved porcine aortic valve leaflets implanted subcutaneously in rats, *Am. J. Pathol.* 113 (1983) 143–155.
- [76] R.J. Levy, F.J. Schoen, S.L. Howard, Mechanism of calcification of porcine bioprosthetic aortic valve cusps: Role of T-lymphocytes, *Am. J. Cardiol.* 52 (1983) 629–631. [https://doi.org/10.1016/0002-9149\(83\)90040-1](https://doi.org/10.1016/0002-9149(83)90040-1).
- [77] G. Guo, L. Jin, B. Wu, H. He, F. Yang, L. Xu, Y. Lei, Y. Wang, A method for simultaneously crosslinking and functionalizing extracellular matrix-based biomaterials as bioprosthetic heart valves with enhanced endothelialization and reduced inflammation, *Acta Biomater.* 119 (2020) 89–100. <https://doi.org/10.1016/j.actbio.2020.10.029>.
- [78] S.J. Bozso, J.J.H. Kang, R. Basu, B. Adam, J.R.B. Dyck, G.Y. Oudit, M.C. Moon, D.H. Freed, J. Nagendran, J. Nagendran, Structural valve deterioration is linked to increased immune infiltrate and chemokine expression, *J. Cardiovasc. Transl. Res.* (2020). <https://doi.org/10.1007/s12265-020-10080-x>.
- [79] C. Veraar, M. Koschutnik, C. Nitsche, M. Laggner, D. Polak, B. Bohle, M. Mildner, A. Mangold, B. Moser, J. Mascherbauer, H.J. Ankersmit, The lost immunological innocence of biological scaffolds for TAVI, Pre-Print. (2020).
- [80] C. Hu, R. Luo, Y. Wang, Heart valves cross-linked with erythrocyte membrane drug-loaded nanoparticles as a biomimetic strategy for anti-coagulation, anti-inflammation, anti-calcification, and endothelialization, *ACS Appl. Mater. Interfaces*. 12 (2020) 41113–41126. <https://doi.org/10.1021/acsami.0c12688>.
- [81] J. Dziki, S. Badylak, M. Yabroudi, B. Sicari, F. Ambrosio, K. Stearns, N. Turner, A. Wyse, M.L. Boninger, E.H.P. Brown, J.P. Rubin, An acellular biologic scaffold treatment for volumetric muscle loss: results of a 13-patient cohort study, *Npj Regen. Med.* 1 (2016) 16008. <https://doi.org/10.1038/npjregenmed.2016.8>.

- [82] J.E. Valentin, N.J. Turner, T.W. Gilbert, S.F. Badylak, Functional skeletal muscle formation with a biologic scaffold, *Biomaterials*. 31 (2010) 7475–7484. <https://doi.org/10.1016/j.biomaterials.2010.06.039>. Functional.
- [83] B.M. Sicari, J.P. Rubin, C.L. Dearth, M.T. Wolf, F. Ambrosio, M. Boninger, N.J. Turner, D.J. Weber, T.W. Simpson, A. Wyse, E.H.P. Brown, J.L. Dziki, L.E. Fisher, S. Brown, S.F. Badylak, An acellular biologic scaffold promotes skeletal muscle formation in mice and humans with volumetric muscle loss., *Sci. Transl. Med.* 6 (2014) 234ra58. <https://doi.org/10.1126/scitranslmed.3008085>.
- [84] V. Mase, J. Hsu, S. Wolf, J. Wenke, D. Baer, J. Owens, S. Badylak, T. Walters, Clinical application of an acellular biologic scaffold for surgical repair of a large, traumatic quadriceps femoris muscle defect, *Orthopedics*. 33 (2010).
- [85] S.F. Badylak, T. Hoppo, A. Nieponice, T.W. Gilbert, J.M. Davison, B.A. Jobe, Esophageal preservation in five male patients after endoscopic inner-layer circumferential resection in the setting of superficial cancer: a regenerative medicine approach with a biologic scaffold., *Tissue Eng. Part A*. 17 (2011) 1643–50. <https://doi.org/10.1089/ten.tea.2010.0739>.
- [86] T. Hoppo, S.F. Badylak, B.A. Jobe, A novel esophageal-preserving approach to treat high-grade dysplasia and superficial adenocarcinoma in the presence of chronic gastroesophageal reflux disease., *World J. Surg.* 36 (2012) 2390–2393. <https://doi.org/10.1007/s00268-012-1698-6>.
- [87] A. Nieponice, F.F. Ciotola, F. Nachman, B.A. Jobe, T. Hoppo, R. Londono, S. Badylak, A.E. Badaloni, Patch esophagoplasty: Esophageal reconstruction using biologic scaffolds, *Ann. Thorac. Surg.* 97 (2014) 283–288. <https://doi.org/10.1016/j.athoracsur.2013.08.011>.
- [88] A. Nieponice, K. McGrath, I. Qureshi, E.J. Beckman, J.D. Luketich, T.W. Gilbert, S.F. Badylak, An extracellular matrix scaffold for esophageal stricture prevention after circumferential EMR, *Gastrointest. Endosc.* 69 (2009) 289–296. <https://doi.org/10.1016/j.gie.2008.04.022>.
- [89] P. Consigliere, I. Polyzois, T. Sarkhel, R. Gupta, O. Levy, A.A. Narvani, Preliminary results of a consecutive series of large & massive rotator cuff tears treated with arthroscopic rotator cuff repairs augmented with extracellular matrix, *Arch Bone Jt Surg.* 5 (2017) 14–21.
- [90] L.M. DeJardin, S.P. Arnoczky, B.J. Ewers, R.C. Haut, R.B. Clarke, Tissue-engineered rotator cuff tendon using porcine small intestine submucosa: Histologic and mechanical evaluation in dogs, *Am. J. Sports Med.* 29 (2001) 175–184. <https://doi.org/10.1177/03635465010290021001>.
- [91] G.J. Gilot, A.M. Alvarez-Pinzon, L. Barcksdale, D. Westerdahl, M. Krill, E. Peck, Outcome of large to massive rotator cuff tears repaired with and without extracellular matrix augmentation: A prospective comparative study, *Arthrosc. J. Arthrosc. Relat. Surg.* 31 (2015) 1459–1465. <https://doi.org/10.1016/j.arthro.2015.02.032>.
- [92] T.W. Gilbert, A.M. Stewart-Akers, A. Simmons-Byrd, S.F. Badylak, Degradation and

- remodeling of small intestinal submucosa in canine Achilles tendon repair., *J. Bone Joint Surg. Am.* 89 (2007) 621–630. <https://doi.org/10.2106/JBJS.E.00742>.
- [93] S.F. Badylak, R. Tullius, K. Kokini, K.D. Shelbourne, T. Klootwyk, S.L. Voytik, M.R. Kraine, C. Simmons, The use of xenogeneic small intestinal submucosa as a biomaterial for Achille's tendon repair in a dog model, *J. Biomed. Mater. Res.* 29 (1995) 977–985. <https://doi.org/10.1002/jbm.820290809>.
- [94] A. V. Boruch, A. Nieponice, I.R. Qureshi, T.W. Gilbert, S.F. Badylak, Constructive remodeling of biologic scaffolds is dependent on early exposure to physiologic bladder filling in a canine partial cystectomy model, *J. Surg. Res.* 161 (2010) 217–225. <https://doi.org/10.1016/j.jss.2009.02.014>.
- [95] B.P. Kropp, B.L. Eppley, C.D. Prevel, M.K. Rippy, R.C. Harruff, S.F. Badylak, M.C. Adams, R.C. Rink, M.A. Keating, Experimental assessment of small intestinal submucosa as a bladder wall substitute, *Urology.* 46 (1995) 396–400. [https://doi.org/https://doi.org/10.1016/S0090-4295\(99\)80227-1](https://doi.org/https://doi.org/10.1016/S0090-4295(99)80227-1).
- [96] S.F. Badylak, B. Kropp, T. McPherson, H. Liang, P.W. Snyder, Small intestinal submucosa: a rapidly resorbed bioscaffold for augmentation cystoplasty in a dog model., *Tissue Eng.* 4 (1998) 379–387. <https://doi.org/10.1089/ten.1998.4.379>.
- [97] P.P. Reddy, D.J. Barrieras, G. Wilson, D.J. Bagli, G.A. McLorie, A.E. Khoury, P.A. Merguerian, Regeneration of functional bladder substitutes using large segment acellular matrix allografts in a porcine model, *J. Urol.* 164 (2000) 936–941. <https://doi.org/10.1097/00005392-200009020-00005>.
- [98] P.A. Merguerian, P.P. Reddy, D.J. Barrieras, G.J. Wilson, K. Woodhouse, D.J. Bagli, G.A. McLorie, A.E. Khoury, Acellular bladder matrix allografts in the regeneration of functional bladders: evaluation of large-segment (> 24 cm) substitution in a porcine model, *BJU Int.* 85 (2000) 894–898.
- [99] F.G. Scholl, M.M. Boucek, K.-C. Chan, L. Valdes-Cruz, R. Perryman, Preliminary experience with cardiac reconstruction using decellularized porcine extracellular matrix scaffold, *World J. Pediatr. Congenit. Hear. Surg.* 1 (2010) 132–136. <https://doi.org/10.1177/2150135110362092>.
- [100] J.W. Wassenaar, R. Gaetani, J.J. Garcia, R.L. Braden, C.G. Luo, D. Huang, A.N. DeMaria, J.H. Omens, K.L. Christman, Evidence for mechanisms underlying the functional benefits of a myocardial matrix hydrogel for post-MI treatment., *J. Am. Coll. Cardiol.* 67 (2016) 1074–86. <https://doi.org/10.1016/j.jacc.2015.12.035>.
- [101] S.F. Badylak, P. V Kochupura, I.S. Cohen, S. V Doronin, A.E. Saltman, T.W. Gilbert, D.J. Kelly, R.A. Ignatz, G.R. Gaudette, The use of extracellular matrix as an inductive scaffold for the partial replacement of functional myocardium., *Cell Transplant.* 15 Suppl 1 (2006) S29-40. <https://doi.org/10.3727/000000006783982368>.
- [102] A. Quarti, S. Nardone, M. Colaneri, G. Santoro, M. Pozzi, Preliminary experience in the

- use of an extracellular matrix to repair congenital heart diseases, *Interact. Cardiovasc. Thorac. Surg.* 13 (2011) 569–572. <http://dx.doi.org/10.1510/icvts.2011.280016>.
- [103] T.W. Gilbert, A. Nieponice, A.R. Spievack, J. Holcomb, S. Gilbert, S.F. Badylak, Repair of the thoracic wall with an extracellular matrix scaffold in a canine model, *J. Surg. Res.* 147 (2008) 61–67. <https://doi.org/https://doi.org/10.1016/j.jss.2007.04.035>.
- [104] P. V Kochupura, E.U. Azeloglu, D.J. Kelly, S. V Doronin, S.F. Badylak, I.B. Krukenkamp, I.S. Cohen, G.R. Gaudette, Tissue-engineered myocardial patch derived from extracellular matrix provides regional mechanical function, *Circulation.* 112 (2005) 144–149. <https://doi.org/10.1161/CIRCULATIONAHA.104.524355>.
- [105] L.D. Knoll, Use of small intestinal submucosa graft for the surgical management of Peyronie’s disease, *J. Urol.* 178 (2007) 2474–2478. <https://doi.org/https://doi.org/10.1016/j.juro.2007.08.044>.
- [106] J.L. Cook, D.B. Fox, K. Kuroki, M. Jayo, P.G. De Deyne, In vitro and in vivo comparison of five biomaterials used for orthopedic soft tissue augmentation., *Am. J. Vet. Res.* 69 (2008) 148–156. <https://doi.org/10.2460/ajvr.69.1.148>.
- [107] H. Kimmel, M. Rahn, T.W. Gilbert, The clinical effectiveness in wound healing with extracellular matrix derived from porcine urinary bladder matrix: A case series on severe chronic wounds, *J. Am. Col. Certif. Wound Spec.* 2 (2010) 55–59. <https://doi.org/http://dx.doi.org/10.1016/j.jcws.2010.11.002>.
- [108] S.E. Geiger, O.A. Deigni, J.T. Watson, B.A. Kraemer, Management of open distal lower extremity wounds with exposed tendons using porcine urinary bladder matrix, *Wounds a Compend. Clin. Res. Pract.* 28 (2016) 306–316.
- [109] S.F. Badylak, The extracellular matrix as a biologic scaffold material, *Biomaterials.* 28 (2007) 3587–3593. <https://doi.org/10.1016/j.biomaterials.2007.04.043>.
- [110] A.J. Allman, T.B. McPherson, L.C. Merrill, S.F. Badylak, D.W. Metzger, The Th2-restricted immune response to xenogeneic small intestinal submucosa does not influence systemic protective immunity to viral and bacterial pathogens, *Tissue Eng.* 8 (2002) 53–62.
- [111] B.N. Brown, R. Londono, S. Tottey, L. Zhang, K.A. Kukla, M.T. Wolf, K.A. Daly, J.E. Reing, S.F. Badylak, Macrophage phenotype as a predictor of constructive remodeling following the implantation of biologically derived surgical mesh materials, *Acta Biomater.* 8 (2012) 978–987. <https://doi.org/10.1016/j.actbio.2011.11.031>.Macrophage.
- [112] B.N. Brown, J.E. Valentin, A.M. Stewart-Akers, G.P. McCabe, S.F. Badylak, Macrophage phenotype and remodeling outcomes in response to biologic scaffolds with and without a cellular component, *Biomaterials.* 30 (2009) 1482–1491. <https://doi.org/10.1016/j.pestbp.2011.02.012>.Investigations.
- [113] S.F. Badylak, J.E. Valentin, A.K. Ravindra, G.P. McCabe, A.M. Stewart-Akers, Macrophage phenotype as a determinant of biologic scaffold remodeling., *Tissue Eng. Part*

- A. 14 (2008) 1835–42. <https://doi.org/10.1089/ten.tea.2007.0264>.
- [114] J.L. Dziki, L. Huleihel, M.E. Scarritt, S.F. Badylak, Extracellular matrix bioscaffolds as immunomodulatory biomaterials, *Tissue Eng. Part A*. 23 (2017) 1152–1159. <https://doi.org/10.1089/ten.tea.2016.0538>.
- [115] V. Agrawal, S.A. Johnson, J. Reing, L. Zhang, S. Tottey, G. Wang, K.K. Hirschi, S. Braunhut, L.J. Gudas, S.F. Badylak, Epimorphic regeneration approach to tissue replacement in adult mammals, *Proc. Natl. Acad. Sci. U. S. A.* 107 (2010) 3351–5. <https://doi.org/10.1073/pnas.0905851106>.
- [116] A.J. Beattie, T.W. Gilbert, J.P. Guyot, A.J. Yates, S.F. Badylak, Chemoattraction of progenitor cells by remodeling extracellular matrix scaffolds., *Tissue Eng. Part A*. 15 (2009) 1119–1125. <https://doi.org/10.1089/ten.tea.2008.0162>.
- [117] J.R. Walton, N.K. Bowman, Y. Khatib, J. Linklater, G.A.C. Murrell, Restore orthobiologic implant: Not recommended for augmentation of rotator cuff repairs, *J. Bone Jt. Surg. - Ser. A*. 89 (2007) 786–791. <https://doi.org/10.2106/JBJS.F.00315>.
- [118] J.A. Soler, S. Gidwani, M.J. Curtis, Early complications from the use of porcine dermal collagen implants (Permacol™) as bridging constructs in the repair of massive rotator cuff tears: A report of 4 cases, *Acta Orthop Belg.* 73 (2007) 432–436.
- [119] K.-L. V Ho, M.N. Witte, E.T. Bird, 8-ply small intestinal submucosa tension-free sling: spectrum of postoperative inflammation., *J. Urol.* 171 (2004) 268–271. <https://doi.org/10.1097/01.ju.0000098680.60020.32>.
- [120] S.G. Selamberg, J.E. Tibone, J.M. Itamura, S. Kasraeian, Six-month magnetic resonance imaging follow-up of large and massive rotator cuff repairs reinforced with porcine small intestinal submucosa., *J. Shoulder Elb. Surg.* 13 (2004) 538–541. <https://doi.org/10.1016/S1058274604001193>.
- [121] T.T. John, N. Aggarwal, A.K. Singla, R.A. Santucci, Intense inflammatory reaction with porcine small intestine submucosa pubovaginal sling or tape for stress urinary incontinence., *Urology*. 72 (2008) 1036–1039. <https://doi.org/10.1016/j.urology.2008.07.043>.
- [122] N.J. Turner, J.S. Badylak, D.J. Weber, S.F. Badylak, Biologic scaffold remodeling in a dog model of complex musculoskeletal injury., *J. Surg. Res.* 176 (2012) 490–502. <https://doi.org/10.1016/j.jss.2011.11.1029>.
- [123] R. Londono, J.L. Dziki, E. Haljasmaa, N.J. Turner, C.A. Leifer, S.F. Badylak, The effect of cell debris within biologic scaffolds upon the macrophage response, *J. Biomed. Mater. Res. - Part A*. 105 (2017) 2109–2118. <https://doi.org/10.1002/jbm.a.36055>.
- [124] T.J. Keane, R. Londono, N.J. Turner, S.F. Badylak, Consequences of ineffective decellularization of biologic scaffolds on the host response, *Biomaterials*. 33 (2012) 1771–1781. <https://doi.org/10.1016/j.biomaterials.2011.10.054>.

- [125] A.H. Morris, J. Chang, T.R. Kyriakides, Inadequate processing of decellularized dermal matrix reduces cell viability in vitro and increases apoptosis and acute inflammation in vivo, *Biores. Open Access*. 5.1 (2016) 177–187. <https://doi.org/10.1089/biores.2016.0021>.
- [126] G.E. Davis, K.J. Bayless, M.J. Davis, G.A. Meininger, Regulation of tissue injury responses by the exposure of matricryptic sites within extracellular matrix molecules, *Am. J. Pathol.* 156 (2000) 1489–1498. [https://doi.org/10.1016/S0002-9440\(10\)65020-1](https://doi.org/10.1016/S0002-9440(10)65020-1).
- [127] V. Agrawal, S. Tottey, S. a. Johnson, J.M. Freund, B.F. Siu, S.F. Badylak, Recruitment of progenitor cells by an extracellular matrix cryptic peptide in a mouse model of digit amputation, *Tissue Eng. Part A*. 17 (2011) 2435–2443. <https://doi.org/10.1089/ten.tea.2011.0036>.
- [128] J.E. Valentin, A.M. Stewart-Akers, T.W. Gilbert, S.F. Badylak, Macrophage participation in the degradation and remodeling of extracellular matrix scaffolds., *Tissue Eng. Part A*. 15 (2009) 1687–1694. <https://doi.org/10.1089/ten.tea.2008.0419>.
- [129] J.L. Dziki, B.M. Sicari, M.T. Wolf, M.C. Cramer, S.F. Badylak, Immunomodulation and mobilization of progenitor cells by extracellular matrix bioscaffolds for volumetric muscle loss treatment, *Tissue Eng. Part A*. 22 (2016) 1129–1139. <https://doi.org/10.1089/ten.TEA.2016.0340>.
- [130] S.L. Hirsh, D.R. McKenzie, N.J. Nosworthy, J.A. Denman, O.U. Sezerman, M.M.M. Bilek, The Vroman effect: Competitive protein exchange with dynamic multilayer protein aggregates, *Colloids Surfaces B Biointerfaces*. 103 (2013) 395–404. <https://doi.org/10.1016/j.colsurfb.2012.10.039>.
- [131] S.F. Badylak, T.W. Gilbert, Immune response to biologic scaffold materials, *Semin. Immunol.* 20 (2008) 109–116. <https://doi.org/10.1016/j.smim.2007.11.003>.Immune.
- [132] S.N. Christo, K.R. Diener, A. Bachhuka, K. Vasilev, J.D. Hayball, Innate immunity and biomaterials at the nexus : Friends or foes, *Biomed Res. Int.* 2015 (2015) 342304.
- [133] S. Franz, S. Rammelt, D. Scharnweber, J.C. Simon, Immune responses to implants - a review of the implications for the design of immunomodulatory biomaterials., *Biomaterials*. 32 (2011) 6692–6709. <https://doi.org/10.1016/j.biomaterials.2011.05.078>.
- [134] C. Mora-Solano, J.H. Collier, Engaging adaptive immunity with biomaterials, *J. Mater. Chem. B*. 2 (2014) 2409–2421. <https://doi.org/10.1039/c3tb21549k>.
- [135] S. Gordon, P.R. Taylor, Monocyte and macrophage heterogeneity, *Nat. Rev. Immunol.* 5 (2005) 953–964. <https://doi.org/10.1038/nri1733>.
- [136] C.D. Mills, K. Kincaid, J.M. Alt, M.J. Heilman, A.M. Hill, M-1/M-2 macrophages and the Th1/Th2 paradigm, *J. Immunol.* 164 (2000) 6166–6173. <https://doi.org/10.4049/jimmunol.164.12.6166>.
- [137] A. Mantovani, A. Sica, S. Sozzani, P. Allavena, A. Vecchi, M. Locati, The chemokine

- system in diverse forms of macrophage activation and polarization, *Trends Immunol.* 25 (2004) 677–686. <https://doi.org/10.1016/j.it.2004.09.015>.
- [138] A. Mantovani, S.K. Biswas, M.R. Galdiero, A. Sica, M. Locati, Macrophage plasticity and polarization in tissue repair and remodelling, *J. Pathol.* 229 (2013) 176–185. <https://doi.org/10.1002/path.4133>.
- [139] A. Berger, Th1 and Th2 responses: what are they ?, *BMJ.* 321 (2000) 424.
- [140] T.R. Mosmann, S. Sad, The expanding universe of T-cell subsets: Th1, Th2 and more, *Immunol. Today.* 17 (1996) 138–146.
- [141] A.J. Allman, T.B. McPherson, S.F. Badylak, L.C. Merrill, B. Kallakury, C. Sheehan, R.H. Raeder, D.W. Metzger, Xenogeneic extracellular matrix grafts elicit a Th2-restricted immune response, *Transplantation.* 71 (2001) 1631–1640.
- [142] B.M. Sicari, J.L. Dziki, B.F. Siu, C.J. Medberry, C.L. Dearth, S.F. Badylak, The promotion of a constructive macrophage phenotype by solubilized extracellular matrix, *Biomaterials.* 35 (2014) 8605–8612. <https://doi.org/10.1016/j.biomaterials.2014.06.060>.
- [143] J.L. Dziki, D.S. Wang, C. Pineda, B.M. Sicari, T. Rausch, S.F. Badylak, Solubilized extracellular matrix bioscaffolds derived from diverse source tissues differentially influence macrophage phenotype, *J. Biomed. Mater. Res. Part A.* 105 (2017) 138–147. <https://doi.org/10.1111/evo.12868>.
- [144] J.M. Fishman, M.W. Lowdell, L. Urbani, T. Ansari, A.J. Burns, M. Turmaine, J. North, P. Sibbons, A.M. Seifalian, K.J. Wood, M.A. Birchall, P. De Coppi, Immunomodulatory effect of a decellularized skeletal muscle scaffold in a discordant xenotransplantation model, *Proc. Natl. Acad. Sci.* 110 (2013) 14360–14365. <https://doi.org/10.1073/pnas.1213228110>.
- [145] K. Sadtler, K. Estrellas, B.W. Allen, M.T. Wolf, H. Fan, A.J. Tam, C.H. Patel, B.S. Lubner, H. Wang, K.R. Wagner, J.D. Powell, F. Housseau, D.M. Pardoll, J.H. Elisseeff, Developing a pro-regenerative biomaterial scaffold microenvironment requires T helper 2 cells, *Science* (80-.). 352 (2016) 366–370.
- [146] T.J. Keane, J. Dziki, E. Sobieski, A. Smoulder, A. Castleton, N. Turne, L.J. White, S.F. Badylak, Restoring mucosal barrier function and modifying macrophage phenotype with an extracellular matrix hydrogel: Potential therapy for ulcerative colitis, *J. Crohn's Colitis.* 11 (2017) 360–368. <https://doi.org/10.1093/ecco-jcc/jjw149>.
- [147] L. Huleihel, J.L. Dziki, J.G. Bartolacci, T. Rausch, M.E. Scarritt, M.C. Cramer, T. Vorobyov, S.T. LoPresti, I.T. Swineheart, L.J. White, B.N. Brown, S.F. Badylak, Macrophage phenotype in response to ECM bioscaffolds, *Semin. Immunol.* 29 (2017) 2–13. <https://doi.org/10.1016/j.smim.2017.04.004>.
- [148] K. Sadtler, B.W. Allen, K. Estrellas, F. Housseau, D.M. Pardoll, J.H. Elisseeff, The scaffold immune microenvironment: Biomaterial-mediated immune polarization in traumatic and nontraumatic applications, *Tissue Eng. - Part A.* 23 (2017) 1044–1053.

<https://doi.org/10.1089/ten.tea.2016.0304>.

- [149] K. Sadtler, M.T. Wolf, S. Ganguly, C.A. Moad, L. Chung, S. Majumdar, F. Housseau, D.M. Pardoll, J.H. Elisseeff, Divergent immune responses to synthetic and biological scaffolds, *Biomaterials*. 192 (2019) 405–415. <https://doi.org/10.1016/j.biomaterials.2018.11.002>.
- [150] M.T. Wolf, S. Ganguly, T.L. Wang, C.W. Anderson, K. Sadtler, R. Narain, C. Cherry, A.J. Parrillo, B. V. Park, G. Wang, F. Pan, S. Sukumar, D.M. Pardoll, J.H. Elisseeff, A biologic scaffold-associated type 2 immune microenvironment inhibits tumor formation and synergizes with checkpoint immunotherapy, *Sci. Transl. Med.* 11 (2019) eaat7973. <https://doi.org/10.1126/scitranslmed.aat7973>.
- [151] L. Huleihel, J.G. Bartolacci, J.L. Dziki, T. Vorobyov, B. Arnold, M.E. Scarritt, C. Pineda Molina, S.T. LoPresti, B.N. Brown, J.D. Naranjo, S.F. Badylak, B.N. Brown, S.F. Badylak, Matrix bound nanovesicles recapitulate extracellular matrix effects on macrophage phenotype, *Tissue Eng Part A*. 23 (2017) Z. <https://doi.org/10.1089/ten.tea.2017.0102>.
- [152] L. Huleihel, G.S. Hussey, J.D. Naranjo, L. Zhang, J.L. Dziki, N.J. Turner, D.B. Stolz, S.F. Badylak, Matrix-bound nanovesicles within ECM bioscaffolds., *Sci. Adv.* 2 (2016) e1600502. <https://doi.org/10.1126/sciadv.1600502>.
- [153] R.M. Wang, T.D. Johnson, J. He, Z. Rong, M. Wong, V. Nigam, A. Behfar, Y. Xu, K.L. Christman, Humanized mouse model for assessing the human immune response to xenogeneic and allogeneic decellularized biomaterials, *Biomaterials*. 129 (2017) 98–110. <https://doi.org/10.1016/j.biomaterials.2017.03.016>.
- [154] S. Haykal, Y. Zhou, P. Marcus, M. Salna, T. Machuca, S.O.P. Hofer, T.K. Waddell, The effect of decellularization of tracheal allografts on leukocyte infiltration and of recellularization on regulatory T cell recruitment, *Biomaterials*. 34 (2013) 5821–5832. <https://doi.org/10.1016/j.biomaterials.2013.04.044>.
- [155] P.M. Crapo, T.W. Gilbert, S.F. Badylak, D.V.M. Badylak, An overview of tissue and whole organ decellularization processes, *Biomaterials*. 32 (2011) 3233–3243. <https://doi.org/10.1016/j.biomaterials.2011.01.057>.
- [156] A.J. Dalgliesh, M. Parvizi, M. Lopera-Higuita, J. Shklover, L.G. Griffiths, Graft-specific immune tolerance is determined by residual antigenicity of xenogeneic extracellular matrix scaffolds, *Acta Biomater.* 79 (2018) 253–264. <https://doi.org/10.1016/j.actbio.2018.08.016>.
- [157] F.W. Meng, P.F. Slivka, C.L. Dearth, S.F. Badylak, Solubilized extracellular matrix from brain and urinary bladder elicits distinct functional and phenotypic responses in macrophages, *Biomaterials*. 46 (2015) 131–140. <https://doi.org/10.1016/j.biomaterials.2014.12.044>.
- [158] S.T. LoPresti, B.N. Brown, Effect of source animal age upon macrophage response to extracellular matrix biomaterials, *J Immunol Regen Med.* 1 (2018) 57–66. <https://doi.org/10.1016/j.bbi.2017.04.008>.

- [159] B.M. Sicari, S.A. Johnson, B.F. Siu, P.M. Crapo, K.A. Daly, H. Jiang, C.J. Medberry, S. Tottey, N.J. Turner, S.F. Badylak, The effect of source animal age upon the in vivo remodeling characteristics of an extracellular matrix scaffold, *Biomaterials*. 33 (2012) 5524–5533. <https://doi.org/10.1016/j.biomaterials.2012.04.017>.
- [160] P.R. Umashankar, P. V. Mohanan, T. V. Kumari, Glutaraldehyde treatment elicits toxic response compared to decellularization in bovine pericardium, *Toxicol. Int.* 19 (2012) 51–58. <https://doi.org/10.4103/0971-6580.94513>.
- [161] M.T. Wolf, Y. Vodovotz, S. Tottey, B.N. Brown, S.F. Badylak, Predicting in vivo responses to biomaterials via combined in vitro and in silico analysis, *Tissue Eng. Part C Methods*. 21 (2015) 148–159. <https://doi.org/10.1089/ten.tec.2014.0167>.
- [162] Y. Van Der Merwe, A.E. Faust, E.T. Sakalli, C.C. Westrick, G. Hussey, I.P. Con, V.L.N. Fu, S.F. Badylak, M.B. Steketee, Matrix-bound nanovesicles prevent ischemia-induced retinal ganglion cell axon degeneration and death and preserve visual function, *Sci. Rep.* 9 (2019) 3482. <https://doi.org/10.1038/s41598-019-39861-4>.
- [163] G.S. Hussey, J.L. Dziki, Y.C. Lee, J.G. Bartolacci, M. Behun, H.R. Turnquist, S.F. Badylak, Matrix bound nanovesicle-associated IL-33 activates a pro-remodeling macrophage phenotype via a non-canonical, ST2-independent pathway, *J. Immunol. Regen. Med.* 3 (2019) 26–35. <https://doi.org/10.1016/j.regen.2019.01.001>.
- [164] K. Eishi, H. Ishibashi-Ueda, K. Nakano, Y. Kosakai, Y. Sasako, J. Kobayashi, C. Yutani, Calcific degeneration of bioprosthetic aortic valves in patients receiving steroid therapy, *J. Heart Valve Dis.* 5 (1996) 668–672. <http://europepmc.org/abstract/MED/8953446>.
- [165] T. Li, Z. Zhang, J.G. Bartolacci, G.K. Dwyer, Q. Liu, L.R. Mathews, M. Velayutham, A.S. Roessing, Y.C. Lee, H. Dai, S. Shiva, M.H. Oberbarnscheidt, J.L. Dziki, S.J. Mullet, S.G. Wendell, J.D. Wilkinson, S.A. Webber, M. Wood-Trageser, S.C. Watkins, A.J. Demetris, G.S. Hussey, S.F. Badylak, H.R. Turnquist, Graft IL-33 regulates infiltrating macrophages to protect against chronic rejection, *J. Clin. Invest.* 130 (2020) 5397–5412. <https://doi.org/10.1172/jci133008>.
- [166] N. Vyavahare, D. Hirsch, E. Lerner, J.Z. Baskin, F.J. Schoen, R. Bianco, H.S. Kruth, R. Zand, R.J. Levy, Prevention of bioprosthetic heart valve calcification by ethanol preincubation: Efficacy and mechanisms, *Circulation*. 95 (1997) 479–488. <https://doi.org/10.1161/01.CIR.95.2.479>.
- [167] Y. Tintut, L.L. Demer, Exosomes: Nanosized cellular messages, *Circ. Res.* 116 (2015) 1281–1283. <https://doi.org/10.1242/jcs.064386.3>.
- [168] T.J. Keane, R. Londono, R.M. Carey, C.A. Carruthers, J.E. Reing, C.L. Dearth, A. D’Amore, C.J. Medberry, S.F. Badylak, Preparation and characterization of a biologic scaffold from esophageal mucosa, *Biomaterials*. 34 (2013) 6729–6737. <https://doi.org/10.1016/j.biomaterials.2013.05.052>.
- [169] P.M. Crapo, C.J. Medberry, J.E. Reing, S. Tottey, Y. van der Merwe, K.E. Jones, S.F.

- Badylak, Biologic scaffolds composed of central nervous system extracellular matrix, *Biomaterials*. 33 (2012) 3539–3547. <https://doi.org/10.1016/j.biomaterials.2012.01.044>.
- [170] J.T. Oxford, J.C. Reeck, M.J. Hardy, Extracellular matrix in development and disease, *Int. J. Mol. Sci.* 20 (2019) 10–14. <https://doi.org/10.3390/ijms20010205>.
- [171] C. Bonnans, J. Chou, Z. Werb, Remodelling the extracellular matrix in development and disease, *Nat. Rev. Mol. Cell Biol.* 15 (2014) 786–801. <https://doi.org/10.1038/nrm3904>.
- [172] A. Falkenham, R. De Antueno, N. Rosin, D. Betsch, T.D.G. Lee, R. Duncan, J.F. L egar e, Nonclassical resident macrophages are important determinants in the development of myocardial fibrosis, *Am. J. Pathol.* 185 (2015) 927–942. <https://doi.org/10.1016/j.ajpath.2014.11.027>.
- [173] R. Villa-Bellosta, M.R. Hamczyk, V. Andr es, Alternatively activated macrophages exhibit an anticalcifying activity dependent on extracellular ATP/pyrophosphate metabolism, *Am. J. Physiol. - Cell Physiol.* 310 (2016) C788–C799. <https://doi.org/10.1152/ajpcell.00370.2015>.
- [174] C. Th ery, K.W. Witwer, E. Aikawa, M.J. Alcaraz, J.D. Anderson, R. Andriantsitohaina, A. Antoniou, T. Arab, F. Archer, G.K. Atkin-Smith, D.C. Ayre, J.M. Bach, D. Bachurski, H. Baharvand, L. Balaj, S. Baldacchino, N.N. Bauer, A.A. Baxter, M. Bebawy, C. Beckham, A. Bedina Zavec, A. Benmoussa, A.C. Berardi, P. Bergese, E. Bielska, C. Blenkinsop, S. Bobis-Wozowicz, E. Boilard, W. Boireau, A. Bongiovanni, F.E. Borr as, S. Bosch, C.M. Boulanger, X. Breakefield, A.M. Breglio, M. Brennan, D.R. Brigstock, A. Brisson, M.L.D. Broekman, J.F. Bromberg, P. Bryl-G orecka, S. Buch, A.H. Buck, D. Burger, S. Busatto, D. Buschmann, B. Bussolati, E.I. Buz as, J.B. Byrd, G. Camussi, D.R.F. Carter, S. Caruso, L.W. Chamley, Y.T. Chang, A.D. Chaudhuri, C. Chen, S. Chen, L. Cheng, A.R. Chin, A. Clayton, S.P. Clerici, A. Cocks, E. Cocucci, R.J. Coffey, A. Cordeiro-da-Silva, Y. Couch, F.A.W. Coumans, B. Coyle, R. Crescitelli, M.F. Criado, C. D’Souza-Schorey, S. Das, P. de Candia, E.F. De Santana, O. De Wever, H.A. del Portillo, T. Demaret, S. Deville, A. Devitt, B. Dhondt, D. Di Vizio, L.C. Dieterich, V. Dolo, A.P. Dominguez Rubio, M. Dominici, M.R. Dourado, T.A.P. Driedonks, F. V. Duarte, H.M. Duncan, R.M. Eichenberger, K. Ekstr om, S. EL Andaloussi, C. Elie-Caille, U. Erdbr ugger, J.M. Falc on-P erez, F. Fatima, J.E. Fish, M. Flores-Bellver, A. F ors onits, A. Frelet-Barrand, F. Fricke, G. Fuhrmann, S. Gabrielsson, A. G amez-Valero, C. Gardiner, K. G artner, R. Gaudin, Y.S. Gho, B. Giebel, C. Gilbert, M. Gimona, I. Giusti, D.C.I. Goberdhan, A. G orgens, S.M. Gorski, D.W. Greening, J.C. Gross, A. Gualerzi, G.N. Gupta, D. Gustafson, A. Handberg, R.A. Haraszti, P. Harrison, H. Hegyesi, A. Hendrix, A.F. Hill, F.H. Hochberg, K.F. Hoffmann, B. Holder, H. Holthofer, B. Hosseinkhani, G. Hu, Y. Huang, V. Huber, S. Hunt, A.G.E. Ibrahim, T. Ikezu, J.M. Inal, M. Isin, A. Ivanova, H.K. Jackson, S. Jacobsen, S.M. Jay, M. Jayachandran, G. Jenster, L. Jiang, S.M. Johnson, J.C. Jones, A. Jong, T. Jovanovic-Taliman, S. Jung, R. Kalluri, S. ichi Kano, S. Kaur, Y. Kawamura, E.T. Keller, D. Khamari, E. Khomyakova, A. Khvorova, P. Kierulf, K.P. Kim, T. Kislinger, M. Klingeborn, D.J. Klinke, M. Kornek, M.M. Kosanovi c,  .F. Kov acs, E.M. Kr amer-Albers, S. Krasemann, M. Krause, I. V. Kurochkin, G.D. Kusuma, S. Kuypers, S. Laitinen, S.M. Langevin, L.R. Languino, J. Lannigan, C. L asser, L.C. Laurent, G. Lavieu, E. L azaro-Ib a nez, S. Le Lay, M.S. Lee, Y.X.F. Lee, D.S. Lemos,

M. Lenassi, A. Leszczynska, I.T.S. Li, K. Liao, S.F. Libregts, E. Ligeti, R. Lim, S.K. Lim, A. Linē, K. Linnemannstöns, A. Llorente, C.A. Lombard, M.J. Lorenowicz, Á.M. Lörincz, J. Lötvall, J. Lovett, M.C. Lowry, X. Loyer, Q. Lu, B. Lukomska, T.R. Lunavat, S.L.N. Maas, H. Malhi, A. Marcilla, J. Mariani, J. Mariscal, E.S. Martens-Uzunova, L. Martin-Jaular, M.C. Martinez, V.R. Martins, M. Mathieu, S. Mathivanan, M. Maugeri, L.K. McGinnis, M.J. McVey, D.G. Meckes, K.L. Meehan, I. Mertens, V.R. Minciocchi, A. Möller, M. Møller Jørgensen, A. Morales-Kastresana, J. Morhayim, F. Mullier, M. Muraca, L. Musante, V. Mussack, D.C. Muth, K.H. Myburgh, T. Najrana, M. Nawaz, I. Nazarenko, P. Nejsun, C. Neri, T. Neri, R. Nieuwland, L. Nimrichter, J.P. Nolan, E.N.M. Nolte-’t Hoen, N. Noren Hooten, L. O’Driscoll, T. O’Grady, A. O’Loghlen, T. Ochiya, M. Olivier, A. Ortiz, L.A. Ortiz, X. Osteikoetxea, O. Ostegaard, M. Ostrowski, J. Park, D.M. Pegtel, H. Peinado, F. Perut, M.W. Pfaffl, D.G. Phinney, B.C.H. Pieters, R.C. Pink, D.S. Pisetsky, E. Pogge von Strandmann, I. Polakovicova, I.K.H. Poon, B.H. Powell, I. Prada, L. Pulliam, P. Quesenberry, A. Radeghieri, R.L. Raffai, S. Raimondo, J. Rak, M.I. Ramirez, G. Raposo, M.S. Rayyan, N. Regev-Rudzki, F.L. Ricklefs, P.D. Robbins, D.D. Roberts, S.C. Rodrigues, E. Rohde, S. Rome, K.M.A. Rouschop, A. Rughetti, A.E. Russell, P. Saá, S. Sahoo, E. Salas-Huenuleo, C. Sánchez, J.A. Saugstad, M.J. Saul, R.M. Schiffelers, R. Schneider, T.H. Schøyen, A. Scott, E. Shahaj, S. Sharma, O. Shatnyeva, F. Shekari, G.V. Shelke, A.K. Shetty, K. Shiba, P.R.M. Siljander, A.M. Silva, A. Skowronek, O.L. Snyder, R.P. Soares, B.W. Sódar, C. Soekmadji, J. Sotillo, P.D. Stahl, W. Stoorvogel, S.L. Stott, E.F. Strasser, S. Swift, H. Tahara, M. Tewari, K. Timms, S. Tiwari, R. Tixeira, M. Tkach, W.S. Toh, R. Tomasini, A.C. Torrecilhas, J.P. Tosar, V. Toxavidis, L. Urbanelli, P. Vader, B.W.M. van Balkom, S.G. van der Grein, J. Van Deun, M.J.C. van Herwijnen, K. Van Keuren-Jensen, G. van Niel, M.E. van Royen, A.J. van Wijnen, M.H. Vasconcelos, I.J. Vechetti, T.D. Veit, L.J. Vella, É. Velot, F.J. Verweij, B. Vestad, J.L. Viñas, T. Visnovitz, K. V. Vukman, J. Wahlgren, D.C. Watson, M.H.M. Wauben, A. Weaver, J.P. Webber, V. Weber, A.M. Wehman, D.J. Weiss, J.A. Welsh, S. Wendt, A.M. Wheelock, Z. Wiener, L. Witte, J. Wolfram, A. Xagorari, P. Xander, J. Xu, X. Yan, M. Yáñez-Mó, H. Yin, Y. Yuana, V. Zappulli, J. Zarubova, V. Žėkas, J. ye Zhang, Z. Zhao, L. Zheng, A.R. Zheutlin, A.M. Zickler, P. Zimmermann, A.M. Zivkovic, D. Zocco, E.K. Zuba-Surma, Minimal information for studies of extracellular vesicles 2018 (MISEV2018): a position statement of the International Society for Extracellular Vesicles and update of the MISEV2014 guidelines, *J. Extracell. Vesicles.* 7 (2018). <https://doi.org/10.1080/20013078.2018.1535750>.

[175] G. Van Niel, G. D’Angelo, G. Raposo, Shedding light on the cell biology of extracellular vesicles, *Nat. Rev. Mol. Cell Biol.* 19 (2018) 213–228. <https://doi.org/10.1038/nrm.2017.125>.

[176] M. Yáñez-Mó, P.R.M. Siljander, Z. Andreu, A.B. Zavec, F.E. Borràs, E.I. Buzas, K. Buzas, E. Casal, F. Cappello, J. Carvalho, E. Colás, A. Cordeiro-Da Silva, S. Fais, J.M. Falcon-Perez, I.M. Ghobrial, B. Giebel, M. Gimona, M. Graner, I. Gursel, M. Gursel, N.H.H. Heegaard, A. Hendrix, P. Kierulf, K. Kokubun, M. Kosanovic, V. Kralj-Iglic, E.M. Krämer-Albers, S. Laitinen, C. Lässer, T. Lener, E. Ligeti, A. Line, G. Lipps, A. Llorente, J. Lötvall, M. Mančėk-Keber, A. Marcilla, M. Mittelbrunn, I. Nazarenko, E.N.M. Nolte-’t Hoen, T.A. Nyman, L. O’Driscoll, M. Olivan, C. Oliveira, É. Pállinger, H.A. Del Portillo, J. Reventós, M. Rigau, E. Rohde, M. Sammar, F. Sánchez-Madrid, N. Santarém, K. Schallmoser, M.S.

- Ostenfeld, W. Stoorvogel, R. Stukelj, S.G. Van Der Grein, M. Helena Vasconcelos, M.H.M. Wauben, O. De Wever, Biological properties of extracellular vesicles and their physiological functions, *J. Extracell. Vesicles.* 4 (2015) 1–60. <https://doi.org/10.3402/jev.v4.27066>.
- [177] B. Mir, C. Goettsch, Extracellular vesicles as delivery vehicles of specific cellular cargo, *Cells.* 9 (2020). <https://doi.org/10.3390/cells9071601>.
- [178] J. Kowal, G. Arras, M. Colombo, M. Jouve, J.P. Morath, B. Primdal-Bengtson, F. Dingli, D. Loew, M. Tkach, C. Théry, Proteomic comparison defines novel markers to characterize heterogeneous populations of extracellular vesicle subtypes, *Proc. Natl. Acad. Sci. U. S. A.* 113 (2016) E968–E977. <https://doi.org/10.1073/pnas.1521230113>.
- [179] E. Bonucci, Fine structure of early cartilage calcification, *J. Ultrastructure Res.* 20 (1967) 33–50. [https://doi.org/10.1016/S0022-5320\(67\)80034-0](https://doi.org/10.1016/S0022-5320(67)80034-0).
- [180] H.C. Anderson, Electron microscopic studies of induced cartilage development and calcification., *J. Cell Biol.* 35 (1967) 81–101. <https://doi.org/10.1083/jcb.35.1.81>.
- [181] G.W. Bernard, D.C. Pease, An electron microscopic study of initial intramembranous osteogenesis, *Am. J. Anat.* 125 (1969) 271–290. <https://doi.org/10.1002/aja.1001250303>.
- [182] E.E. Golub, Role of matrix vesicles in biomineralization, *Biochim. Biophys. Acta.* 1790 (2009) 1592–1598. <https://doi.org/10.1016/j.bbagen.2009.09.006>.
- [183] E.G. Trams, C.J. Lauter, J. Norman Salem, U. Heine, Exfoliation of membrane ectoenzymes in the form of micro-vesicles, *BBA - Biomembr.* 645 (1981) 63–70. [https://doi.org/10.1016/0005-2736\(81\)90512-5](https://doi.org/10.1016/0005-2736(81)90512-5).
- [184] R.M. Johnstone, M. Adam, J.R. Hammond, L. Orr, C. Turbide, Vesicle formation during reticulocyte maturation. Association of plasma membrane activities with released vesicles (exosomes)., *J. Biol. Chem.* 262 (1987) 9412–9420. [https://doi.org/10.1016/s0021-9258\(18\)48095-7](https://doi.org/10.1016/s0021-9258(18)48095-7).
- [185] A. Ibrahim, E. Marban, Exosomes: Fundamental biology and roles in cardiovascular physiology, *Annu Rev Physiol.* 78 (2016) 67–83. <https://doi.org/10.1146/annurev-physiol-021115-104929>.Exosomes.
- [186] G.S. Hussey, C.P. Molina, M.C. Cramer, Y.Y. Tyurina, V.A. Tyurin, Y.C. Lee, S.O. El-Mossier, M.H. Murdock, P.S. Timashev, V.E. Kagan, S.F. Badylak, Lipidomics and RNA sequencing reveal a novel subpopulation of nanovesicle within extracellular matrix biomaterials, *Sci. Adv.* 6 (2020) 1–14. <https://doi.org/10.1126/sciadv.aay4361>.
- [187] S.C. Chaudhary, M. Kuzynski, M. Bottini, E. Beniash, T. Dokland, C.G. Mobley, M.C. Yadav, A. Poliard, O. Kellermann, J.L. Millán, D. Napierala, Phosphate induces formation of matrix vesicles during odontoblast-initiated mineralization in vitro, *Matrix Biol.* 52–54 (2016) 284–300. <https://doi.org/10.1016/j.matbio.2016.02.003>.

- [188] G.V. Shelke, C. Lässer, Y.S. Gho, J. Lötvall, Importance of exosome depletion protocols to eliminate functional and RNA-containing extracellular vesicles from fetal bovine serum, *J. Extracell. Vesicles*. 3 (2014) 1–8. <https://doi.org/10.3402/jev.v3.24783>.
- [189] Y. Lai, Y. Sun, C.M. Skinner, E.L. Son, Z. Lu, R.S. Tuan, R.L. Jilka, J. Ling, X.-D.D. Chen, Reconstitution of marrow-derived extracellular matrix ex vivo: A robust culture system for expanding large-scale highly functional human mesenchymal stem cells, *Stem Cells Dev*. 19 (2010) 1095–1107. <https://doi.org/10.1089/scd.2009.0217>.
- [190] Y.Y. Tyurina, E.R. Kisin, A. Murray, V.A. Tyurin, V.I. Kapralova, L.J. Sparvero, A.A. Amoscato, A.K. Samhan-Arias, L. Swedin, R. Lahesmaa, B. Fadeel, A.A. Shvedova, V.E. Kagan, Global phospholipidomics analysis reveals selective pulmonary peroxidation profiles upon inhalation of single-walled carbon nanotubes, *ACS Nano*. 5 (2011) 7342–7353. <https://doi.org/10.1021/nn202201j>.
- [191] E. Boilard, Extracellular vesicles and their content in bioactive lipid mediators: more than a sack of microRNA, *J. Lipid Res.* (n.d.) 1–25.
- [192] T. Skotland, K. Sandvig, A. Llorente, Lipids in exosomes: Current knowledge and the way forward, *Prog. Lipid Res.* 66 (2017) 30–41. <https://doi.org/10.1016/j.plipres.2017.03.001>.
- [193] J. Lötvall, A.F. Hill, F. Hochberg, E.I. Buzás, D. Di Vizio, C. Gardiner, Y.S. Gho, I. V. Kurochkin, S. Mathivanan, P. Quesenberry, S. Sahoo, H. Tahara, M.H. Wauben, K.W. Witwer, C. Théry, Minimal experimental requirements for definition of extracellular vesicles and their functions: A position statement from the International Society for Extracellular Vesicles, *J. Extracell. Vesicles*. 3 (2014) 1–6. <https://doi.org/10.3402/jev.v3.26913>.
- [194] A. Bakhshian Nik, J.D. Hutcheson, E. Aikawa, Extracellular vesicles as mediators of cardiovascular calcification, *Front. Cardiovasc. Med.* 4 (2017). <https://doi.org/10.3389/fcvm.2017.00078>.
- [195] I.M. Shapiro, W.J. Landis, M. V Risbud, Matrix vesicles: Are they anchored exosomes?, *Bone*. 79 (2015) 29–36. <https://doi.org/10.1515/jci-2013-0007>. Targeted.
- [196] R.J. Simpson, S.S. Jensen, J.W.E. Lim, Proteomic profiling of exosomes: Current perspectives, *Proteomics*. 8 (2008) 4083–4099. <https://doi.org/10.1002/pmic.200800109>.
- [197] X. Zhou, Y. Cui, J. Luan, X. Zhou, G. Zhang, X. Zhang, J. Han, Label-free quantification proteomics reveals novel calcium binding proteins in matrix vesicles isolated from mineralizing Saos-2 cells, *Biosci. Trends*. 7 (2013) 144–151. <https://doi.org/10.5582/bst.2013.v7.3.144>.
- [198] G.M. Saed, Z. Jiang, M.P. Diamond, H.M. Abu-Soud, The role of myeloperoxidase in the pathogenesis of postoperative adhesions, *Wound Repair Regen*. 17 (2009) 531–539. <https://doi.org/10.1111/j.1524-475X.2009.00500.x>.
- [199] M.O. DeNichilo, V. Panagopoulos, T.E. Rayner, R.A. Borowicz, J.E. Greenwood, A.

- Evdokiou, Peroxidase enzymes regulate collagen extracellular matrix biosynthesis, *Am. J. Pathol.* 185 (2015) 1372–1384. <https://doi.org/10.1016/j.ajpath.2015.01.013>.
- [200] T. Kirsch, H.D. Nah, D.R. Demuth, G. Harrison, E.E. Golub, S.L. Adams, M. Pacifici, Annexin V-mediated calcium flux across membranes is dependent on the lipid composition: Implications for cartilage mineralization, *Biochemistry.* 36 (1997) 3359–3367. <https://doi.org/10.1021/bi9626867>.
- [201] T. Kirsch, G. Harrison, E.E. Golub, H.D. Nah, The roles of annexins and types II and X collagen in matrix vesicle-mediated mineralization of growth plate cartilage, *J. Biol. Chem.* 275 (2000) 35577–35583. <https://doi.org/10.1074/jbc.M005648200>.
- [202] G. Harrison, I.M. Shapiro, E.E. Golub, The phosphatidylinositol-glycolipid anchor on alkaline phosphatase facilitates mineralization initiation in vitro, *J. Bone Miner. Res.* 10 (1995) 568–573. <https://doi.org/10.1002/jbmr.5650100409>.
- [203] H.C. Anderson, Matrix vesicles and calcification., *Curr. Rheumatol. Rep.* 5 (2003) 222–226. <https://doi.org/10.1007/s11926-003-0071-z>.
- [204] B.R. Genge, X. Cao, L.N.Y. Wu, W.R. Buzzi, R.W. Showman, A.L. Arsenault, Y. Ishikawa, R.E. Wuthier, Establishment of the primary structure of the major lipid-dependent Ca²⁺ binding proteins of chicken growth plate cartilage matrix vesicles: Identity with anchorin cii (annexin V) and annexin II, *J. Bone Miner. Res.* 7 (1992) 807–819. <https://doi.org/10.1002/jbmr.5650070710>.
- [205] K.S. Lee, J. Lee, H.K. Kim, S.H. Yeom, C.H. Woo, Y.J. Jung, Y.E. Yun, S.Y. Park, J. Han, E. Kim, J.H. Sul, J.M. Jung, J.H. Park, J.S. Choi, Y.W. Cho, D.G. Jo, Extracellular vesicles from adipose tissue-derived stem cells alleviate osteoporosis through osteoprotegerin and miR-21-5p, *J. Extracell. Vesicles.* 10 (2021). <https://doi.org/10.1002/jev2.12152>.
- [206] T. Hasegawa, Ultrastructure and biological function of matrix vesicles in bone mineralization, *Histochem. Cell Biol.* 149 (2018) 289–304. <https://doi.org/10.1007/s00418-018-1646-0>.
- [207] L. Cui, D.A. Houston, C. Farquharson, V.E. MacRae, Characterisation of matrix vesicles in skeletal and soft tissue mineralisation, *Bone.* 87 (2016) 147–158. <https://doi.org/10.1016/j.bone.2016.04.007>.
- [208] R.E. Wuthier, Lipid composition of isolated epiphyseal cartilage cells, membranes and matrix vesicles, *Biochim. Biophys. Acta (BBA)/Lipids Lipid Metab.* 409 (1975) 128–143. [https://doi.org/10.1016/0005-2760\(75\)90087-9](https://doi.org/10.1016/0005-2760(75)90087-9).
- [209] R.E. Wuthier, Lipids of matrix vesicles., *Fed. Proc.* 35 (1976) 117–121.
- [210] B.D. Boyan, Z. Schwartz, L.D. Swain, A. Khare, Role of lipids in calcification of cartilage, *Anat. Rec.* 224 (1989) 211–219. <https://doi.org/10.1002/ar.1092240210>.
- [211] R.J. Majeska, D.L. Holwerda, R.E. Wuthier, Localization of phosphatidylserine in isolated

- chick epiphyseal cartilage matrix vesicles with trinitrobenzenesulfonate, 1979. <https://doi.org/10.1007/BF02441159>.
- [212] C. Subra, D. Grand, K. Laulagnier, A. Stella, G. Lambeau, M. Paillasse, P. De Medina, B. Monsarrat, B. Perret, S. Silvente-Poirot, M. Poirot, M. Record, Exosomes account for vesicle-mediated transcellular transport of activatable phospholipases and prostaglandins, *J. Lipid Res.* 51 (2010) 2105–2120. <https://doi.org/10.1194/jlr.M003657>.
- [213] L. V. Yang, C.G. Radu, L. Wang, M. Riedinger, O.N. Witte, Gi-independent macrophage chemotaxis to lysophosphatidylcholine via the immunoregulatory GPCR G2A, *Blood.* 105 (2005) 1127–1134. <https://doi.org/10.1182/blood-2004-05-1916>.
- [214] J. Donoso-Quezada, S. Ayala-Mar, J. González-Valdez, The role of lipids in exosome biology and intercellular communication: Function, analytics and applications, *Traffic.* 22 (2021) 204–220. <https://doi.org/10.1111/tra.12803>.
- [215] S.C. Frasch, K. Zemski-Berry, R.C. Murphy, N. Borregaard, P.M. Henson, D.L. Bratton, Lysophospholipids of different classes mobilize neutrophil secretory vesicles and induce redundant signaling through G2A, *J. Immunol.* 178 (2007) 6540–6548. <https://doi.org/10.4049/jimmunol.178.10.6540>.
- [216] T. Matsui, F. Osaki, S. Hiragi, Y. Sakamaki, M. Fukuda, ALIX and ceramide differentially control polarized small extracellular vesicle release from epithelial cells, *EMBO Rep.* 22 (2021) 1–11. <https://doi.org/10.15252/embr.202051475>.
- [217] R. Garcia-Martin, G. Wang, B.B. Brandão, T.M. Zanotto, S. Shah, S.K. Patel, B. Schilling, C.R. Kahn, MicroRNA sequence codes for small extracellular vesicle release and cellular retention, *Nature.* (2021). <https://doi.org/10.1038/s41586-021-04234-3>.
- [218] M. Schlame, M.L. Greenberg, Biosynthesis, remodeling and turnover of mitochondrial cardiolipin, *Biochim. Biophys. Acta - Mol. Cell Biol. Lipids.* 1862 (2017) 3–7. <https://doi.org/10.1016/j.bbali.2016.08.010>.
- [219] P.E. Glaser, R.W. Gross, Plasmenylethanolamine facilitates rapid membrane fusion: A stopped-flow kinetic investigation correlating the propensity of a major plasma membrane constituent to adopt an HII phase with its ability to promote membrane fusion, *Biochemistry.* 33 (1994) 5805–5812. <https://doi.org/10.1021/bi00185a019>.
- [220] X. Han, R.W. Gross, Plasmenylcholine and phosphatidylcholine membrane bilayers possess distinct conformational motifs, *Biochemistry.* 29 (1990) 4992–4996. <https://doi.org/10.1021/bi00472a032>.
- [221] T. Rog, A. Koivuniemi, The biophysical properties of ethanolamine plasmalogens revealed by atomistic molecular dynamics simulations, *Biochim. Biophys. Acta - Biomembr.* 1858 (2016) 97–103. <https://doi.org/10.1016/j.bbamem.2015.10.023>.
- [222] R. Ray, V. Rai, Lysophosphatidic acid converts monocytes into macrophages in both mice and humans, *Blood.* 129 (2017) 1177–1183. <https://doi.org/10.1182/blood-2016-10->

- [223] A.M. Tager, P. LaCamera, B.S. Shea, G.S. Campanella, M. Selman, Z. Zhao, V. Polosukhin, J. Wain, B.A. Karimi-Shah, N.D. Kim, W.K. Hart, A. Pardo, T.S. Blackwell, Y. Xu, J. Chun, A.D. Luster, The lysophosphatidic acid receptor LPA1 links pulmonary fibrosis to lung injury by mediating fibroblast recruitment and vascular leak, *Nat. Med.* 14 (2008) 45–54. <https://doi.org/10.1038/nm1685>.
- [224] K. Masuda, S. Haruta, K. Orino, M. Kawaminami, S. Kurusu, Autotaxin as a novel, tissue-remodeling-related factor in regressing corpora lutea of cycling rats, *FEBS J.* 280 (2013) 6600–6612. <https://doi.org/10.1111/febs.12565>.
- [225] K.M. Hines, S. Ashfaq, J.M. Davidson, S.R. Opalenik, J.P. Wikswo, J.A. McLean, Biomolecular signatures of diabetic wound healing by structural mass spectrometry, *Anal. Chem.* 85 (2013) 3651–3659. <https://doi.org/10.1021/ac303594m>.
- [226] L. Xu, Y. Liu, Y. Sun, B. Wang, Y. Xiong, W. Lin, Q. Wei, H. Wang, W. He, B. Wang, G. Li, Tissue source determines the differentiation potentials of mesenchymal stem cells: A comparative study of human mesenchymal stem cells from bone marrow and adipose tissue, *Stem Cell Res. Ther.* 8 (2017). <https://doi.org/10.1186/s13287-017-0716-x>.
- [227] I.S. Anand, R. Latini, V.G. Florea, M.A. Kuskowski, T. Rector, S. Masson, S. Signorini, P. Mocarelli, A. Hester, R. Glazer, J.N. Cohn, C-reactive protein in heart failure: Prognostic value and the effect of Valsartan, *Circulation.* 112 (2005) 1428–1434. <https://doi.org/10.1161/CIRCULATIONAHA.104.508465>.
- [228] P. Pellicori, J. Zhang, J. Cuthbert, A. Urbinati, P. Shah, S. Kazmi, A.L. Clark, J.G.F. Cleland, High-sensitivity C-reactive protein in chronic heart failure: Patient characteristics, phenotypes, and mode of death, *Cardiovasc. Res.* 116 (2020) 91–100. <https://doi.org/10.1093/cvr/cvz198>.
- [229] M. Lu, Q. Lu, Y. Zhang, G. Tian, ApoB/apoA1 is an effective predictor of coronary heart disease risk in overweight and obesity, *J. Biomed. Res.* 25 (2011) 266–273. [https://doi.org/10.1016/S1674-8301\(11\)60036-5](https://doi.org/10.1016/S1674-8301(11)60036-5).
- [230] G. Florvall, S. Basu, A. Larsson, Apolipoprotein A1 is a stronger prognostic marker than are HDL and LDL cholesterol for cardiovascular disease and mortality in elderly men, *Journals Gerontol. - Ser. A Biol. Sci. Med. Sci.* 61 (2006) 1262–1266. <https://doi.org/10.1093/gerona/61.12.1262>.
- [231] C. Zhai, Q. Qian, G. Tang, B. Han, H. Hu, D. Yin, H. Pan, S. Zhang, MicroRNA-206 protects against myocardial ischaemia-reperfusion injury in rats by targeting Gadd45 β , *Mol. Cells.* 40 (2017) 916–924. <https://doi.org/10.14348/molcells.2017.0164>.
- [232] F. Altaf, C. Vesely, A.M. Sheikh, R. Munir, S.T.A. Shah, A. Tariq, Modulation of ADAR mRNA expression in patients with congenital heart defects, *PLoS One.* 14 (2019) 1–14. <https://doi.org/10.1371/journal.pone.0200968>.

- [233] S. Ock, W.S. Lee, J. Ahn, H.M. Kim, H. Kang, H.-S. Kim, D. Jo, E.D. Abel, T.J. Lee, J. Kim, Deletion of IGF-1 receptors in cardiomyocytes attenuates cardiac aging in male mice, *Endocrinology*. 157 (2016) 336–345.
- [234] S. Hirth, A. Bühler, J.B. Bührdel, S. Rudeck, T. Dahme, W. Rottbauer, S. Just, Paxillin and focal adhesion kinase (FAK) regulate cardiac contractility in the Zebrafish heart, *PLoS One*. 11 (2016) 3–7. <https://doi.org/10.1371/journal.pone.0150323>.
- [235] F. Marino, M. Scalise, E. Cianflone, T. Mancuso, I. Aquila, V. Agosti, M. Torella, D. Paolino, V. Mollace, B. Nadal-Ginard, D. Torella, Role of c-kit in myocardial regeneration and aging, *Front. Endocrinol. (Lausanne)*. 10 (2019) 1–15. <https://doi.org/10.3389/fendo.2019.00371>.
- [236] R. Kolhe, M. Hunter, S. Liu, R.N. Jadeja, C. Pundkar, A.K. Mondal, B. Mendhe, M. Drewry, M. V. Rojiani, Y. Liu, C.M. Isales, R.E. Guldborg, M.W. Hamrick, S. Fulzele, Gender-specific differential expression of exosomal miRNA in synovial fluid of patients with osteoarthritis, *Sci. Rep.* 7 (2017). <https://doi.org/10.1038/s41598-017-01905-y>.
- [237] E. Eitan, J. Green, M. Bodogai, N.A. Mode, R. Bæk, M.M. Jørgensen, D.W. Freeman, K.W. Witwer, A.B. Zonderman, A. Biragyn, M.P. Mattson, N. Noren Hooten, M.K. Evans, Age-related changes in plasma extracellular vesicle characteristics and internalization by leukocytes, *Sci. Rep.* 7 (2017) 1–14. <https://doi.org/10.1038/s41598-017-01386-z>.
- [238] L. Chung, D.R. Maestas, F. Housseau, J.H. Elisseeff, Key players in the immune response to biomaterial scaffolds for regenerative medicine, *Adv. Drug Deliv. Rev.* 114 (2017) 184–192. <https://doi.org/10.1016/j.addr.2017.07.006>.
- [239] D.P. Vasconcelos, A.P. Águas, M.A. Barbosa, P. Pelegrín, J.N. Barbosa, The inflammasome in host response to biomaterials: Bridging inflammation and tissue regeneration, *Acta Biomater.* 83 (2019) 1–12. <https://doi.org/10.1016/j.actbio.2018.09.056>.
- [240] D.M. Mosser, J.P. Edwards, Exploring the full spectrum of macrophage activation, *Nat Rev Immunol.* 8 (2008) 958–969. <https://doi.org/10.1038/nri2448.Exploring>.
- [241] G.S. Hussey, J.L. Dziki, S.F. Badylak, Extracellular matrix-based materials for regenerative medicine, *Nat. Rev. Mater.* 3 (2018) 1–15. <https://doi.org/10.1038/s41578-018-0023-x>.
- [242] A. Costa, J.D. Naranjo, R. Londono, S.F. Badylak, Biologic scaffolds, *Cold Spring Harb. Perspect. Biol.* 7 (2017) a025676.
- [243] E.S. Baekkevold, M. Roussigne, T. Yamanaka, F.-E.E. Johansen, F.L. Jahnsen, F.F. Amalric, P. Brandtzaeg, M. Erard, G. Haraldsen, J.-P.P. Girard, M. Roussigné, T. Yamanaka, F.-E.E. Johansen, F.L. Jahnsen, F.F. Amalric, P. Brandtzaeg, M. Erard, G. Haraldsen, J.-P.P. Girard, Molecular characterization of NF-HEV, a nuclear factor preferentially expressed in human high endothelial venules, *Am. J. Pathol.* 163 (2003) 69–79. [https://doi.org/10.1016/S0002-9440\(10\)63631-0](https://doi.org/10.1016/S0002-9440(10)63631-0).
- [244] V. Carriere, L. Roussel, N. Ortega, D.D.-A. Lacorre, L. Americh, L. Aguilar, J.J.-P. Girard,

- G. Bouche, J.J.-P. Girard, IL-33, the IL-1-like cytokine ligand for ST2 receptor, is a chromatin-associated nuclear factor in vivo, *Proc. Natl. Acad. Sci.* 104 (2007) 2–7. <https://doi.org/10.1073/pnas.0606854104>.
- [245] M. Pichery, E. Mirey, P. Mercier, E. Lefrancais, A. Dujardin, N. Ortega, J.-P. Girard, Endogenous IL-33 is highly expressed in mouse epithelial barrier tissues, lymphoid organs, brain, embryos, and inflamed tissues: In situ analysis using a novel Il-33-LacZ gene trap reporter strain, *J. Immunol.* 188 (2012) 3488–3495. <https://doi.org/10.4049/jimmunol.1101977>.
- [246] C. Cayrol, J.P. Girard, Interleukin-33 (IL-33): A nuclear cytokine from the IL-1 family, *Immunol. Rev.* 281 (2018) 154–168. <https://doi.org/10.1111/imr.12619>.
- [247] F.Y. Liew, J.-P. Girard, H.R. Turnquist, Interleukin-33 in health and disease, *Nat. Rev. Immunol.* 16 (2016) 676–689. <https://doi.org/10.1038/nri.2016.95>.
- [248] M.W. Dahlgren, S.W. Jones, K.M. Cautivo, A. Dubinin, J.F. Ortiz-Carpena, S. Farhat, K.S. Yu, K. Lee, C. Wang, A. V. Molofsky, A.D. Tward, M.F. Krummel, T. Peng, A.B. Molofsky, Adventitial stromal cells define group 2 innate lymphoid cell tissue niches, *Immunity.* 50 (2019) 707–722.e6. <https://doi.org/10.1016/j.immuni.2019.02.002>.
- [249] P.T. Nguyen, L.C. Dorman, S. Pan, I.D. Vainchtein, R.T. Han, H. Nakao-Inoue, S.E. Taloma, J.J. Barron, A.B. Molofsky, M.A. Kheirbek, A. V. Molofsky, Microglial remodeling of the extracellular matrix promotes synapse plasticity, *Cell.* 182 (2020) 388–403.e15. <https://doi.org/10.1016/j.cell.2020.05.050>.
- [250] D.K. Reichenbach, V. Schwarze, B.M. Matta, V. Tkachev, E. Lieberknecht, Q. Liu, B.H. Koehn, D. Pfeifer, P.A. Taylor, G. Prinz, H. Dierbach, N. Stickel, Y. Beck, M. Warncke, T. Junt, A. Schmitt-Graeff, S. Nakae, M. Follo, T. Wertheimer, L. Schwab, J. Devlin, S.C. Watkins, J. Duyster, J.L.M. Ferrara, H.R. Turnquist, R. Zeiser, B.R. Blazar, The IL-33/ST2 axis augments effector T-cell responses during acute GVHD, *Blood.* 125 (2015) 3183–3192. <https://doi.org/10.1182/blood-2014-10-606830>.
- [251] P. Aparicio-Domingo, H. Cannelle, M.B. Buechler, S. Nguyen, S.M. Kallert, S. Favre, N. Alouche, N. Papazian, B. Ludewig, T. Cupedo, D.D. Pinschewer, S.J. Turley, S.A. Luther, Fibroblast-derived IL-33 is dispensable for lymph node homeostasis but critical for CD8 T-cell responses to acute and chronic viral infection, *Eur. J. Immunol.* 51 (2021) 76–90. <https://doi.org/10.1002/eji.201948413>.
- [252] R. Kakkar, R.T. Lee, The IL-33/ST2 pathway: therapeutic target and novel biomarker, *Nat. Rev. Drug Discov.* 7 (2008) 827–840. <https://doi.org/10.1038/nrd2660>.
- [253] S. Ali, A. Mohs, M. Thomas, J. Klare, R. Ross, M.L. Schmitz, M.U. Martin, The dual function cytokine IL-33 interacts with the transcription factor NF- κ B to dampen NF- κ B-stimulated gene transcription, *J. Immunol.* 187 (2011) 1609–1616. <https://doi.org/10.4049/jimmunol.1003080>.
- [254] Y. Ni, L. Tao, C. Chen, H. Song, Z. Li, Y. Gao, J. Nie, M. Piccioni, G. Shi, B. Li, The

- deubiquitinase USP17 regulates the stability and nuclear function of IL-33, *Int. J. Mol. Sci.* 16 (2015) 27956–27966. <https://doi.org/10.3390/ijms161126063>.
- [255] E.J. Lee, M.W. So, S. Hong, Y.G. Kim, B. Yoo, C.K. Lee, Interleukin-33 acts as a transcriptional repressor and extracellular cytokine in fibroblast-like synoviocytes in patients with rheumatoid arthritis, *Cytokine*. 77 (2016) 35–43. <https://doi.org/10.1016/j.cyto.2015.10.005>.
- [256] F. Gatti, S. Mia, C. Hammarström, N. Frerker, B. Fosby, J. Wang, W. Pietka, O. Sundnes, J. Hol, M. Kasprzycka, G. Haraldsen, Nuclear IL-33 restrains the early conversion of fibroblasts to an extracellular matrix-secreting phenotype, *Sci. Rep.* 11 (2021) 1–13. <https://doi.org/10.1038/s41598-020-80509-5>.
- [257] V. Gautier, C. Cayrol, D. Farache, S. Roga, B. Monsarrat, O. Burette-Schiltz, A. Gonzalez De Peredo, J.P. Girard, Extracellular IL-33 cytokine, but not endogenous nuclear IL-33, regulates protein expression in endothelial cells, *Sci. Rep.* 6 (2016) 1–12. <https://doi.org/10.1038/srep34255>.
- [258] J. Travers, M. Rochman, C.E. Miracle, J.E. Habel, M. Brusilovsky, J.M. Caldwell, J.K. Rymer, M.E. Rothenberg, Chromatin regulates IL-33 release and extracellular cytokine activity, *Nat. Commun.* 9 (2018) 1–15. <https://doi.org/10.1038/s41467-018-05485-x>.
- [259] Y. bin He, J. hong Guo, C. Wang, D. Zhu, L. ming Lu, IL-33 promotes the progression of nonrheumatic aortic valve stenosis via inducing differential phenotypic transition in valvular interstitial cells, *J. Cardiol.* 75 (2020) 124–133. <https://doi.org/10.1016/j.jjcc.2019.06.011>.
- [260] T. Kukolj, D. Trivanović, S. Mojsilović, I. Okić Djordjević, H. Obradović, J. Krstić, A. Jauković, D. Bugarski, IL-33 guides osteogenesis and increases proliferation and pluripotency marker expression in dental stem cells, *Cell Prolif.* 52 (2019) 1–17. <https://doi.org/10.1111/cpr.12533>.
- [261] K. Seki, S. Sanada, A.Y. Kudinova, M.L. Steinhauser, V. Handa, J. Gannon, R.T. Lee, Interleukin-33 prevents apoptosis and improves survival after experimental myocardial infarction through ST2 signaling, *Circ. Hear. Fail.* 2 (2009) 684–691. <https://doi.org/10.1161/CIRCHEARTFAILURE.109.873240>.
- [262] A.H. Chester, I. El-Hamamsy, J.T. Butcher, N. Latif, S. Bertazzo, M.H. Yacoub, The living aortic valve: From molecules to function, *Glob. Cardiol. Sci. Pract.* 2014 (2014) 11. <https://doi.org/10.5339/gcsp.2014.11>.
- [263] C.S. Samuel, E.N. Unemori, I. Mookerjee, R.A.D. Bathgate, S.L. Layfield, J. Mak, G.W. Tregear, X.J. Du, Relaxin modulates cardiac fibroblast proliferation, differentiation, and collagen production and reverses cardiac fibrosis in vivo, *Endocrinology*. 145 (2004) 4125–4133. <https://doi.org/10.1210/en.2004-0209>.
- [264] Y. Xu, H. Xiao, H. Luo, Y. Chen, Y. Zhang, L. Tao, Y. Jiang, Y. Chen, X. Shen, Inhibitory effects of oxymatrine on TGF- β 1-induced proliferation and abnormal differentiation In rat

- cardiac fibroblasts via the p38MAPK and ERK1/2 signaling pathways, *Mol. Med. Rep.* 16 (2017) 5354–5362. <https://doi.org/10.3892/mmr.2017.7277>.
- [265] I.C.L. Pillai, S. Li, M. Romay, L. Lam, Y. Lu, J. Huang, N. Dillard, M. Zemanova, L. Rubbi, Y. Wang, J. Lee, M. Xia, O. Liang, Y.H. Xie, M. Pellegrini, A.J. Lusic, A. Deb, Cardiac fibroblasts adopt osteogenic fates and can be targeted to attenuate pathological heart calcification, *Cell Stem Cell.* 20 (2017) 218–232.e5. <https://doi.org/10.1016/j.stem.2016.10.005>.
- [266] M.J. Townsend, P.G. Fallon, D.J. Matthews, H.E. Jolin, A.N.J. McKenzie, T1/ST2-deficient mice demonstrate the importance of T1/ST2 in developing primary T helper cell type 2 responses, *J. Exp. Med.* 191 (2000) 1069–1075. <https://doi.org/10.1084/jem.191.6.1069>.
- [267] K. Oboki, T. Ohno, N. Kajiwara, K. Arae, H. Morita, A. Ishii, A. Nambu, T. Abe, H. Kiyonari, K. Matsumoto, K. Sudo, K.K. Okumura, H. Saito, S. Nakae, H. Morita, N. Kajiwara, A. Nambu, T. Ohno, K. Arae, K. Matsumoto, K. Sudo, T. Abe, K.K. Okumura, S. Nakae, H. Saito, K. Oboki, A. Ishii, IL-33 is a crucial amplifier of innate rather than acquired immunity, *Proc. Natl. Acad. Sci. U. S. A.* 107 (2010) 18581–18586. <https://doi.org/10.1073/pnas.1003059107>.
- [268] M.I. Love, W. Huber, S. Anders, Moderated estimation of fold change and dispersion for RNA-seq data with DESeq2, *Genome Biol.* 15 (2014) 1–21. <https://doi.org/10.1186/s13059-014-0550-8>.
- [269] J. Bai, N. Zhang, Y. Hua, B. Wang, L. Ling, A. Ferro, B. Xu, Metformin inhibits angiotensin II-induced differentiation of cardiac fibroblasts into myofibroblasts., *PLoS One.* 8 (2013) 1–7. <https://doi.org/10.1371/journal.pone.0072120>.
- [270] P.J. Lijnen, V. V. Petrov, R.H. Fagard, Angiotensin II-induced stimulation of collagen secretion and production in cardiac fibroblasts is mediated via angiotensin II subtype 1 receptors, *JRAAS - J. Renin-Angiotensin-Aldosterone Syst.* 2 (2001) 117–122. <https://doi.org/10.3317/jraas.2001.012>.
- [271] S. Goto, M.A. Rogers, M.C. Blaser, H. Higashi, L.H. Lee, F. Schlotter, S.C. Body, M. Aikawa, S.A. Singh, E. Aikawa, Standardization of human calcific aortic valve disease in vitro modeling reveals passage-dependent calcification, *Front. Cardiovasc. Med.* 6 (2019) 1–12. <https://doi.org/10.3389/fcvm.2019.00049>.
- [272] T. Schöneberg, J. Meister, A.B. Knierim, A. Schulz, The G protein-coupled receptor GPR34 – The past 20 years of a grownup, *Pharmacol. Ther.* 189 (2018) 71–88. <https://doi.org/10.1016/j.pharmthera.2018.04.008>.
- [273] B. Faz-López, J. Morales-Montor, L.I. Terrazas, Role of macrophages in the repair process during the tissue migrating and resident helminth infections, *Biomed Res. Int.* 2016 (2016). <https://doi.org/10.1155/2016/8634603>.
- [274] S. Chakarov, H.Y. Lim, L. Tan, S.Y. Lim, P. See, J. Lum, X.M. Zhang, S. Foo, S. Nakamizo,

- K. Duan, W.T. Kong, R. Gentek, A. Balachander, D. Carbajo, C. Bleriot, B. Malleret, J.K.C. Tam, S. Baig, M. Shabeer, S.A.E.S. Toh, A. Schlitzer, A. Larbi, T. Marichal, B. Malissen, J. Chen, M. Poidinger, K. Kabashima, M. Bajenoff, L.G. Ng, V. Angeli, F. Ginhoux, Two distinct interstitial macrophage populations coexist across tissues in specific subtissular niches, *Science* (80-). 363 (2019). <https://doi.org/10.1126/science.aau0964>.
- [275] L. Estrada-Capetillo, L. Aragonese-Fenoll, Á. Domínguez-Soto, S. Fuentelsaz-Romero, C. Nieto, M. Simón-Fuentes, B. Alonso, P. Portolés, A.L. Corbí, J.M. Rojo, A. Puig-Kröger, CD28 is expressed by macrophages with anti-inflammatory potential and limits their T-cell activating capacity, *Eur. J. Immunol.* 51 (2021) 824–834. <https://doi.org/10.1002/eji.202048806>.
- [276] S.A. Rudge, M.J.O. Wakelam, Phosphatidylinositolphosphate phosphatase activities and cancer, *J. Lipid Res.* 57 (2016) 176–192. <https://doi.org/10.1194/jlr.R059154>.
- [277] U.M. Gundra, N.M. Girgis, D. Ruckerl, S. Jenkins, L.N. Ward, Z.D. Kurtz, K.E. Wiens, M.S. Tang, U. Basu-Roy, A. Mansukhani, J.E. Allen, P. Loke, Alternatively activated macrophages derived from monocytes and tissue macrophages are phenotypically and functionally distinct, *Blood.* 123 (2014) 110–122. <https://doi.org/10.1182/blood-2013-08-520619>.
- [278] C. Gabay, Interleukin-6 and chronic inflammation, *Arthritis Res. Ther.* 8 (2006) 1–6. <https://doi.org/10.1186/ar1917>.
- [279] N. Shahzad, T. Munir, M. Javed, F. Tasneem, B. Aslam, M. Ali, Z. Mutahir, M.A. Ali, M. Umer, M. Ahmad, K. Farooq, U. Hassan, T. Mustafa, R.S. Anjum, A.R. Shakoori, SHISA3, an antagonist of the Wnt/ β -catenin signaling, is epigenetically silenced and its ectopic expression suppresses growth in breast cancer, *PLoS One.* 15 (2020) 1–16. <https://doi.org/10.1371/journal.pone.0236192>.
- [280] E.S. Malsin, S. Kim, A.P. Lam, C.J. Gottardi, Macrophages as a source and recipient of Wnt signals, *Front. Immunol.* 10 (2019) 1813. <https://doi.org/10.3389/fimmu.2019.01813>.
- [281] K.A. Zimmerman, C.J. Song, Z. Li, J.M. Lever, D.K. Crossman, A. Rains, E.J. Aloria, N.M. Gonzalez, J.R. Bassler, J. Zhou, M.R. Crowley, D.Z. Revell, Z. Yan, D. Shan, E.N. Benveniste, J.F. George, M. Mrug, B.K. Yoder, Tissue-resident macrophages promote renal cystic disease, *J. Am. Soc. Nephrol.* 30 (2019) 1841–1856. <https://doi.org/10.1681/ASN.2018080810>.
- [282] L. Tserel, M. Limbach, M. Saare, K. Kisand, A. Metspalu, L. Milani, P. Peterson, CpG sites associated with NRP1, NRXN2 and miR-29b-2 are hypomethylated in monocytes during ageing, *Immun. Ageing.* 11 (2014) 1–5. <https://doi.org/10.1186/1742-4933-11-1>.
- [283] J.C. Gensel, T.J. Kopper, B. Zhang, M.B. Orr, W.M. Bailey, Predictive screening of M1 and M2 macrophages reveals the immunomodulatory effectiveness of post spinal cord injury azithromycin treatment, *Sci. Rep.* 7 (2017) 1–10. <https://doi.org/10.1038/srep40144>.
- [284] D.D. MacDougall, Z. Lin, N.L. Chon, S.L. Jackman, H. Lin, J.D. Knight, A. Anantharam,

- The high-affinity calcium sensor synaptotagmin-7 serves multiple roles in regulated exocytosis, *J. Gen. Physiol.* 150 (2018) 783–807. <https://doi.org/10.1085/jgp.201711944>.
- [285] X. Ma, W. Yan, H. Zheng, Q. Du, L. Zhang, Y. Ban, N. Li, F. Wei, Regulation of IL-10 and IL-12 production and function in macrophages and dendritic cells, *F1000Research*. 4 (2015) 1–13. <https://doi.org/10.12688/f1000research.7010.1>.
- [286] Y.-T. Azuma, H. Nakajima, T. Takeuchi, IL-19 as a potential therapeutic in autoimmune and inflammatory diseases, *Curr. Pharm. Des.* 17 (2011) 3776–3780. <https://doi.org/10.2174/138161211798357845>.
- [287] Y.H. Hsu, P.P. Hsieh, M.S. Chang, Interleukin-19 blockade attenuates collagen-induced arthritis in rats, *Rheumatology*. 51 (2012) 434–442. <https://doi.org/10.1093/rheumatology/ker127>.
- [288] R. Marzio, E. Jirillo, A. Ransijn, J. Mauël, S.B. Corradin, Expression and function of the early activation antigen CD69 in murine macrophages, *J. Leukoc. Biol.* 62 (1997) 349–355. <https://doi.org/10.1002/jlb.62.3.349>.
- [289] K. Yamauchi, Y. Kasuya, F. Kuroda, K. Tanaka, J. Tsuyusaki, S. Ishizaki, H. Matsunaga, C. Iwamura, T. Nakayama, K. Tatsumi, Attenuation of lung inflammation and fibrosis in CD69-deficient mice after intratracheal bleomycin, *Respir. Res.* 12 (2011) 1–10. <https://doi.org/10.1186/1465-9921-12-131>.
- [290] P. Ruytinx, P. Proost, J. Van Damme, S. Struyf, Chemokine-induced macrophage polarization in inflammatory conditions, *Front. Immunol.* 9 (2018) 1–12. <https://doi.org/10.3389/fimmu.2018.01930>.
- [291] A.W. Roberts, G-CSF: A key regulator of neutrophil production, but that’s not all!, *Growth Factors*. 23 (2005) 33–41. <https://doi.org/10.1080/08977190500055836>.
- [292] J. Schmitz, A. Owyang, E. Oldham, Y. Song, E. Murphy, T.K. McClanahan, G. Zurawski, M. Moshrefi, J. Qin, X. Li, D.M. Gorman, J.F. Bazan, R.A. Kastelein, IL-33, an interleukin-1-like cytokine that signals via the IL-1 receptor-related protein ST2 and induces T helper type 2-associated cytokines, *Immunity*. 23 (2005) 479–490. <https://doi.org/10.1016/j.immuni.2005.09.015>.
- [293] C. Moussion, N. Ortega, J.P. Girard, The IL-1-like cytokine IL-33 is constitutively expressed in the nucleus of endothelial cells and epithelial cells in vivo: A novel “Alarmin”?, *PLoS One*. 3 (2008) 1–8. <https://doi.org/10.1371/journal.pone.0003331>.
- [294] M. Nechama, J. Kwon, S. Wei, A.T. Kyi, R.S. Welner, I.Z. Ben-Dov, M.S. Arredouani, J.M. Asara, C.H. Chen, C.Y. Tsai, K.F. Nelson, K.S. Kobayashi, E. Israel, X.Z. Zhou, L.K. Nicholson, K.P. Lu, The IL-33-PIN1-IRAK-M axis is critical for type 2 immunity in IL-33-induced allergic airway inflammation, *Nat. Commun.* 9 (2018). <https://doi.org/10.1038/s41467-018-03886-6>.
- [295] M.S. Zaibi, M.A. Kępczyńska, P. Harikumar, S.Y. Alomar, P. Trayhurn, IL-33 stimulates

- expression of the GPR84 (EX33) fatty acid receptor gene and of cytokine and chemokine genes in human adipocytes, *Cytokine*. 110 (2018) 189–193. <https://doi.org/10.1016/j.cyto.2018.05.008>.
- [296] K. Gao, X. Li, L. Zhang, L. Bai, W. Dong, K. Gao, G. Shi, X. Xia, L. Wu, L. Zhang, Transgenic expression of IL-33 activates CD8⁺ T cells and NK cells and inhibits tumor growth and metastasis in mice, *Cancer Lett.* 335 (2013) 463–471. <https://doi.org/10.1016/j.canlet.2013.03.002>.
- [297] C. Dreis, F.M. Ottenlinger, M. Putyrski, A. Ernst, M. Huhn, K.G. Schmidt, J.M. Pfeilschifter, H.H. Radeke, Tissue cytokine IL-33 modulates the cytotoxic CD8T lymphocyte activity during nutrient deprivation by regulation of lineage-specific differentiation programs, *Front. Immunol.* 10 (2019) 1–15. <https://doi.org/10.3389/fimmu.2019.01698>.
- [298] P.C. McCarthy, I.R. Phair, C. Greger, K. Pardali, V.A. McGuire, A.R. Clark, M. Gaestel, J.S.C. Arthur, IL-33 regulates cytokine production and neutrophil recruitment via the p38 MAPK-activated kinases MK2/3, *Immunol. Cell Biol.* 97 (2019) 54–71. <https://doi.org/10.1111/imcb.12200>.
- [299] R. Joulia, F.E. L’Faqihi, S. Valitutti, E. Espinosa, IL-33 fine tunes mast cell degranulation and chemokine production at the single-cell level, *J. Allergy Clin. Immunol.* 140 (2017) 497–509. <https://doi.org/10.1016/j.jaci.2016.09.049>.
- [300] K.D. Mertz, L.F. Mager, M.H. Wasmer, T. Thiesler, V.H. Koelzer, G. Ruzzante, S. Joller, J.R. Murdoch, T. Brümmendorf, V. Genitsch, A. Lugli, G. Cathomas, H. Moch, A. Weber, I. Zlobec, T. Junt, P. Krebs, The IL-33/ST2 pathway contributes to intestinal tumorigenesis in humans and mice, *Oncoimmunology*. 5 (2016) 1–11. <https://doi.org/10.1080/2162402X.2015.1062966>.
- [301] H. Sandig, C.E. Jobbings, N.G. Roldan, J.K. Whittingham-Dowd, Z. Orinska, O. Takeuchi, S. Akira, S. Bulfone-Paus, IL-33 causes selective mast cell tolerance to bacterial cell wall products by inducing IRAK1 degradation, *Eur. J. Immunol.* 43 (2013) 979–988. <https://doi.org/10.1002/eji.201242786>.
- [302] Q. Espinassous, E. Garcia-de-Paco, I. Garcia-Verdugo, M. Synguelakis, S. von Aulock, J.-M. Sallenave, A.N.J. McKenzie, J. Kanellopoulos, IL-33 enhances lipopolysaccharide-induced inflammatory cytokine production from mouse macrophages by regulating lipopolysaccharide receptor complex, *J. Immunol.* 183 (2009) 1446–1455. <https://doi.org/10.4049/jimmunol.0803067>.
- [303] R. Kakkar, H. Hei, S. Dobner, R.T. Lee, Interleukin 33 as a mechanically responsive cytokine secreted by living cells, *J. Biol. Chem.* 287 (2012) 6941–6948. <https://doi.org/10.1074/jbc.M111.298703>.
- [304] M.A. Ansari, V.V. Singh, S. Dutta, M.V. Veetil, D. Dutta, L. Chikoti, J. Lu, D. Everly, B. Chandran, Constitutive interferon-inducible protein 16-inflammasome activation during Epstein-Barr virus latency I, II, and III in B and epithelial cells, *J. Virol.* 87 (2013) 8606–

8623. <https://doi.org/10.1128/jvi.00805-13>.

- [305] D. Shao, F. Perros, G. Caramori, C. Meng, P. Dormuller, P.C. Chou, C. Church, A. Papi, P. Casolari, D. Welsh, A. Peacock, M. Humbert, I.M. Adcock, S.J. Wort, Nuclear IL-33 regulates soluble ST2 receptor and IL-6 expression in primary human arterial endothelial cells and is decreased in idiopathic pulmonary arterial hypertension, *Biochem. Biophys. Res. Commun.* 451 (2014) 8–14. <https://doi.org/10.1016/j.bbrc.2014.06.111>.
- [306] S. Sanada, D. Hakuno, L.J. Higgins, E.R. Schreiter, A.N.J. McKenzie, R.T. Lee, IL-33 and ST2 comprise a critical biomechanically induced and cardioprotective signaling system, *J. Clin. Invest.* 117 (2007) 1538–1549. <https://doi.org/10.1172/JCI30634>.
- [307] J. Zhu, W. Carver, Effects of interleukin-33 on cardiac fibroblast gene expression and activity, *Cytokine.* 58 (2012) 368–379. <https://doi.org/10.1016/j.cyto.2012.02.008>.
- [308] C. Mora-Navarro, A. Badileanu, A. Gracioso Martins, E. Ozpinar, L. Gaffney, I. Huntress, E. Harrell, J. Enders, X. Peng, R. Branski, D. Freytes, Porcine vocal fold lamina propria-derived biomaterials modulate TGF- β 1 mediated fibroblast activation in vitro, *ACS Appl. Mater. Interfaces.* 6 (2020) 1690–1703. <https://doi.org/10.1021/acsbiomaterials.9b01837>. Porcine.
- [309] L.M. Quijano, J.D. Naranjo, S. El-Mossier, N.J. Turner, C. Pineda Molina, J. Bartolacci, L. Zhang, L. White, H. Li, S.F. Badylak, Matrix-bound nanovesicles: The effects of isolation method upon yield, purity and function, *Tissue Eng. Part C Methods.* 26 (2020) 528–540. <https://doi.org/10.1089/ten.tec.2020.0243>.
- [310] S. Saidi, F. Bouri, P. Lencel, L. Duplomb, M. Baud’huin, S. Delplace, D. Leterme, F. Miellot, D. Heymann, P. Hardouin, G. Palmer, D. Magne, IL-33 is expressed in human osteoblasts, but has no direct effect on bone remodeling, *Cytokine.* 53 (2011) 347–354. <https://doi.org/10.1016/j.cyto.2010.11.021>.
- [311] L. Ginaldi, M. De Martinis, S. Saitta, M.M. Sirufo, C. Mannucci, M. Casciaro, F. Ciccarelli, S. Gangemi, Interleukin-33 serum levels in postmenopausal women with osteoporosis, *Sci. Rep.* 9 (2019) 1–7. <https://doi.org/10.1038/s41598-019-40212-6>.
- [312] H. Saleh, D. Eeles, J.M. Hodge, G.C. Nicholson, R. Gu, S. Pompolo, M.T. Gillespie, J.M.W. Quinn, Interleukin-33, a target of parathyroid hormone and oncostatin m, increases osteoblastic matrix mineral deposition and inhibits osteoclast formation in vitro, *Endocrinology.* 152 (2011) 1911–1922. <https://doi.org/10.1210/en.2010-1268>.
- [313] J. Schulze, T. Bickert, F.T. Beil, M.M. Zaiss, J. Albers, K. Wintges, T. Streichert, K. Klaetschke, J. Keller, T.N. Hissnauer, A.S. Spiro, A. Gessner, G. Schett, M. Amling, A.N.J. McKenzie, A.K. Horst, T. Schinke, Interleukin-33 is expressed in differentiated osteoblasts and blocks osteoclast formation from bone marrow precursor cells, *J. Bone Miner. Res.* 26 (2011) 704–717. <https://doi.org/10.1002/jbmr.269>.
- [314] A. Danjo, T. Yamaza, M.A. Kido, D. Shimohira, T. Tsukuba, T. Kagiya, Y. Yamashita, K. Nishijima, S. Masuko, M. Goto, T. Tanaka, Cystatin C stimulates the differentiation of

- mouse osteoblastic cells and bone formation, *Biochem. Biophys. Res. Commun.* 360 (2007) 199–204. <https://doi.org/10.1016/j.bbrc.2007.06.028>.
- [315] B. Warriar, R. Mallipeddi, P.K. Karla, C.H. Lee, The functional role of C-reactive protein in aortic wall calcification, *Cardiology.* 104 (2005) 57–64. <https://doi.org/10.1159/000086686>.
- [316] R. Li, L. Peng, L. Ren, H. Tan, L. Ye, Hepatocyte growth factor exerts promoting functions on murine dental papilla cells., *J. Endod.* 35 (2009) 382–388. <https://doi.org/10.1016/j.joen.2008.11.031>.
- [317] K. Sadtler, S.D. Sommerfeld, M.T. Wolf, X. Wang, S. Majumdar, L. Chung, D.S. Kelkar, A. Pandey, J.H. Elisseeff, Proteomic composition and immunomodulatory properties of urinary bladder matrix scaffolds in homeostasis and injury, *Semin. Immunol.* 29 (2017) 14–23. <https://doi.org/10.1016/j.smim.2017.05.002>.
- [318] O.R. Mahon, D.C. Browe, P.J. Diaz-Payno, P. Pitacco, K.T. Cunningham, K.H.G. Mills, A. Dunne, D.J. Kelly, Extracellular matrix scaffolds derived from different musculoskeletal tissues drive distinct macrophage phenotypes and direct tissue-specific cellular differentiation, *J. Immunol. Regen. Med.* 12 (2021) 100041. <https://doi.org/10.1016/j.regen.2021.100041>.
- [319] R. Londono, S.F. Badylak, Factors which affect the host response to biomaterials, in: S.F. Badylak (Ed.), *Host Response to Biomater. Impact Host Response Biomater. Sel.*, Academic Press, Oxford, 2015: pp. 1–12. <https://doi.org/https://doi.org/10.1016/B978-0-12-800196-7.00001-3>.
- [320] Y.H. Joung, Development of implantable medical devices: From an engineering perspective, *Int. Neurourol. J.* 17 (2013) 98–106. <https://doi.org/10.5213/inj.2013.17.3.98>.
- [321] L. Parisi, A. Toffoli, G. Ghiacci, G.M. Macaluso, Tailoring the interface of biomaterials to design effective scaffolds, *J. Funct. Biomater.* 9 (2018) 1–31. <https://doi.org/10.3390/jfb9030050>.
- [322] D. Williams, Biomaterials and biomedical materials, in: D. Williams, X. Zhang (Eds.), *Mater. Today Defin. Biomater. Twenty-First Century*, Elsevier, 2019: pp. 15–23. <https://doi.org/https://doi.org/10.1016/B978-0-12-818291-8.00002-X>.
- [323] D.F. Williams, On the mechanisms of biocompatibility, *Biomaterials.* 29 (2008) 2941–2953. <https://doi.org/10.1016/j.biomaterials.2008.04.023>.
- [324] M.T. Wolf, C.L. Dearth, C.A. Ranallo, S. LoPresti, L. Carey, K.A. Daly, B.N. Brown, S.F. Badylak, Macrophage polarization in response to ECM coated polypropylene mesh, *Biomaterials.* 35 (2014) 6838–6849. <https://doi.org/10.1530/ERC-14-0411.Persistent>.
- [325] O. Veiseh, J.C. Doloff, M. Ma, A.J. Vegas, H. Hei, A.R. Bader, J. Li, E. Langan, J. Wyckoff, W.S. Loo, S. Jhunjhunwala, A. Chiu, S. Siebert, K. Tang, S. Aresta-dasilva, M. Bochenek, J. Mendoza-elias, Y. Wang, M. Qi, D.M. Lavin, M. Chen, N. Dholakia, I. Lacík, G.C. Weir, J. Oberholzer, D.L. Greiner, R. Langer, D.G. Anderson, Size- and shape-dependent foreign body immune response to materials implanted in rodents and non-human primates, *Nat*

- Mater. 14 (2015) 643–651. <https://doi.org/10.1038/nmat4290>.Size-
- [326] D.R. Johnston, E.G. Soltesz, N. Vakil, J. Rajeswaran, E.E. Roselli, J.F. Sabik, N.G. Smedira, L.G. Svensson, B.W. Lytle, E.H. Blackstone, Long-term durability of bioprosthetic aortic valves: Implications from 12,569 implants, *Ann. Thorac. Surg.* 99 (2015) 1239–1247. <https://doi.org/10.1016/j.athoracsur.2014.10.070>.
- [327] C.R. Deeken, L. Melman, E.D. Jenkins, S.C. Greco, M.M. Frisella, B.D. Matthews, Histologic and biomechanical evaluation of crosslinked and non-crosslinked biologic meshes in a porcine model of ventral incisional hernia repair, *J Am Coll Surg.* 212 (2011) 880–888. <https://doi.org/10.1016/j.jamcollsurg.2011.01.006>.Histologic.
- [328] M. Cramer, J. Chang, M. Cox, H. Li, A. Serrero, M. El-kurdi, S.F. Badylak, F.J. Schoen, Tissue response, macrophage phenotype, and intrinsic calcification induced by cardiovascular biomaterials: Can clinical regenerative potential be predicted in a rat subcutaneous implant model?, *J Biomed Mater Res Part A.* (2021) 1–12. <https://doi.org/10.1002/jbm.a.37280>.
- [329] B. Wernly, M. Lichtenauer, P. Jirak, S. Eder, C. Reiter, J. Kammler, A. Kypta, C. Jung, M. Franz, U.C. Hoppe, U. Landmesser, H.R. Figulla, A. Lauten, Soluble ST2 predicts 1-year outcome in patients undergoing transcatheter aortic valve implantation, *Eur. J. Clin. Invest.* 47 (2017) 149–157. <https://doi.org/10.1111/eci.12719>.
- [330] J.W. Tsao, R.J. Levy, F.J. Schoen, Compressive mechanical deformation inhibits calcification of bovine pericardium used in cardiac valve bioprosthesis, in: 13th Annu. Meet. Soc. Biomater., 1987: p. 180.
- [331] F.J. Schoen, J.W. Tsao, R.J. Levy, Calcification of bovine pericardium used in cardiac valve bioprostheses: Implications for the mechanisms of bioprosthetic tissue mineralization, *Am J Pathol.* 123 (1986) 134–145. <https://doi.org/10.1021/acsnano.9b03050>.
- [332] M.C. Fishbein, R.J. Levy, V.J. Ferrans, L.C. Dearden, A. Nashef, A.P. Goodman, A. Carpentier, Calcification of cardiac valve bioprostheses. Biochemical, histologic, and ultrastructural observations in a subcutaneous implantation model system, *J. Thorac. Cardiovasc. Surg.* 83 (1982) 602–609. [https://doi.org/10.1016/s0022-5223\(19\)37251-4](https://doi.org/10.1016/s0022-5223(19)37251-4).
- [333] D. Hachim, N. Wang, S.T. Lopresti, E.C. Stahl, Y.U. Umeda, R.D. Rege, S.T. Carey, D. Mani, B.N. Brown, Effects of aging upon the host response to implants, *J. Biomed. Mater. Res. - Part A.* 105 (2017) 1281–1292. <https://doi.org/10.1002/jbm.a.36013>.
- [334] C.G.A. McGregor, A. Carpentier, N. Lila, J.S. Logan, G.W. Byrne, Cardiac xenotransplantation technology provides materials for improved bioprosthetic heart valves, *J. Thorac. Cardiovasc. Surg.* 141 (2011) 269–275. <https://doi.org/10.1016/j.jtcvs.2010.08.064>.
- [335] B. Meuris, S. Ozaki, P. Herijgers, E. Verbeken, W. Flameng, Bioprosthetic tissue calcification: Influence of blood contact and arterial pressure. An experimental study in rats and sheep, *J. Heart Valve Dis.* 12 (2003) 392–399.